POLITECNICO DI TORINO

Master's Degree in Civil Engineering

Master's Degree Thesis

Impact of Climate Change on Global Wave Energy Resource

Supervisors

Dr. Davide Poggi

Dr. Joan Pau Sierra

Candidate

Michele Montefusco

December 2019

TABLE OF CONTENTS

LIST OF FIGURES

ABSTRACT

The Intergovernmental Panel on Climate Change (IPCC) is the main organization about the analysis of climate change. This organization collects studies and processes all the information obtained with the aim of producing assessment reports about the state of the Earth climate and its potential future evolution. The last IPCC report is the "Fifth Assessment Report" (AR5), which was published in 2014. In it the AR5, together with the past climate evolution, some future climate projections are presented, in which different rates of greenhouse gas emissions are expected, assembling a number of climate models.

The wave energy is a field of renewable energy which try to extract the energy stored in wind waves. In the last years many attempts to produce energy from this resource have been made using prototypes that benefit from waves using different methods such as their kinetic energy, the motion of swinging or rotation caused by waves to floating devices, and also the pressure inducted by the oscillating sea level into closed chambers moored on the nearshore area. Potentially, marine energy is considered a powerful resource despite the majority of technologies are still in an experimental state. In fact, it is estimated that energy extractable from oceans could cover the entire global energy requirement.

The five data sets (obtained from 5 series of numerical models) used for this work provide a total of twenty files output, ten for wave heights and ten for peak wave periods. Each set of ten is divided into five outputs of past period (1979-2005) and five of future period (2081-2100). For the process of wave energy's assessment, between all the points available in the models only 1310 have been selected. This permits to form a grid all over the sea surface with a point every 5° of latitude and longitude, so that the distance between two subsequent points vary depending on the latitude and has a mean length of 400 km.

The results of the global wave power averaged on every point for the entire time interval of twenty years in the past (1986-2005) and in the future (2081-2100) show that all five model sets agree on considering the Southern Hemisphere as the most powerful area with peaks of mean wave power around 170 kW/m in the area located in southwestern Australia. In addition, the Northern Hemisphere is also considered by all five model sets as a high power area, with some models estimating the North Atlantic as more powerful than Pacific Ocean (BCC-CSM1-1 and EC-EARTH) while other models (INMCM4 and MIROC5) estimate the opposite.

All models seem to agree with the patterns of wave power's variations between past and future periods, projecting an increment in the Southern Hemisphere, especially in the Indian Ocean where up to 20 kW/m more will be expected. All models also estimate, but with different rates, an increase of wave power in the eastern Pacific Ocean and a decrease in the Northern Hemisphere of the Atlantic Ocean. Moreover, the results outputted that the maximums values of monthly and seasonal variability are found in the Northern Hemisphere but the climate change projects to decrease these coefficients in such Hemisphere and, by contrast, increase their values in all the Southern Hemisphere.

ACKNOWLEDGMENTS

I would like to thank my supervisor Dr Joan Pau Sierra from the Univesidad Politecnica de Cataluña for his support and for his valuable advices that permitted to perform a great work. Thanks also to my professor Dr Davide Poggi for giving me the opportunity to live an experience in a foreign country and to Dr. Mercè Casas-Prat from Environment and Climate Change Canada for providing the data needed to carry out the study.

Finally I must express gratitude to my family that supported me during the years and encourage me for chasing my goals. A final important thanks goes to all my friends from Turin, Lecce and from Barcelona, without whom these years would not have been so specials.

1. INTRODUCTION

The purpose of this thesis is to study the effects that climate change will have on the energy resource originated from seas and oceans.

Nowadays the population on the planet is increasing and it is estimated that in year 2100 there will be around 11 billions of people on Earth (United Nations, DESA, 2019). From this growth will arise an ever increasing demand of electricity so, in terms of infrastructure, an increasing of installed capacity. Moreover, it is a common thought of many scientists and an objective fact for IPCC (Intergovernmental Panel on Climate Change) that climate change is occurring on our planet manifesting mainly with the rise of the mean sea level and the mean of air temperature (IPCC, 2013).

The increasing of energy demand risks to accelerate the growth of carbon emission in the atmosphere caused by the production of energy from fossil fuels. From this problem the need of developing technologies with take advantage of renewable resources was born. The trend of their employment is rising thanks to funding from the governments and it will be crucial to expand the installed capacity of the most exercised one, such as hydropower, solar energy, wind energy etc., but also to implement new technologies which use other green resources in order to diversify the production of energy.

One form of energy which is still not widespread is ocean energy. Around the seas and the oceans there is a huge amount of energy which is still not tapped. This energy resides not only in waves but also in currents, tides and thermic gradients. Nowadays there are a lot of prototypes built for capturing these energies, but only few of them are near to the marketing step.

The focus of this thesis will be to understand if wave energy technologies could take advantage or not of the climate change and how much this renewable resource could help to satisfying the ever increasing global demand of energy. Therefore, the main goal of this work is to assess, at a global scale, how climate change can modify the available wave energy resource.

This main goal will be developed through the following ancillary objectives:

- To assess the wave energy resource for present and future conditions, analysing the changes in such resource at a global scale,
- To analyse changes in the resource at a regional scale.
- To study alterations in the variability of the resource.
- To analyse seasonal changes in the wave energy resource.

2. STATE OF THE CLIMATE CHANGE

2.1 IPCC and AR5

The Intergovernmental Panel on Climate Change (IPCC) is the main organization about the analysis of climate change.

It was established in 1988 by the World Meteorological Organization (WMO) and the United Nations Environment Program (UNEP) as a goal from United Nations to unify the world scientific knowledge on climate change and provide to the governments around the world a complete vision of what is one of the main problems of modern society, what could be its impact on environment and on global society and economy.

An important feature about IPCC is that it does not do research on climate change or monitoring of climate data, it simply evaluate the studies of thousands of volunteer scientists from all over the 195 member states that give to IPCC their contribution with their own research. This organization, then, collects, studies and processes all the information obtained with the aim of producing final reports, focused at grouping the most important information which can serve to society to better understand the problem and to governments to deal with it developing climate policies.

The IPCC started publishing reports in 1990, and continued its work every 6 years on average. The second report, made in 1995, contributed in the making of Kyoto Protocol of 1997, the last report, the "Fifth Assessment Report" (AR5) was published in 2013 (IPCC, 2013) and the next one is programmed to be released in 2022.

The working group for AR5 is divided into three subgroups with different goals. These objectives are the physical science basis of climate change, the impact, adaption and vulnerability of climate change and the mitigation of it. In this report the key messages that IPCC wanted to spread were that "it is extremely likely that we are the dominant cause of warming since the mid-20th century" and this warning is supported in the IPCC's document in four topics: "Observed Changes and their Causes", "Future Climate Changes, Risk and Impacts", "Future Pathways for Adaption, Mitigation and Sustainable Development" and "Adaption and Mitigation" (IPCC, 2013).

2.2 Observed Changes

The studies of scientists who took part in the AR5 (IPCC, 2013) affirm that the last three decades have been successively the warmest from 1850 as can be seen in *figure 2.1 (a)*, and probably these last thirty years have been the warmest of the last 800 years in the North Hemisphere. In the period which goes from 1880 to 2012 the combined temperature of land and ocean increased 0.85 °C, this energy has been collected mostly by the oceans, which store 90% of it against only 1% of atmosphere (*figure 2.1 (b)*).

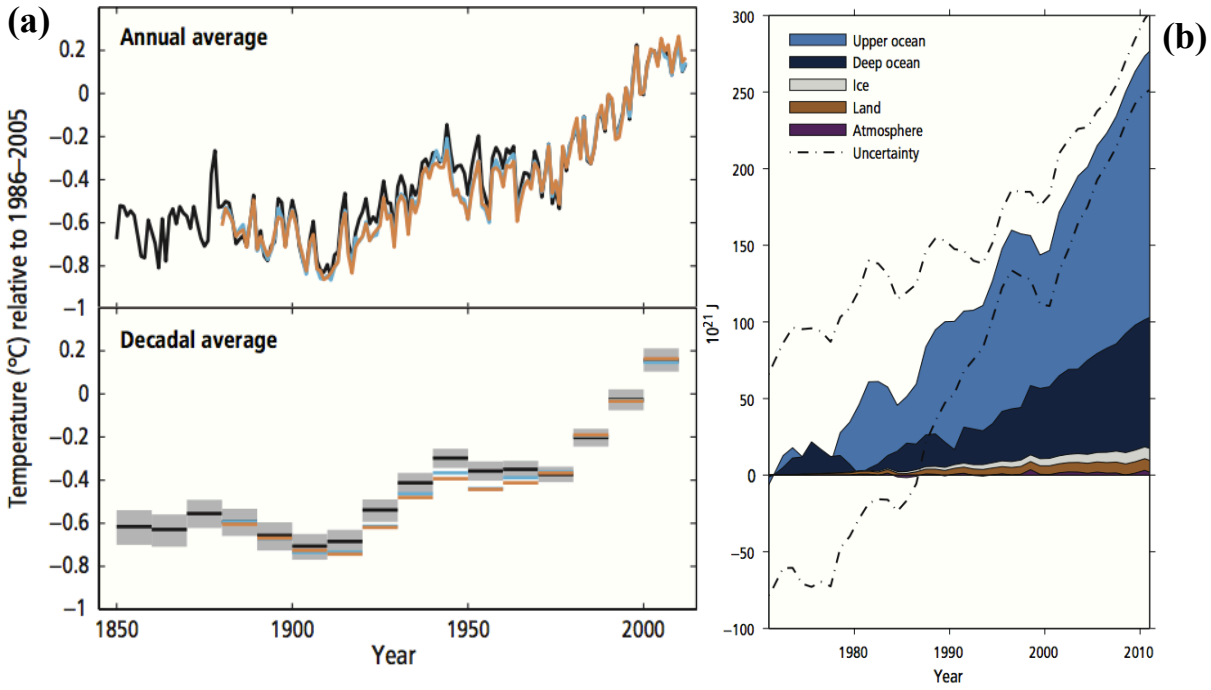

Figure 2.1: a) Temperature anomaly from 1850 to 2005 shown in annual and decadal time scale, relative to the mean of the period 1986-2005. **b)** Division of energy accumulation between oceans, ice and lands caused by global warming in the period 1971-2010 (Source: IPCC, 2013).

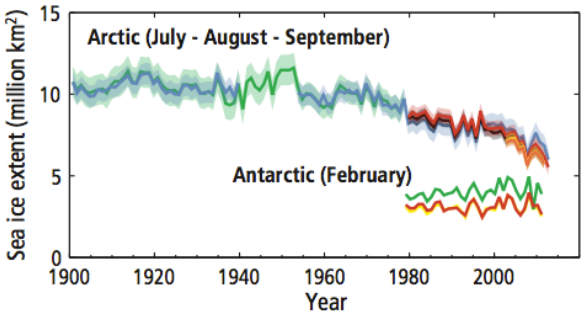

Figure 2.2: Sea ice extend in Arctic (from 1900 to 2012) and Antarctic (from 1980 to 2012) (Source: IPCC, 2013).

Regarding the ocean warming, it has been evaluated that the zone between the surface and 75 meters underwater had a warming rate of 0.11°C per decade from 1971 to 2010 and also the water portions gradually deeper are warming in more recent years. Another change in the environment is the acidification of oceans, where the PH has decreased of 0.1 corresponding to an acidity growth by 26% (IPCC,2013), measured in terms of hydrogen ion's concentration.

Moreover, one of the most well-known effects of climate change is the cryosphere's reduction. From 1979, when satellites started monitoring the North Pole, the frozen area has been continuously decreasing with a rate of around 4% per decade and, especially in summer, the mean ice mass decrease reached a reduction rate between 9.4% and 13.6% per decade, which means around 1 million of km^2 per decade (*figure 2.2*).

Glaciers' melting, combined with thermal expansion of water due to temperature increasing, is producing a sea level rise. This rise is estimated to be 20 centimeters over the period 1901-2010, with a mean of 1.7 mm/year, against the mean in the period 1993-2010 which is almost double, 3.2 mm/year (*figure 2.3*).

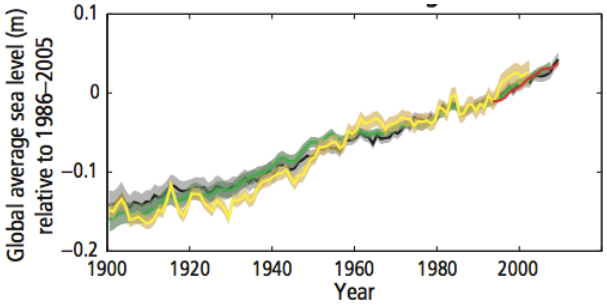

Figure 2.3: Global mean sea level change relative to the mean sea level of 1986-2005's period (Source: IPCC, 2013).

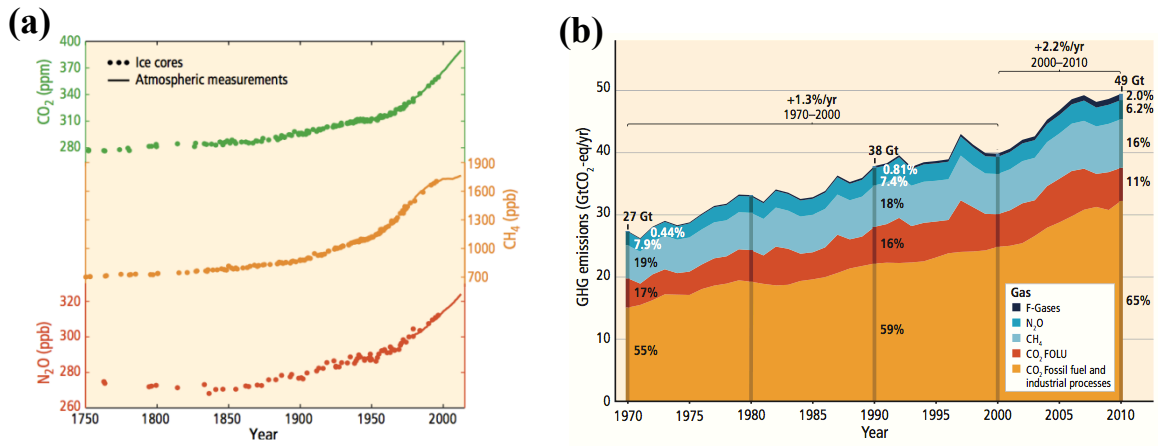

Figure 2.4: a) Observed changes in greenhouse gas concentrations of CO_2 (green), CH_4 (orange) and N_2O (red). **b)** Total annual anthropogenic GHGs emissions for the period 1970-2010 (Source: IPCC, 2013).

The past and recent drivers of climate change can be found certainly in greenhouse gas emissions (GHGs), which have increased with population and economy. The concentration value of the most common GHGs as CO_2, CH_4 are N_2O are subjected to growths of respectively 40%, 150%, 20% since 1750 (*figure 2.4 (a)*). The total anthropogenic radiative forcing is estimated to be 2.3 W/m^2 (a positive value means a warming effect) in the period between 1750 and 2011 with a continuously increasing trend in the last decades since 1970 and, moreover, in 2011 it resulted 43% higher than the prevision of AR4 (IPCC, 2007). Regarding the natural radiative forcings from solar irradiance and volcanic eruptions, their contribution is estimated at -0.9 W/m^2, which means they contribute with a cooling effect on global temperature (IPCC, 2013).

The trend of CO_2 emissions have been increasing more than usual in the 20^{th} century and between 2000 and 2010 the largest growth ever took place, with 49 billions of carbon dioxide tons emitted in the atmosphere in 2010, these numbers can be appreciated in *figure 2.4 (b)*, where it also can be noted that 76% of total GHGs emissions is attributable to CO_2, followed by methane (16%) and N_2O (6.2%). Apart from global warming, another negative effect of the carbon dioxide is that around 40% of it remains in the atmosphere, letting the ocean to adsorb it and becoming itself every year more acid (IPCC, 2013).

2.3 Future Climate Change

The attribution of climate change is extremely likely caused by anthropogenic forcings, due to humans' continuous emissions, which will cause an irreversible damage to ecosystems and climate system.

In the AR5 (IPCC, 2013) some future climate projections are discussed, in which different rates of greenhouse gas emissions are expected, assembling different climate models. These models can be made with complex mathematical circulation equations of atmosphere and oceans or with easier simple idealized models. The first ones are called General Circulation Models (GCM) and they simulate many parameters as wind, temperature, precipitation, ocean currents etc. As mentioned before, another important parameter that can have an important role is the projection of GHGs emissions, which could depend by factors like the population growth and lifestyle and climate policies. The diversification of all these parameters generates different scenarios, which in the AR5 are called Representative Concentration Pathways (RCPs).

The RCPs show four pathways of GHGs emissions, modelled with Integrated Assessment Modelling (IAM), which represent three different kinds of scenarios: one optimistic (RCP2.6), two intermediates (RCP4.5 and RCP6.0) and one corresponding to high GHGs emissions (RCP8.5). Their trends are represented in *figure 2.5 (a, b, c, d)*.

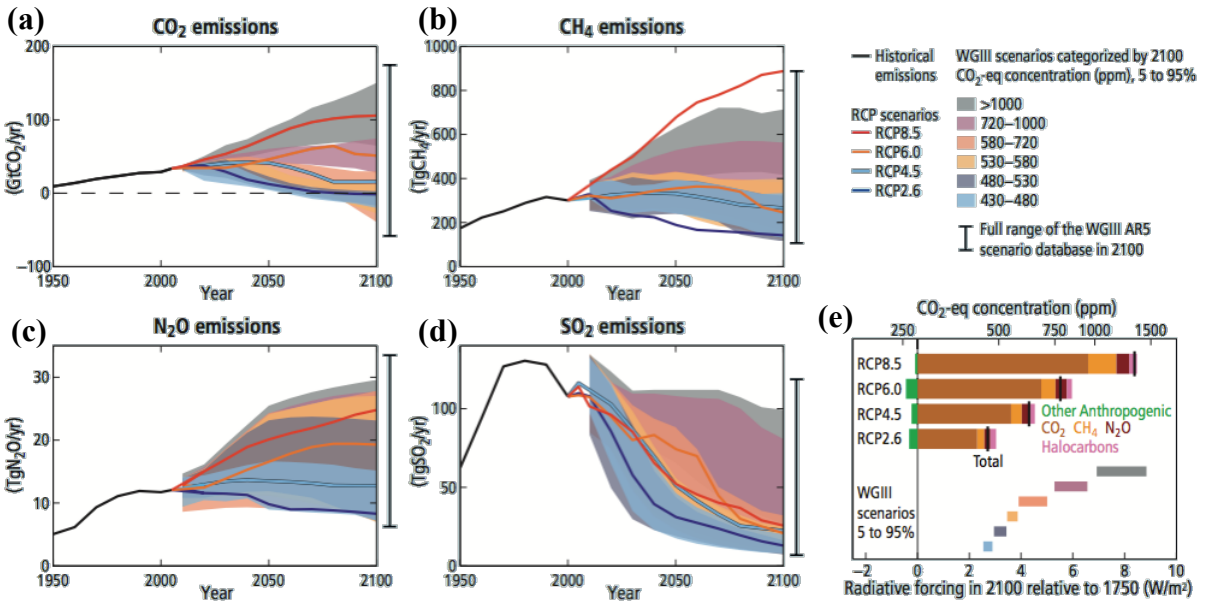

Figure 2.5: a, b, c, d) Emission scenarios regarding the four Representative Concentration Pathways (lines) and the associated scenarios categories used in Working Group III (coloured areas) for four different GHGs (CO_2, CH_4, N_2O and SO_2). **e)** Radiative forcing levels computed in equivalent CO_2 concentrations for the RCPs and WGIII scenarios (Source: IPCC, 2013).

In all the four scenarios the surface temperature is estimated to rise, so that there will occur more often and more durable heat waves. The global mean temperature will rise up to 3.7°C in the period 2081-2100 for RCP8.5, while for the more cautious scenario it will be 1.0°C higher relative to the period 1986-2005 (*figures 2.6* and *2.7*). Therefore, there will be a strong dependence on the choice of emissions' scenarios, assuming that in the studied period volcanic eruptions and sudden changes in solar irradiance will not happen. Changings in global temperature will affect wind patternes causing an alteration of the wave energy resource. Indeed the increase and decrease of mean temperature in different areas will modify how the air mass (cold and hot) interact, transforming the wind patterns and as a consequence the wave power. Moreover, it is esteemed that wave height is more sensitive to climate change than wind, as a

matter of fact a positive alteration of 20% in wind speed would produce an increase of the wave height of 44% (Harrisonn and Wallace, 2006).

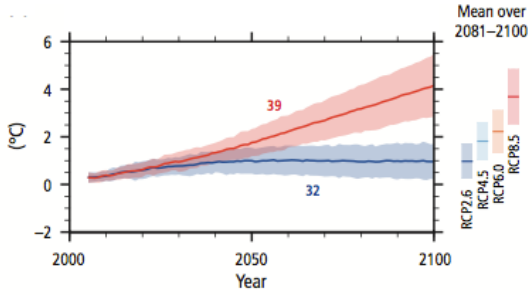

Figure 2.6: Global average surface temperature change for RCP8.5 and 2.6 relative to mean of 1986-2005 period (Source: IPCC, 2013).

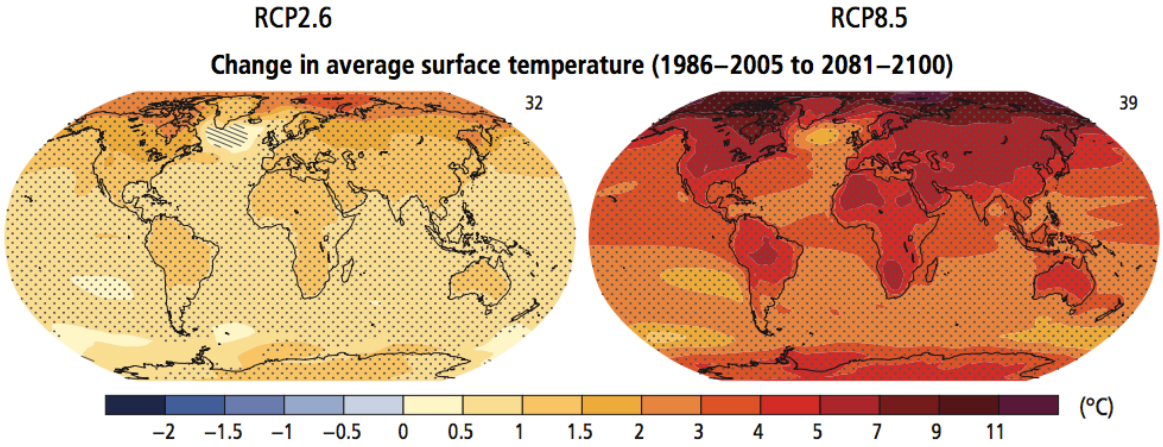

Figure 2.7: Comparison of surface temperature's change between the worst (RCP8.5) and the best scenarios (RCP2.6) (Source: IPCC, 2013).

The water cycle will undergo a non-uniform change (*figure 2.8*). Along the equator, at high latitudes and in wet mid-latitude regions the precipitations will increase, while at mid-latitude dry regions a decreasing trend will occur. On average, extreme rain events will become more frequent and stronger.

The ocean waters will warm, especially in tropical regions and in Northern Hemisphere subtropical regions. The Atlantic Meridional Overturning Circulation (AMOC), famous for bringing hot water from the south of the Atlantic Ocean to the North Pole and cold water back to south, will weaken from 11% to 34%, depending by the scenario, at the end of 21st century.

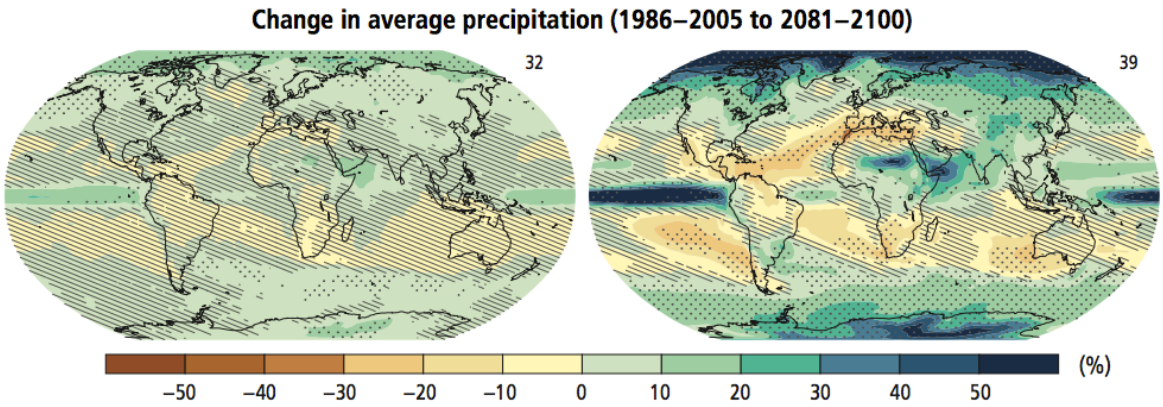

Figure 2.8: Comparison of precipitation changes between RCP2.6 (left) and RCP8.5 (right) (Source: IPCC, 2013).

The acidification of oceans will continue for all the four scenarios, due to absorption of anthropogenic carbon dioxide and the variations of pH will be in the range 0.07-0.06 for RCP2.6 and 0.32-0.33 for RCP8.5 (*figure 2.9*).

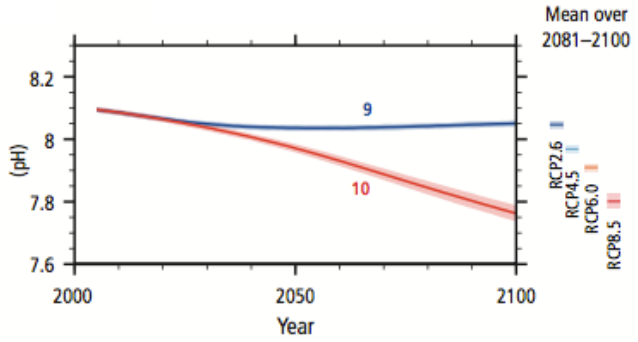

Figure 2.9: Variation of global surface ocean's PH in RCP2.6 (blue line) and RCP8.5 (red line) (Source: IPCC, 2013).

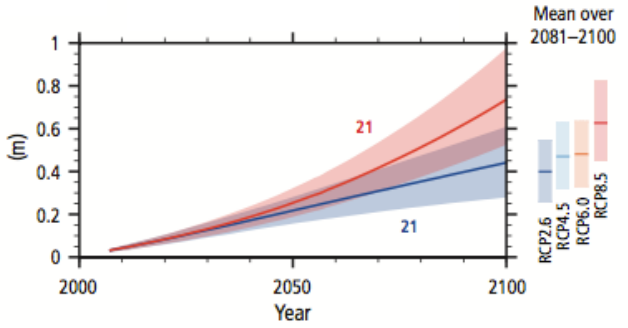

Figure 2.10: Global mean sea level rise relative to 1986-2005 period for RCP2.6 (blue line) and RCP8.5 (red line) (Source: IPCC, 2013).

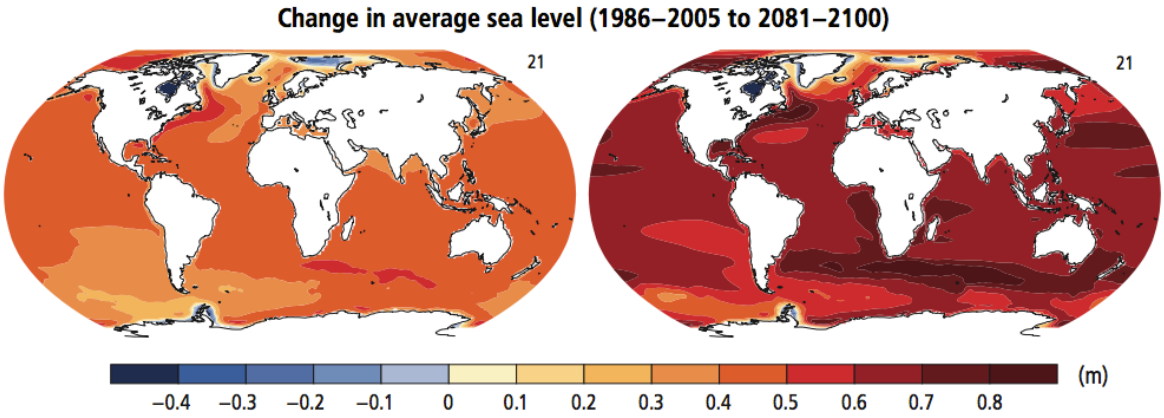

Figure 2.11: Comparison between two periods (1986-2005 and 2081-2100) of changes in average sea level between RCP2.6 (left) and RCP8.5 (right) (Source: IPCC, 2013).

All scenarios project a reduction of Arctic sea ice during the entire year (*figure 2.12*), in contrast to the Antarctic, where the projection is a bit different and there is a low confidence result that ice will melt in the future. However, the ice that will melt will contribute to sea level rise (*figure 2.10*), that in all RCP scenarios will increase in almost all the ocean areas (95%), as can be seen in *figure 2.11*. The sea level rise will exceed that of the 1971-2010 period, which was of 2 mm/year reaching the range 8-16 mm/year in 2081-2100 for RCP8.5.

An alteration of sea level would affect how the waves propagate through coastal waters, where their height and period is influenced by the bathymetry and water depth (Dean and Dalrymple, 2002). Apart from the possible modification of coastal morphology due to coast's erosion caused by the waves, there would be also changes in the resource from which onshore wave energy converters benefit.

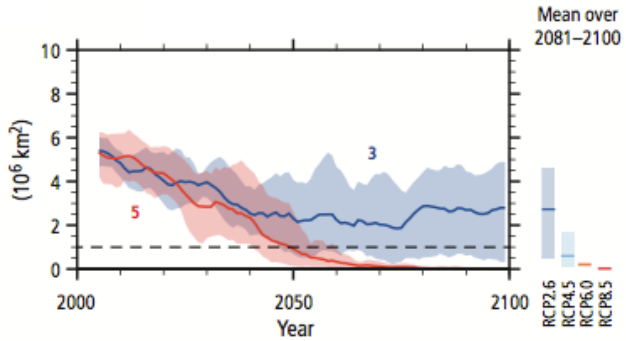

Figure 2.12: Northern Hemisphere sea ice extent in September in RCP2.6 (blue) and RCP8.5 (red) (Source: IPCC, 2013).

Concerning sea waves, in the last 40 years significant changes in wave patterns have been detected in a number of oceanic areas. Although there is no clear evidence that such changes are generated by climate change, it is proven that atmospheric circulation patterns are conditioned by CO_2 concentrations in the atmosphere (Déqué et al., 2007). Therefore, the probability that the increase of GHGs emissions could modify wave climate is high. As a consequence, wave parameters such as wave height and period may change, affecting the energetic potential of waves. Some authors (e.g. Nikulin et al., 2011) pointed out that storms would be less frequent but more intense, as a consequence of the changes in wind patterns that could be expected.

To project future wave conditions under climate change scenarios there are two approaches:

- A statistical downscaling (e.g. Wang et al., 2010; Mori et al., 2013; Casas-Prat et al., 2014).
- A dynamic downscaling.

This last method is more widely used and consists of running numerical wave models that are forced by winds simulated using global and regional circulation models (GCMs and RCMs respectively). Examples of this approach are Mori et al. (2010), Hemer et al. (2013, 2016), Wang et al. (2014) and Casas-Prat et al. (2018) at the global scale and Grabemann and Weisse (2008), Lionello et al. (2008), Charles et al. (2012), hemer et al. (2012) and casas-Prat and Sierra (2013) at a regional scale.

2.4 Future Risks

Climate change will produce risks for human and natural systems, extending those risks which already exist and creating new ones in a non-uniform way. People who are already in a dangerous situation will probably experience a worst change.

The main systems that are in danger are those who can be vulnerable to an irreversible change in the climate or those whose change affects fragile balances of natural species or delicate economic systems. Considering that risk is a product of vulnerability, probability of occurrence and value, it is important to evaluate the risk of systems with low probability of happening but with a high value, since a damage to this type of system could have catastrophic outcomes.

An increase of 1°C of global mean temperature could cause considerable consequences while an increase of 4°C could create problems to the entire ecosystem.

Between the main risks of climate change, beyond global warming, there is the variation in the amount of precipitation which can cause as well the releasing of ground's carbon stored in the atmosphere. Another problem is the risk of extinction of many vegetal and animal species who are unable to adapt to these changes, as well as deforestation. These ecosystems' endangerment can cause then a reduction of food production, that means a loss of livelihood and incomes which can be dangerous especially for already poor communities.

Another risk is the rise of mean sea level, which can create problems to low-lying coastal regions because they could face floods and coastal erosion. From the ocean another risk which could occur is the acidification with the subsequent change of many species habitats. This would have repercussions on those communities who benefit from fishing as there would be a movement of species away from zones with a low rate of oxygen, that are estimated to be especially at low latitudes.

Moreover, extreme events also could bring danger, with strong storms and precipitations which are estimated to increase in power and frequency, potentially endangering to human lives as well as to the operation of services and to solidity of infrastructure networks and constructions.

3. STATE OF ART OF WAVE ENERGY

3.1 Types of marine energies

The renewable energy which benefits from the energy contained in sea and oceans is called marine energy. Potentially, marine energy is considered as a powerful resource, despite the majority of technologies are still in an experimental state. In fact, it is estimated that energy extractable from oceans could cover the entire global energy requirement.

There are technologies whose purpose is to extract the kinetic energy stored in waves and tides and other which try to gain energy from thermal and chemical (salinity) gradients:

- Wave energy
- Tidal energy
- Marine current energy
- Ocean thermal energy
- Osmotic power

3.2 Wave energy

Wave energy is the process of extracting energy stored in wind waves, which are those waves generated from winds, that propagate across sea and ocean. Their power is influenced by the duration and the velocity of the winds but also by the fetch, that is the distance on which the wind blows to generate the wave, and by the depth and the bathymetry.

The multiple technologies of wave power converters (WEC) developed in recent years are distinguished by their mode of operation as compared to wave direction and their location in the water.

Attenuator are floating devices with the peculiar dimension in the direction of the wave which is longer than the wave length. The production of energy occurs at the passage of the wave, which causes an opposed motion between two separate parts of the device. One of the technologies that take advantage of this fundamental principle is *Pelamis Wave Power* (*figure 3.1*), which was inaugurated in 2004 and was the first offshore WEC that generated electricity in the national grid (EMEC).

Point Absorber are usually buoy shaped devices moored to the bottom of the sea that use their floating feature for moving up and down when the waves pass over them. They can be positioned on the surface or under it and through the relative movement between the device and the bottom they generate electricity. A well-known point absorber is *CorPower C3* (*figure 3.2 (b)*), made by a Swedish company, which is trying to take advantage from the resonance between the movement of the wave and the device in order to produce more energy.

Figure 3.1: Pelamis Wave Power WEC, Orkney Islands.

(a)

(b)

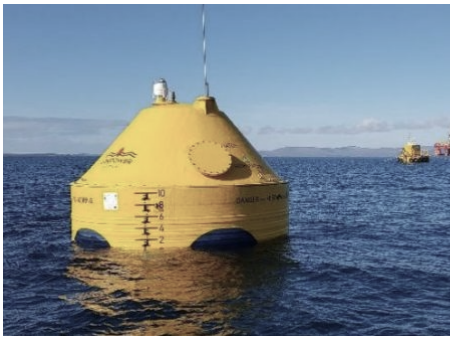

Figure 3.2: a) Wave Energy Dragon, Denmark. **b)** CorPower C3 point absorber, Orkney Islands.

A similar function of point absorber is carried out by **Submerged Pressure Differential**. The theory behind this technology comes from the Archimedes' effect. As a matter of fact, while the moving of both the devices is vertical, the submerged WEC stays usually below the surface and its motion of rise and fall is caused by the difference in depth given by the passage of the waves.

Overtopping devices usually have one or more ramps who benefit from kinetic energy for driving the water to a higher level above sea level where it fills a reservoir in order to whirl the water back to the sea with a turbine. These prototypes are obviously located on the surface and can be moored offshore or placed on the coast. An example of overtopping is *Wave Energy Dragon* (*figure 3.2 (a)*) which was the first offshore WEC installed outside the coast of

Denmark. It is structured with two wave reflectors and low head turbines in the water reservoir (Knapp et al, 2011).

The **Oscillating Water Columns (OWC)** are usually constructions installed onshore which consist of a closed chamber where the sea level, due to waves coming, moves continuously up and down generating an alternating high pressure-low pressure area that give power to an air turbine. An alternative way of these devices is to benefit not from the pressure of the chamber but from the motion of the water which activate a water turbine. An example of this typology is the *Mutriku Wave Energy Plant* OWC in Basque Country, constructed in 2006, which is a 100 meters long device placed on the port breakwater (Torre-Enciso et al. 2009). In *figure 3.3 (a, b)* a sketch of the closed chamber's section (where the air turbine is installed) is shown.

(a) **(b)**

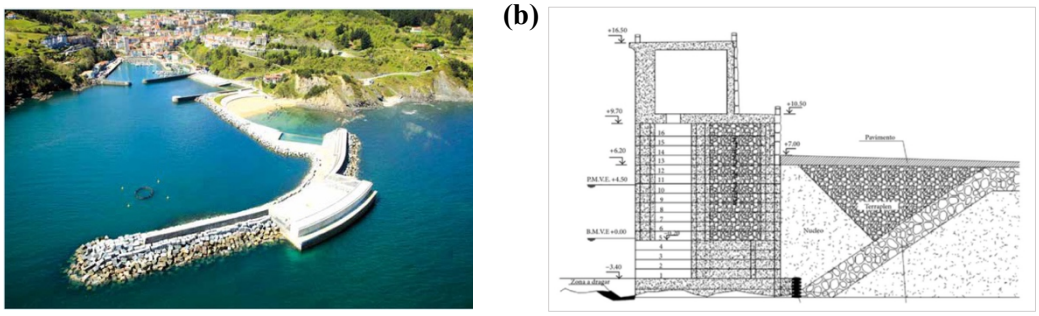

Figure 3.3: a) Mutriku Wave Energy Plant OWC, Spain**. b)** Side section of the Mutriku OWC converter.

The **Oscillating Wave Surge Converter (OWSC)** are submerged devices installed nearshore or onshore. They use the hydrodynamic forces of the wave, whose water particles in shallow water assume a horizontal motion, creating a rotation around the horizontal axis on the bottom, near the mooring system, that activate the power take-off of WECs. A wave energy converter that tries to benefit from these forces is the *Oyster Aquamarine Power* prototype (*figure 3.4 (b)*), around 10-12 meters high, which was installed in Orkney Islands at EMEC.

The **Bulge Wave** WEC starts a low head turbine located at the end of a long tube-shaped device which permits the wave to push water inside it and conducts then the water to the turbine with the help of the pressure increase inside the pipe due to the wave itself. Instead, some other type of bulge wave WECs are made with more complex materials which generate electricity when deformed.

(a)  **(b)** 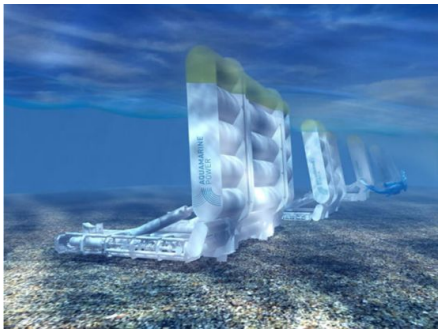

Figure 3.4: a) Inertial Sea Wave Energy Converter from Politecnico of Turin. **b)** Oyster Aquamarine Power WEC.

The **Rotating Mass** devices are usually floating objects that can be moored nearshore or offshore and generate electricity either with an eccentric mass inside them which rotate around a vertical axis or with the swaying of the device caused by waves which create a reacting inertial effect of a gyroscope. An example of rotating mass is the *ISWEC (Inertial Sea Wave Energy Converter)* (*figure 3.4 (a)*) that takes advantage from the rocking motion and generate electricity with a gyroscope. It was produced by Wave for Energy, a spinoff of Politecnico di Torino.

3.3 Tidal Energy

The global tidal resource is estimated at 1200 TWh/year (OES, 2012). Tide is a renewable resource which can be exploited either onshore for the difference in water height that generate or offshore with the current flow created from the tidal wave.

The tidal range is very variable among different parts of the world. In open ocean this value is usually relatively short, around 30-50 centimetres, while near the coasts due to the seabed morphology it can be much bigger with measures of the order of meters. In particular, there are places where this range can be extremely high, for example values of ten metres in Brittany, fourteen meters in Argentina or up to seventeen metres in Nova Scotia's Fundy Bay. Moreover tidal energy is predictable as tides work with lunar motion and this is a fundamental quality when compared to other renewable resources like sun, wind and waves which do not have this capability.

The approach usually used to take advantage of tidal energy is to select a natural lagoon where to build a dam in order to generate an hydraulic head and then whirling the water with a low head turbine. This process has the good intrinsic propriety that it is possible to turbine the water

in two different ways, inside and outside the dam, depending on the low or high tide. Power stations like these are already operating, for example the power plant of La Rance in Saint-Malo in Brittany (*figure 3.5 (a)*), built on a river mouth in 1966, which has a power of 240 MW (Rolandez et al., 2014).

The other type of tidal energy converter consists of Tidal Stream Generators (TSG). These devices are structured with watermills under the surface of the sea and they extract the kinetic energy contained in currents. As a matter of fact, the flow speed can reach values between one and three meters/second which are enough to spin the blades of a TSG, that compared with an air mill can produce similar energy (although current velocities are lower since water has more density than air). During the last years many prototypes such as SeaGen (*figure 3.5 (b)*) have been tested in particular places where the morphology helps the current to accelerate. SeaGen was installed in 2008 and removed in 2016, and during this period it exported 11.6 GWh to UK's grid (NS Energy, 2019).

(a)  **(b)** 

Figure 3.5: a) Tidal power plant in the estuary of La Rance, Saint-Malo, Britany, France. **b)** SeaGen tidal stream generator, Northern Ireland.

3.4 Marine current energy

This type of energy can be achieved with the same technologies of TSG exposed in the previous *subchapter 4.1.2* because the physics of the motion of water is identical. The only distinction between marine current energy and tidal current energy is the nature of the water flow forcing.

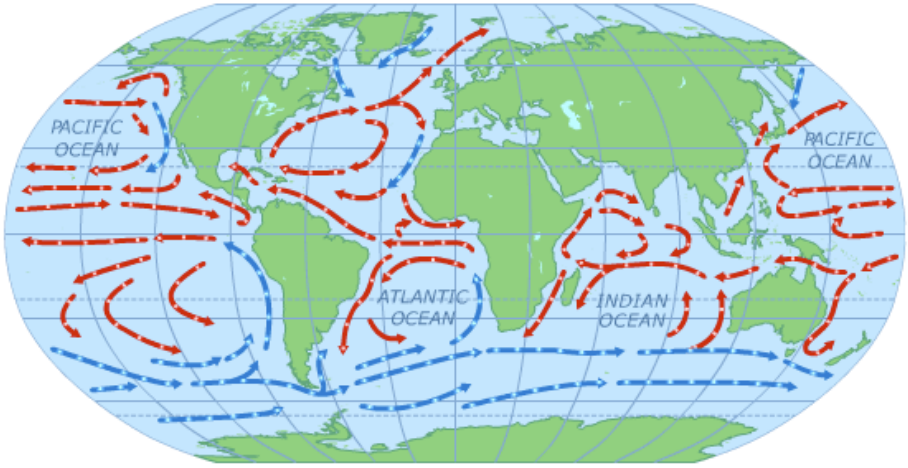

Figure 3.6: Main ocean currents around the world. (Source: EarthLabs)

On one hand ocean currents are more scattered around the world (*Figure 3.6*) while tidal currents are usually located only in landscape's bottlenecks, in places where tidal ranges are relevant. On the other hand it is more difficult to benefit from flows in the middle of the ocean as it would be too much expensive to connect technologies to the electric grid and to reach them for maintenance.

3.5 Ocean thermal energy

Ocean thermal energy conversion, also known by the acronym OTEC, is an energy conversion which takes advantage of the temperature's difference between the surface water, which usually is warmer and deep cold water.

The principle for producing electricity is similar to that of thermoelectric power plants. The vapour generated from a fluid's evaporation is used to spin a turbine. In open-cycle OTECs seawater is used, while in closed-cycle OTECs the ammonia is preferred due to its low boiling temperature, which is similar to that of the sea surface. As a matter of fact, usually this energy conversion is preferable for those places with a surface water temperature around 25-28 °C and where it is also possible to reach depths of the order of hundreds of metres, where the temperature is about 0-4 °C. Another good quality of open-cycle OTECs is that they can produce drinking water from the condensed vapour, which is pure water without salt or other contaminants.

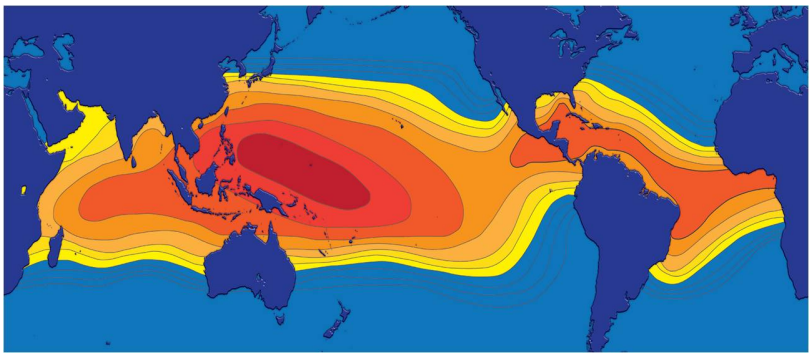

Figure 3.7: Areas of the world with temperatures suitable for OTECs. The dark-red area correspond to 24°C or more of temperature's difference between surface and 1000 metres depth, while the blue area to 18°C or less. (Source: UTM OTEC)

Prototypes of OTEC can be built onshore or offshore and these last ones can be floating or shelf-based structures. Offshore sites are less attractive due to the high costs of the structure, which have to be resistant especially in the surf zone, and for the pipes which connect them to the land. Moreover, floating OTECs can face mooring difficulties to make the power plants stable. Onshore plants are certainly favourable despite the high cost of pipes, which in certain cases can be very long in order to reach the right depth when the seabed decreases slowly.

Figure 3.8: OTEC developed by Makai Ocean.

Nowadays some experimental plants have been tested and in favourable places like those located at tropical waters (*figure 3.7*). Between the power plants that have been installed, one is located on one island of Hawaii (*figure 3.8*). The project developed by Makai Ocean Engineering started in 2015 and consists of a 100 kW turbine (Makai Ocean Engineering, 2013).

3.6 Osmotic Power

Osmotic power is a renewable energy which takes advantage of the difference of salinity between seawater and freshwater. As a matter of fact, when a river flows into oceans a relevant quantity of energy is released between the two liquids.

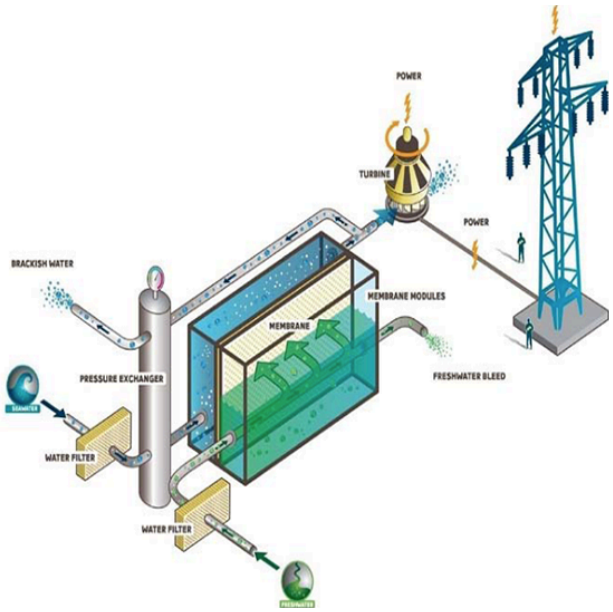

Figure 3.9: Sketch of an osmotic power plant. (Source: changemakers)

The osmotic process is launched when two different chambers, one filled with freshwater and the other with seawater, are separated by a special membrane which permits to be passed through by water molecules while it stops the salt particles. Due to the difference in salt concentration between the two sides of the membrane the water will start to flow from the freshwater chamber to the salted one (because of its high osmotic pressure value) in order to dilute it. This will implicate an increase of pressure in the seawater chamber, so that the air contained inside would spin an air turbine and power the generator that produces electrical energy (*figure 3.9*).

Initially this renewable resource was not considered due to the high cost of the membrane, but a lower cost membrane built with electrically modified polyethylene plastic could face the commercial stage. One of the first osmotic power plant prototypes was built in 2009 in Norway by Stratkraft company and had a power of 10 kW.

3.7 Wave energy resource

In the bibliography there are numerous studies carried out to assess the power of the waves at global scale (e.g. Cornett et al., 2008; Arinaga and Cheung, 2012; Gunn and Stock-Williams, 2012) and local or regional scales (e.g. Iglesias and Carballo, 2010, 2011; Rusu and Guedes Soares 2012a, 2012b; Liberti et al., 2013; Stopa et al., 2013; Vicinanza et al., 2013; Sierra et al., 2013, 2014, 2016, 2017a; Gonçalves et al., 2014; Gillou and Chapalain, 2015; Besio et al., 2016).

In spite of this, only few studies have addressed the impact of climate change on wave energy (e.g. Harrison and Wallace, 2005; Mackay et al., 2010a, 2010b; Sierra et al., 2017b).

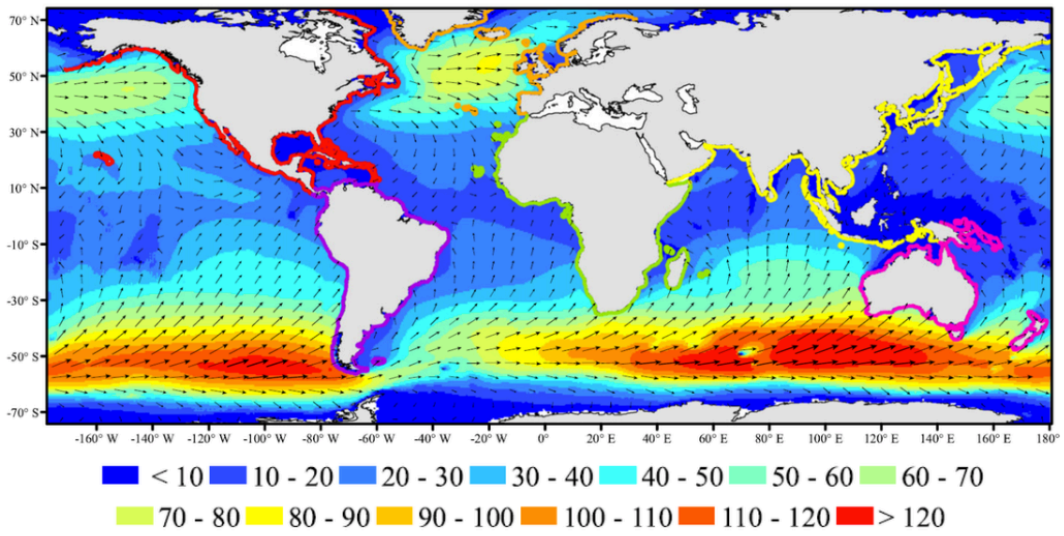

Figure 3.10: Average wave power stated in kW/m by Gunn and Stock-William (2012).

Focusing on the asses of wave power at global scale for present conditions, the studies conducted by Gunn and Stock-Williams (2012) (*figure 3.10*) show that the Southern Hemisphere is the most powerful area, especially in the South of Indian Ocean and Pacific Ocean where the wave power annual average peak reach over 120 kW/m. Also the North Atlantic and North Pacific prove to be notable area with values of the order of 70-80 kW/m.

4. MATERIAL AND METHODS

4.1 Model data

4.1.1 CMIP5 and presentation of the models

The Coupled Model Intercomparison Project Phase 5 (CMIP5) is a framework of research groups and universities who collaborate developing multiple models of climate systems. The CMIP5 (Taylor et al., 2012) derive from 2014 IPCC's Fifth Assessment Report (discussed in *paragraph 2.1*) and is the last and largest ensemble of climate models.

In this thesis work five of these models will be used, which outline the projected changes in ocean surface at a global scale considering both past conditions from 1979 to 2005 and future conditions from 2081 to 2100 using one of the Representative Concentration Pathways (RCPs) discussed in *paragraph 2.3* named RCP8.5, which evaluates the scenario where the harsher concentrations of greenhouse gasses emission are predicted. The models evaluate twenty members for significant wave height H_s, considering dynamical and statistical simulations, along with four members for mean wave period T_m and five members for the mean wave direction θ_m (Casas-Prat et al., 2018), which however will not be deepened in this work.

One of the most important features that characterize these models is the implementation of the computation on Arctic and Antarctic areas, where some obstacle to physical wave modelling usually occurs. These areas will be excluded from this work (as it will be explained in *section 4.2*) but it is very important their insertion in the models as they change the values of wave height and period in those areas that are considered. Indeed, the areas over 60° of latitude (North and South) modify the characteristics of the remaining ocean area adding fetch to the propagation of waves and, moreover, Arctic and Antarctic storms generate waves that then spread in studied areas.

The main difficulty is composed by the computational grid, because of the diminishing size of cells that in all models are built with a constant delta of latitude and longitude. This means that at high latitudes the physical distance between two cells is so small that cause a computationally unaffordable time step (Courant-Friederichs-Lewy restriction). Furthermore another problem of the presence of ice is that it makes laborious the computation of wave propagation, due to the difficult evaluation of how the waves interact with the presence of icebergs which dissipate kinetic energy and or reflect waves.

In spite of these problems, the used data constitute a unique set of wave data at global scale that allow to assess the evolution of wave energy along the 21st century.

The five considered models are the following:

- BCC-CSM1-1 from Beijing Climate Center.
- INM-CM4 from Institute for Numerical Mathematics of the Russian Academy of Sciences.
- MIROC5 from the University of Tokyo, National Institute of Environmental Studies (Japan) and Japan Agency for Marine-Earth Sciences and Technology.
- GFDL-ESM2M from Geophysical Fluid Dynamics Laboratory of Princeton University.
- EC-EARTH from European Community Earth System Models.

From these five models the wave height H_s and the peak wave period T_p were obtained. For achieving this, Casas-Prat et al. (2018) implemented the WAVEWATCH III wave model (Tolman et al., 2014), known as WW3, running in it surface wind (10 meters from the sea) with a 3 hours-time step and daily sea ice concentration (SIC) simulated in the five CMIP5 models. The wave parametrization used was the conventional one used in ocean waves (Ardhuin et al., 2010), with a computational time step of 1 hour, using 29 frequency bins.

4.1.2 Models output

The five models provide a total of twenty files output, ten for wave heights and ten for peak wave periods, where each set of ten is divided into five output of past period (1979-2005) and five of future period (2081-2100). In all the files it is possible to read the following variables:

- H_s: wave height [m] (only in ten out of twenty files)
- T_p: peak wave period [s] (only in ten out of twenty files)
- Longitude [East degrees]
- Latitude [North degrees]
- Time [h]

The outputs are available in files with a NetCDF (Network Command Data Form) format '*.nc*' which can be read and managed with Matlab®, where using the command `ncdisp` the software can inform the user of the variables contained in the file (*figure 4.1*).

In the case of the BCC-CSM1-1 model shown in *figure 4.1* the length of the latitude, longitude and time vectors and the wave height array can be seen. The dimension of the coordinates states

that 32516 points are considered while the time vector length, as described by the plot, is 236520 cells long, that are the hours included in the period from the 1st of January 1979 to the 31st of December 2005. Furthermore the 'hs' dimension is described as a 32516 x 236520 array, which means that every row correspond to a point and its values in the columns are a function of the time. The attributes of the coordinate variables inform the user that longitude is displayed with East degrees which means that the points will have a value between 0° East and 360° East where the zero correspond to Greenwich Meridian while the latitude goes from 90° North to -90° North where positive values are in the northern hemisphere.

```
Command Window
>> ncdisp('BCC-CSM1-1.hs.1979-2005.nc')
Source:
           /Users/MicheleMontefusco/Desktop/Master Thesis/BCC-CSM1-1.hs.1979-2005.nc
Format:
           classic
Dimensions:
           ncells = 32516
           time   = 236520 (UNLIMITED)
Variables:
    lon
           Size:       32516x1
           Dimensions: ncells
           Datatype:   double
           Attributes:
                       standard_name = 'longitude'
                       units         = 'degrees_east'
    lat
           Size:       32516x1
           Dimensions: ncells
           Datatype:   double
           Attributes:
                       standard_name = 'latitude'
                       units         = 'degrees_north'
    time
           Size:       236520x1
           Dimensions: time
           Datatype:   double
           Attributes:
                       standard_name = 'time'
                       units         = 'hours since 1979-01-01 00:00:00'
                       calendar      = '365_day'
    hs
           Size:       32516x236520
           Dimensions: ncells,time
           Datatype:   single
           Attributes:
                       units         = 'units'
                       grid_type     = 'unstructured'
                       coordinates   = 'lon lat'
```

Figure 4.1: Example of the Matlab script used for reading the data.

If instead of a wave height file a wave peak period had been plotted, the variables would have been the ame apart from 'tp' in place of 'hs' but with the same dimensions.

It is important to specify that for all the twenty files used, the coordinate vectors of the points are the same. As a matter of fact, despite the input grids of any singular model can be different from the others, the output grids (of all the models) used for the computation of this thesis are uniform in all the files.

4.1.3 Description of model's points

As mentioned in previous *section 4.1.2* the number of points used in the models equals to 32516 (*figure 4.2*). The points present in the models can be divided into two parts:

- Coastline points
- Open sea grid points

The first part of the model consists of 7599 points located on the coasts with a resolution of 0.46° in latitude and 0.70° in longitude. They form a matrix more dense in order to perform a more reliable computation where the bathymetry changes faster close to coasts. In addition, another favourable consequence of this high resolution is that the shape of the coasts and the islands can be well-defined.

In the second part of the file there are the remaining 24917 points located in open sea areas. They form five different zones of square grids (*table 4.1*), differentiating each other for the distance between the points in order to maintain a density of points per area similar around all globe. This is because such point density would not be approximately constant if the longitude interval remained the same all over the surface because of the shape of the earth itself on the poles. The problems that will occur without this differentiation have been already explained in *section 4.1.1.*

Zone	**Latitude limits [° N]**		**Latitude grid interval [° N]**	**Vertical distance between following points [km]**	**Longitude grid interval [°E]**	**Horizontal distance between following points [km]**	
	max	**min**				**max**	**min**
1	87.7°	85.8°	0.94°	104.3	22.5°	142.3	101.5
2	85.8°	82°	0.94°	104.3	11.25°	152.8	91.8
3	82°	74.5°	0.94°	104.3	5.625°	157.0	86.8
4	74.5°	60.5°	0.94°	104.3	2.8125°	153.5	83.1
5	60.5°	0°	0.94°	104.3	1.40625°	155.7	79.0

Table 4.1: Definition of the main features of the five areas used in open sea.

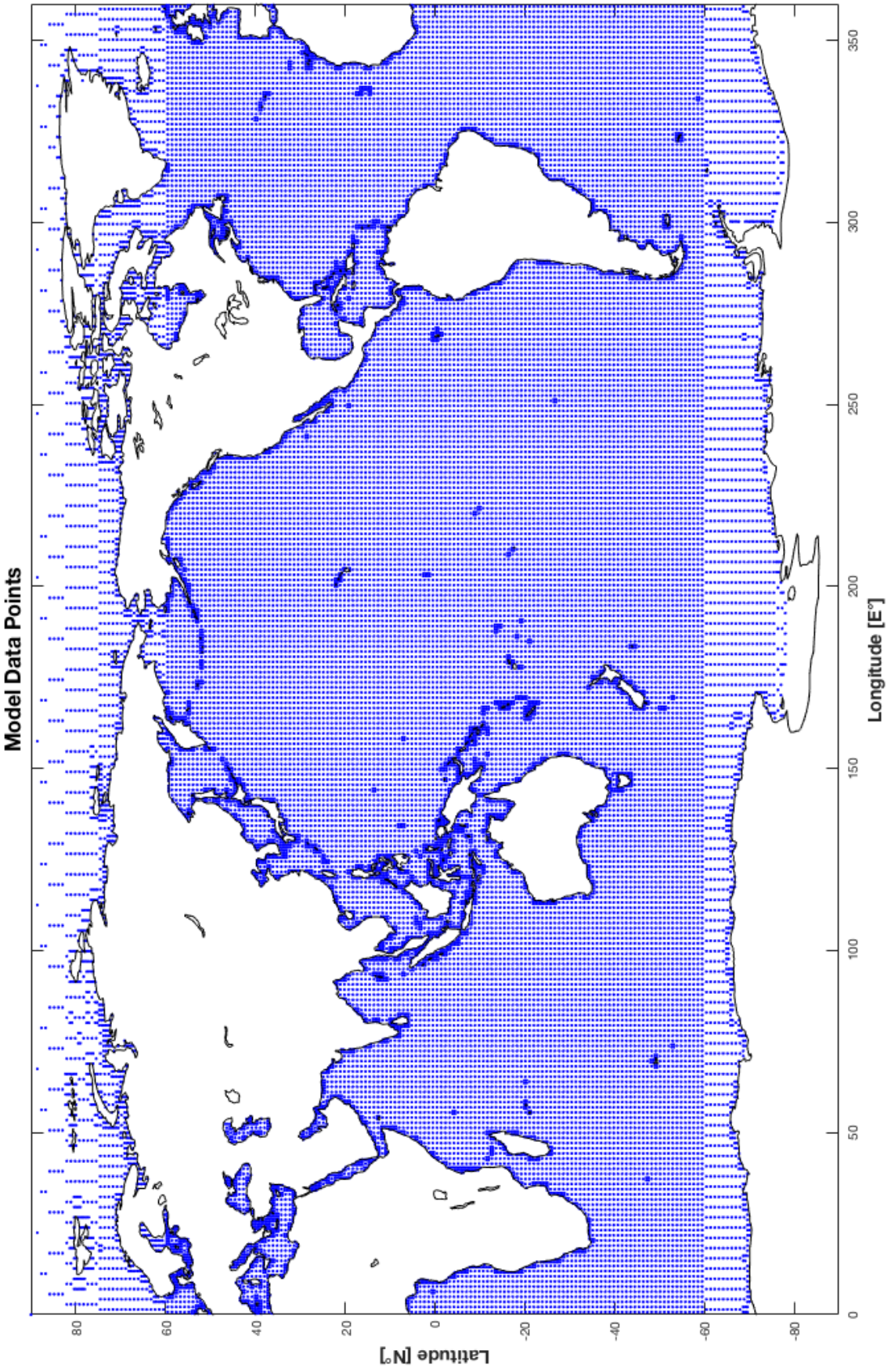

Figure 4.2: Points with wave data.

4.1.4 Description of model's time vectors

The time vector described previously is 236520 cells long, which means that it includes the hourly sequence from the 1st of January 1979 to the31st of December 2005 that consists of a total of 27 years. This vector length is different between past and future data since this last set includes hourly data from the 1st of January 2081 to the 31st of December 2100 for a total of 20 years. Therefore, the future data vector has a smaller length and contains 175200 cells.

4.1.5 Description of wave height and peak period's array

In the output the wave's information provided by the models essentially consists of two parameters:

- Significant wave height H_S
- Peak wave period T_P

An example of data extracted from the files can be seen in *figure 4.3*, where a time series of one year (1986) of data of the BCC-CSM1 model in a point in the Bay of Biscay is plotted.

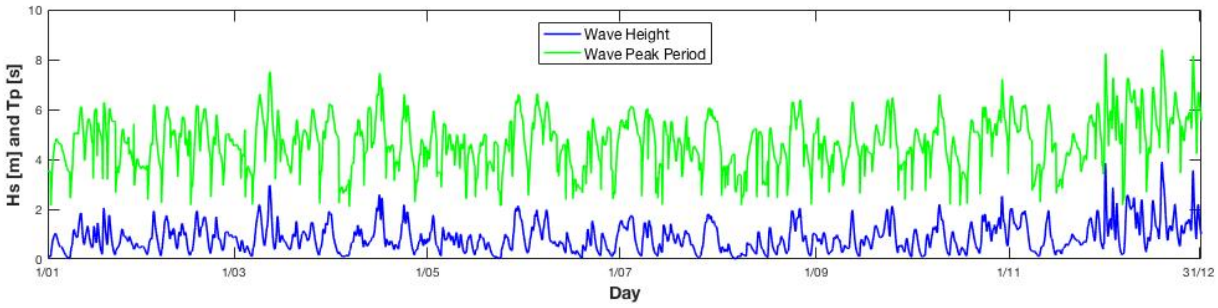

Figure 4.3: Example of one year of data obtained from BCC-CSM1 model.

These two quantities, which will be explained in *paragraph 4.3.1*, are chosen due to the fact that they are necessary to assess the wave power.

The different length of time vectors described in previous paragraphs obviously influences the dimensions of wave height and wave peak period arrays of future data files. In fact, they maintain 32516 rows but they reduce their columns from 236520 to 175200.

4.2 Description of the area

4.2.1 Description of chosen points

For the process of assessment of wave energy between all the points available in the models, only a few have been selected in order to proceed with the computation, which has been done with Matlab®.

Actually, the firsts four zones listed in *table 4.1* will not be taken into account. It was decided to exclude those points with a latitude higher than 60.5° North and 60.5° South in order to not consider the Arctic and Antarctic Oceans due to their tendency to freeze for most part of the year which also involves the exclusion of these places for a potential exploitation of the energy resource supplied from waves.

All the five zones mentioned in *table 4.1*have a specular nature respect to the equator. As a matter of fact the fifth zone, the only one studied, which actually goes from 60.5° North to 60.5° South presents an average interval of 117 kilometres between two consecutive points located on the same latitude but with different longitude coordinates. The range in which the interval oscillates is 155.7 km at the equator and 79 km at 60.5° North or South.

It was decided to select 1310 points (*figure 4.5*) among those available, forming a grid all over the sea surface with a point every 5° of latitude and longitude. This interval is not constant due to model points nature, which have a latitude that is a multiple of 1.4° and a longitude multiple of 0.93°. Since the software programmed selected all the points with a multiple of 5 as an integer number, it can happen that one of these points could be missed. In this case, it was decided to select the point with the nearest coordinate of latitude or longitude to the missed point.

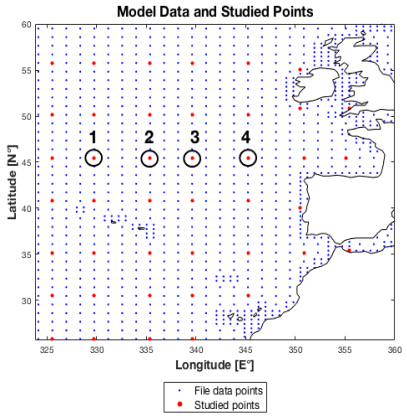

Figure 4.4: Example of point selection.

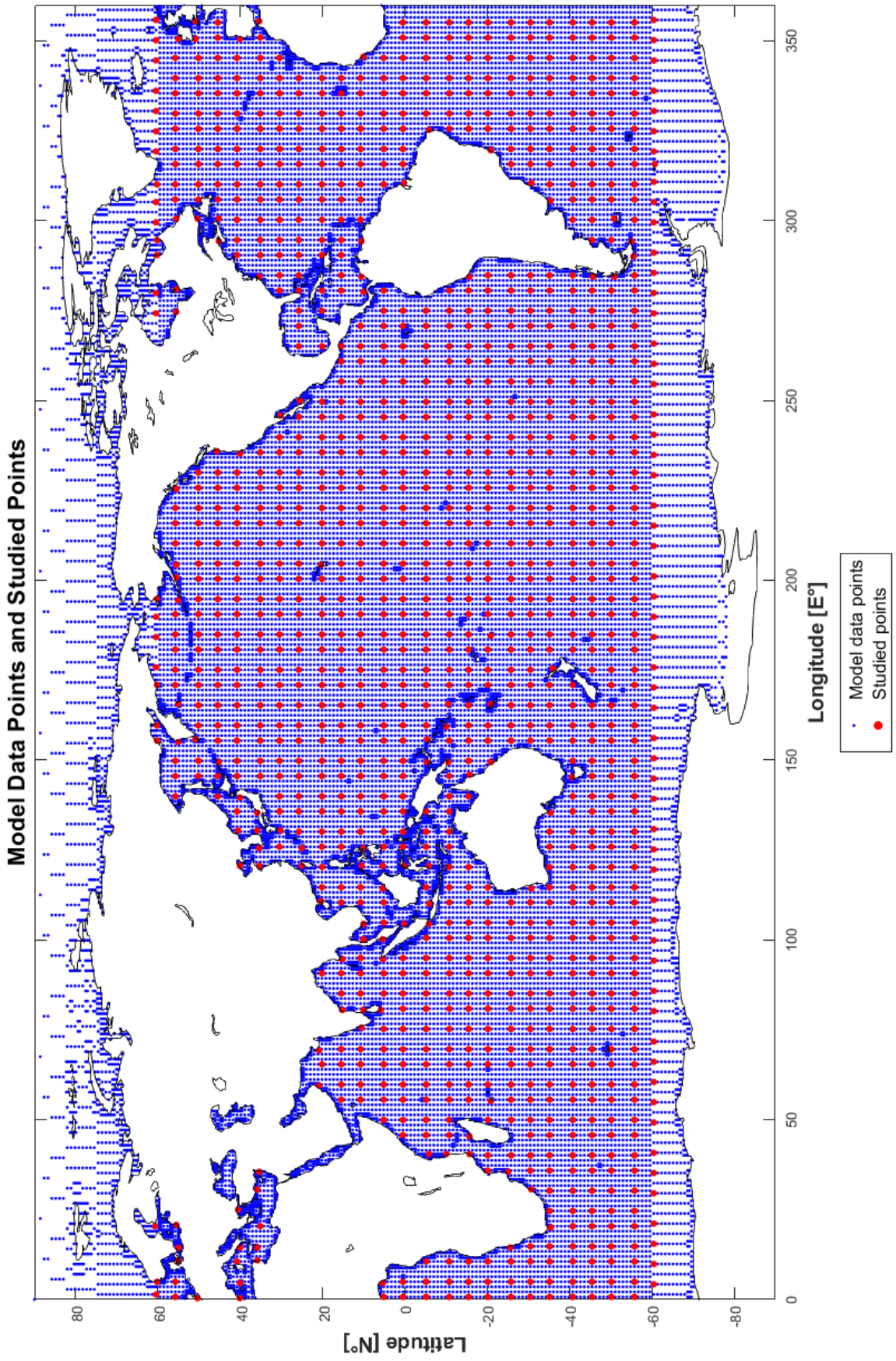

Figure 4.5: Selected points.

An example of this circumstance is seen in *figure 4.4* where the longitude of points from 1 to 4 is 329.8 °E – 335.4 °E – 339.6 °E – 345.2 °E. This means that the interval can vary between two values, being the largest 5.6° while the smallest is 4.2°.

The same principle occurs between latitude with points where the largest interval is 5.62° against 4.69° for the nearest points.

Considering these point properties, for the same reason explained in *section 4.2.2*, the physical distance between the selected points varies depending on the latitude. An example of the distances is explained in *table 4.2*:

Latitude		**0°**	**± 10°**	**± 20°**	**± 30°**	**± 40°**	**± 50°**	**± 60°**
Distance between consecutive selected points [km]	**max**	633.9	624.4	595.7	549.0	485.6	407.4	316.9
	min	467.2	460.0	439.0	404.5	357.8	300.2	233.5

Table 4.2: Distance between consecutive points.

The distance between two consecutive selected points with the same longitude is the same at all latitudes, and equals to 521.6 kilometres when the difference is 4.69° and 625.1 kilometres when it is 5.62°.

4.2.2 Time interval and time step

In order to simplify the amount of calculus for the Matlab® computation of this work, it was decided to consider a time step of three hours. Since it is very common to use this value of Δt in climate computations, this assumption has proved to be suitable for the purpose of streamlining the calculation.

Moreover, another reduction of the number of columns was obtained with the exclusion of the firsts 61320 columns of past data, or rather the first seven years from the 1st of January 1979 to the 31st of December 1985. Since the future data consist of 20 years of values (2081-2100), it was decided to use the same time interval for past ones, starting therefore from the 1st January of 1986.

The time vectors described in *paragraph 4.1.4* were 236520 cells long in past conditions and 175200 cells in future conditions but, after the assumption made in this paragraph, the final array dimensions are 1310 rows (one for every point) and 58400 columns.

4.2.3 Ocean area division

In order to obtain some results that will be explained in *chapter 6*, it has been necessary to divide oceans in several areas so as to make the results more understandable having a separated vision of how climate change will interact with the different areas.

The Atlantic Ocean, the Pacific Ocean and the Indian Ocean have been divided into a total of eleven areas, showed in *figure 4.6*.

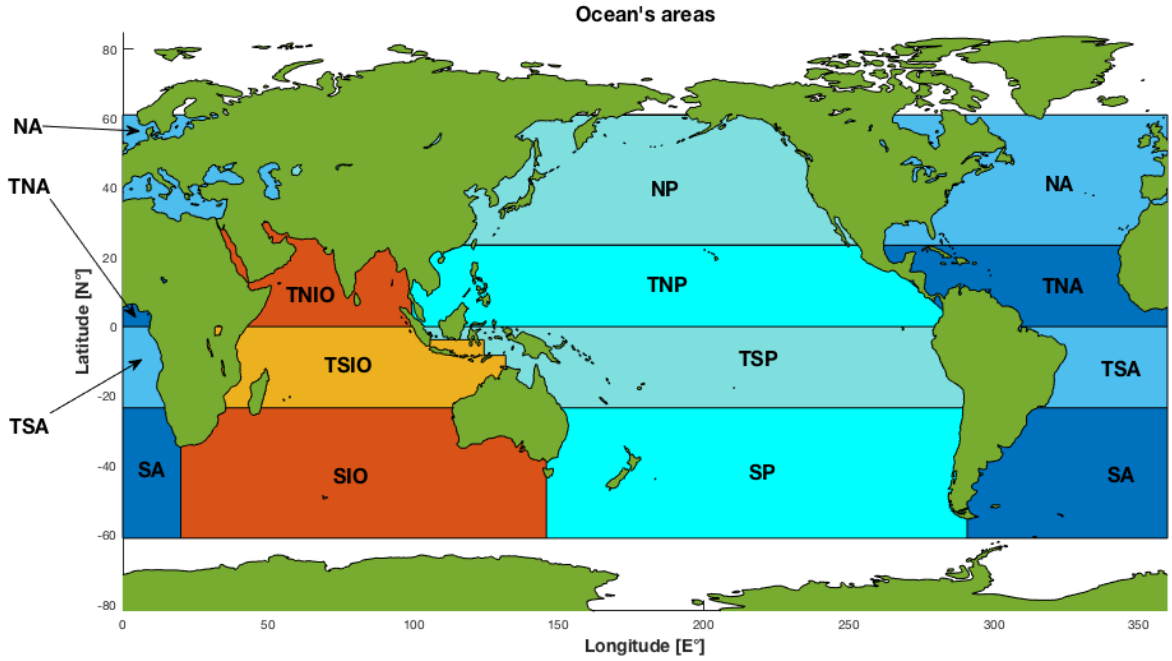

Figure 4.6: Distance between consecutive points.

The limits between the three oceans are geographically made by lands. The Atlantic Ocean is divided from Pacific Ocean at South-West by Cape Horn in Chile and from Indian Ocean at South-East by Cape Agulhas in South Africa. The Pacific Ocean and the Indian Ocean are separated by the southernmost part of Tasmania and by Indonesian archipelago.

Moreover, the three oceans are subdivided by the latitude:

- Atlantic Ocean is divided into four areas: North Atlantic (NA), Tropical North Atlantic (TNA), Tropical South Atlantic (TSA) and South Atlantic (SA).
- Pacific Ocean is also divided into four areas: North Pacific (NP), Tropical North Pacific (TNP), Tropical South Pacific (TSP) and South Pacific (SP).
- India Ocean is divided into three areas: Tropical North Indian Ocean (TNIO), Tropical South Indian Ocean (TSIO) and South Indian Ocean (SIO).

The tropical areas are divided from southernmost and northernmost areas at 23°26'16" North or South and from each other by the equator. Furthermore the North and South Areas end at latitudes superior than 60° North or South, where the Arctic and Antarctic Oceans begin.

4.3 Methodology

4.3.1 Definition of the variables

Mainly two variables are extracted from the data contained in the model files, the significant wave height and the peak wave period.

The *significant wave height* H_S is stated in metres in the files and its definition is known in physical oceanography as the mean wave height of the highest one third of waves of a sea state

The *peak wave period* T_P, stated in seconds, derives from the wave spectrum, where the peak frequency f_P is considered the frequency associated to the most energetic waves. The peak period is then the inverse of the frequency.

4.3.2 Wave power

The *wave power P* is one of the most common parameters used in wave energy field for assessing the real potential of an area's energy resource and it will be one of the variables on which this work will focus.

The formula used for calculating the wave power is the following:

$$P = \frac{\rho g^2}{64\pi} \cdot H_s^2 \cdot T_e \simeq 0.49 \cdot H_s^2 \cdot T_e \qquad \left[kW/m\right] \qquad [1]$$

Where:

- ρ is the seawater density, assumed to be 1025 kg/m^3
- g is the gravity acceleration, assumed to be 9.81 m/s^2
- H_S is the significant wave height [m]
- T_e is the wave energy period [s]

The *wave energy period* T_e can be obtained following two different methods: the first uses the formula [2] while the second applies a coefficient to the wave peak period [4]. The first formula make use of the spectral moments of order 0 and -1:

$$T_e = \frac{m_{-1}}{m_0} \qquad [s] \qquad [2]$$

The moment of order *n* is computed as:

$$m_n = \sum_i f_i^n \cdot S_i \cdot \Delta f_i \qquad [3]$$

Where:

- f_i is the ith discrete frequency [Hz]
- S_i is the spectral density over the ith discrete frequency [m^2/Hz]
- Δf_i is the frequency width of the spectral density of the ith discrete frequency [Hz]

The other method consists of the simple relation between the two periods:

$$T_e = \alpha \cdot T_p \qquad [4]$$

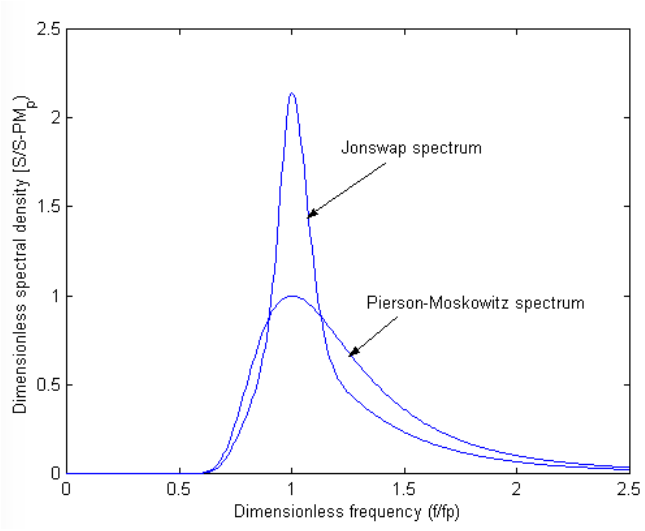

Figure 4.7: Types of spectrum more frequent.

The value of the coefficient α has a range of possible values between 0.86 and 1, depending on the shape of the wave spectrum (*figure 4.7*). For example Pierson-Moskowitz set α=0.86 while a JONWASP spectrum has a higher value.

In this work the formula [4] will be used assuming α = 0.9, so that the wave energy period will be considered as the 90% of the wave peak period.

4.3.3 Monthly variability index

The monthly variability index is computed by [5] and describes how the wave power can change across the months in an assigned area. It is defined as follows:

$$MV = \frac{P_{M1} - P_{M12}}{P_{year}} \qquad [-] \qquad [5]$$

Where:

- P_{M1} is the mean wave power of the highest energy month [kW/m]
- P_{M12} is the mean wave power of the lowest energy month [kW/m]
- P_{year} is the annual mean wave power [kW/m]

High values of MV indicate a major difference between months with high resource of energy and months with a lower one, while values which tend towards zero would mean a constant trend of wave power.

Since the analysed period both for past and future conditions is twenty years length, the variables presented in [5] concern about the months of the years ensemble and not of every year, so the monthly variability of a single point will produce only one output value and not twenty.

4.3.4 Seasonal variability index

Seasonal variability index [6] has similar proprieties of MV and describes the changing of wave power between the high and the low season. It is defined as follows:

$$SV = \frac{P_{S1} - P_{S4}}{P_{year}} \qquad [-] \qquad [6]$$

Where:

- P_{S1} is the mean wave power of the highest energy season [kW/m]
- P_{S4} is the mean wave power of the lowest energy season [kW/m]
- P_{year} is the annual mean wave power [kW/m]

The meaning of SV values is the same of MV ones. In fact a result which tends towards zero would indicate a constant value of wave power during the seasons. Nevertheless, actually is very common to have summers that coincide with the low season and winters where usually high values of wave power occur, therefore this index always present non-zero values. Moreover, the values of seasonal variability are lower than monthly ones, due to the fact that SV index includes in it three months.

As for MV, the output seasonal variability for every point will consist in only one value instead of twenty.

5. RESULTS

Using the output plots of the Matlab® software's computation in this chapter the results of those wave energy variables already descripted in *section 4.3* will be shown. These variables can help in assessing if and how climate change could produce an alteration of wave energy resource and/or a change in its distribution along months or seasons:

- The Wave Power ***P*** in past and future conditions for understanding the resource's potential that some ocean areas could gain or lose with esteemed climate change.
- The Monthly Variability Index ***MV*** and Seasonal Variability Index ***SV*** for evaluate the regularity of the resource or instead its alternation across months and seasons which can be crucial in the selection of a point where to install a wave energy converter.
- The ***absolute difference*** and the ***relative difference*** between the historic period 1986-2005 and the future forecasted conditions of 2081-2100 of the three above-mentioned variables. These variables are useful for esteeming the size of the changings.

5.1 Average Wave Power

The results of the Wave Power computed using formula [1] can be seen in the following images:

- The images of the average wave power's results obtained from every single model.
- An image of the average wave power of models' ensemble.
- The images of the absolute and relative differences obtained from every single model.
- An image of the absolute and relative differences of models' ensemble.

For every picture listed above there will be two results, one for each time series: the past conditions which refer to the 1986-2005 period and the future conditions which refer to the 2081-2100 period.

It is important to notice that for evaluate better the variations between past and future results of every model the same colorbar scale was used. This means that the range of colorbar's values vary between a minimum value (zero) and a maximum wave power value which is the highest wave power between the two results. A first example can be seen in *figures 5.1 and 5.2* where the maximum value of the wave power's map in *figure 5.1* does not correspond to the maximum value of its colorbar on the right side of the picture (185 kW/m) which instead is the maximum value of *figure 5.2*'s map.

In figures that show the difference occurred between the past and future computations grey areas can be noticed, for example around the coast of North America in *figure 5.12*, near Africa in *figure 5.16* and around Thailand in *figure 5.20*. These grey areas represent those points where the wave power's relative difference of models was not computed because the computation outputted high values. This problem occurred due to some very small values of mean wave power (of the order of 10^{-2} kW/m) that created extremely high or low values of relative differences despite small variations between past and future results.

Below, from *section 5.1.1 to 5.1.6*, the results of the wave power's computation for each model and models ensemble in both past and future periods are presented (*figures 5.1, 5.2, 5.5, 5.6, 5.9, 5.10, 5.13, 5.14, 5.17, 5.18, 5.21 and 5.22*), as well as the absolute and relative differences between them (*figures 5.3, 5.4, 5.7, 5.8, 5.11, 5.12, 5.15, 5.16, 5.19, 5.20, 5.23 and 5.24*).

5.1.1 Results of BCC-CSM1.1 model

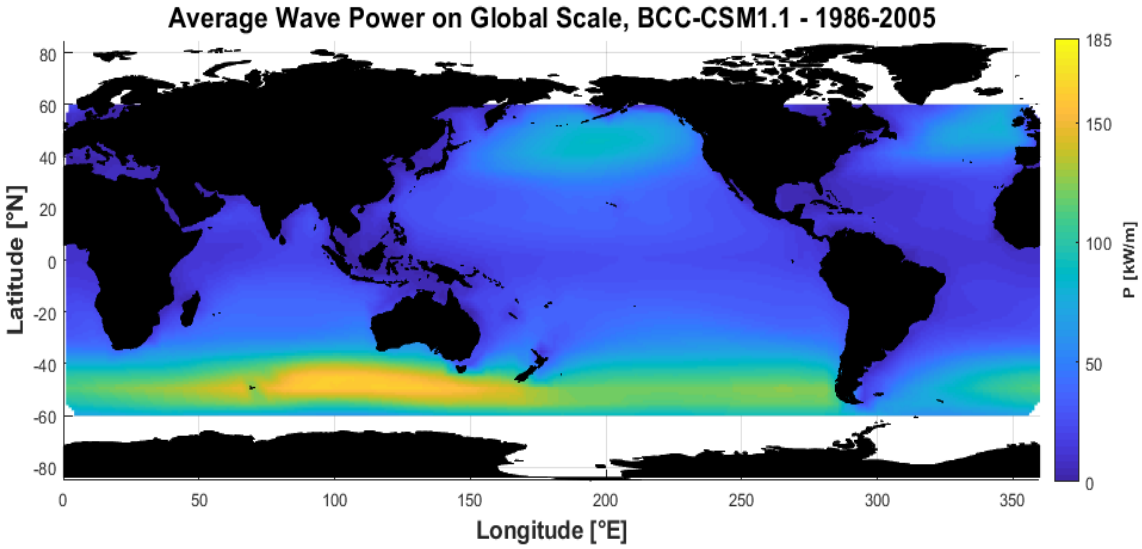

Figure 5.1: Wave power results of BCC in past conditions .

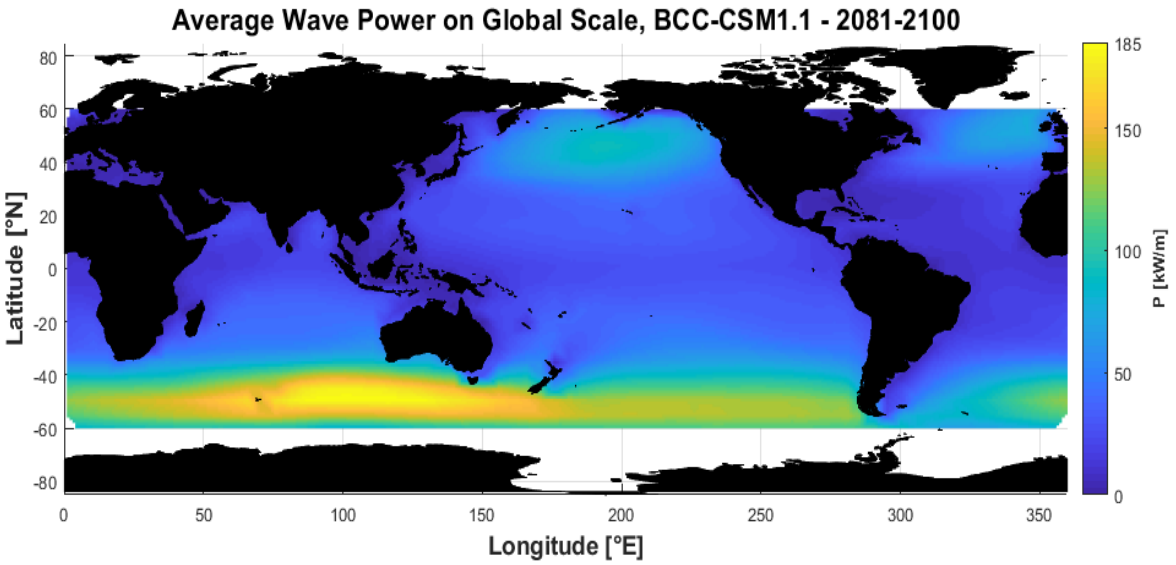

Figure 5.2: Wave power results of BCC in future conditions.

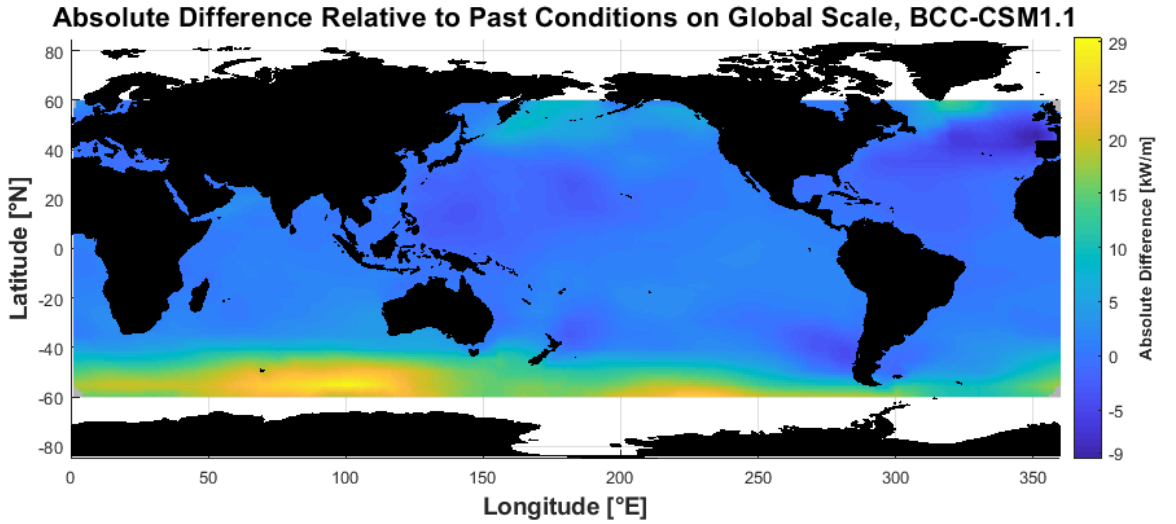

Figure 5.3: Wave power's bias of BCC model relative to past conditions.

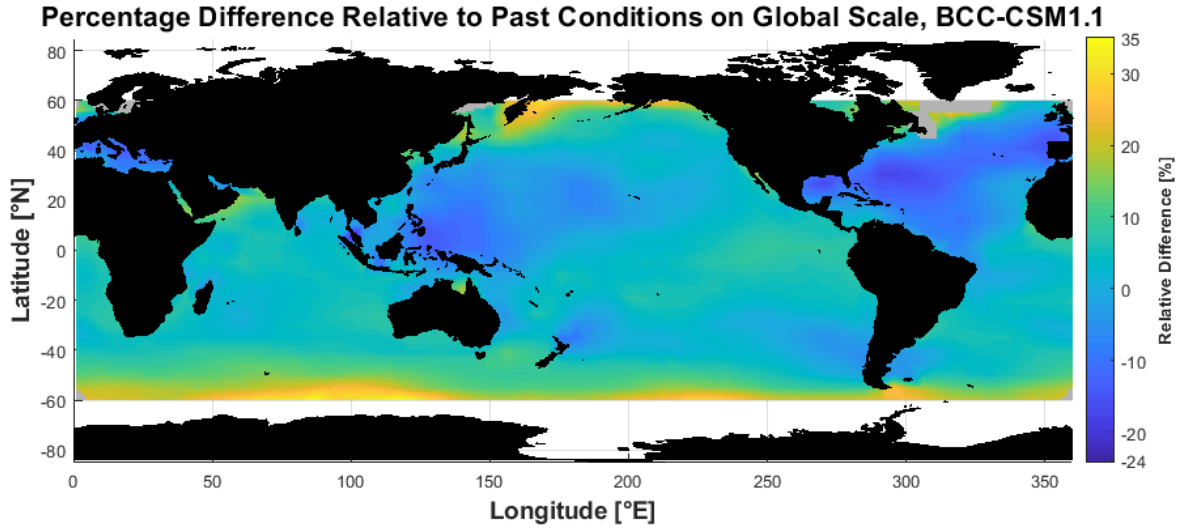

Figure 5.4: Wave power's relative difference of BCC model relative to past conditions.

5.1.2 Results of EC-EARTH model

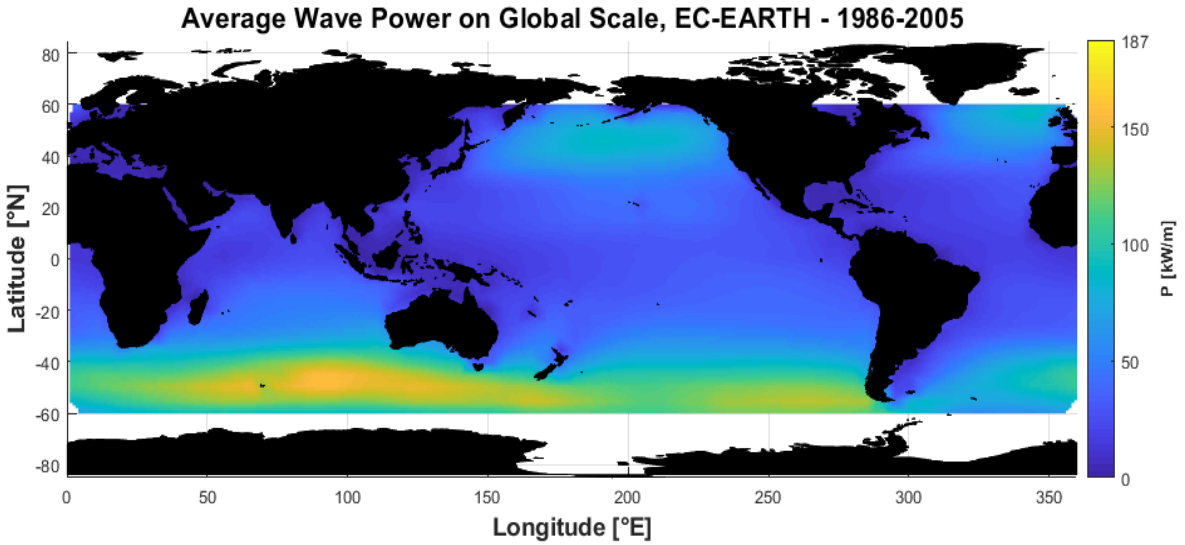

Figure 5.5: Wave power results of EC-EARTH model in past conditions

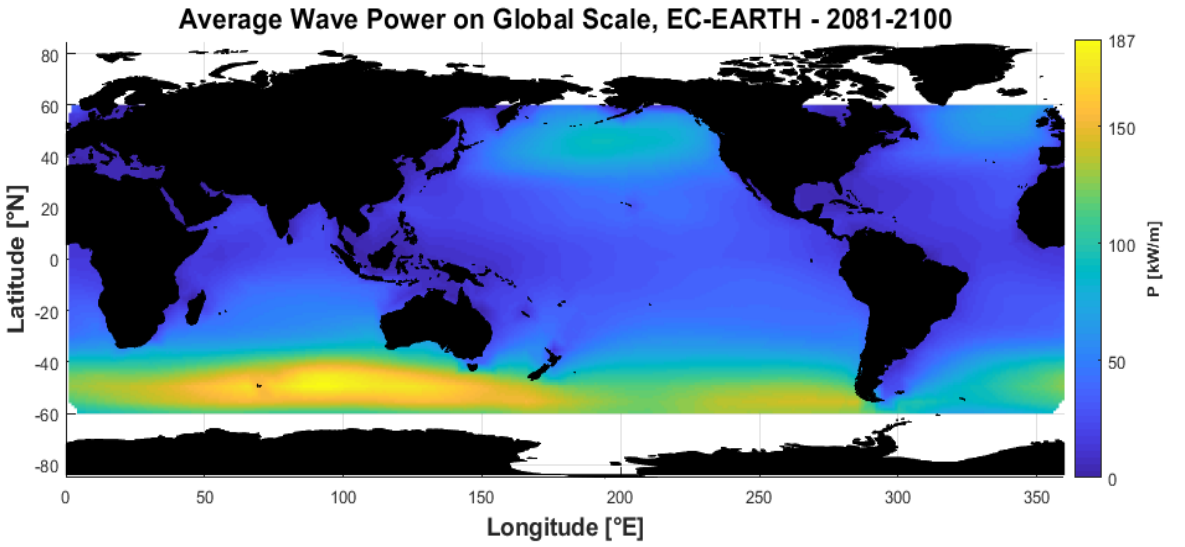

Figure 5.6: Wave power results of EC-EARTH model in future conditions

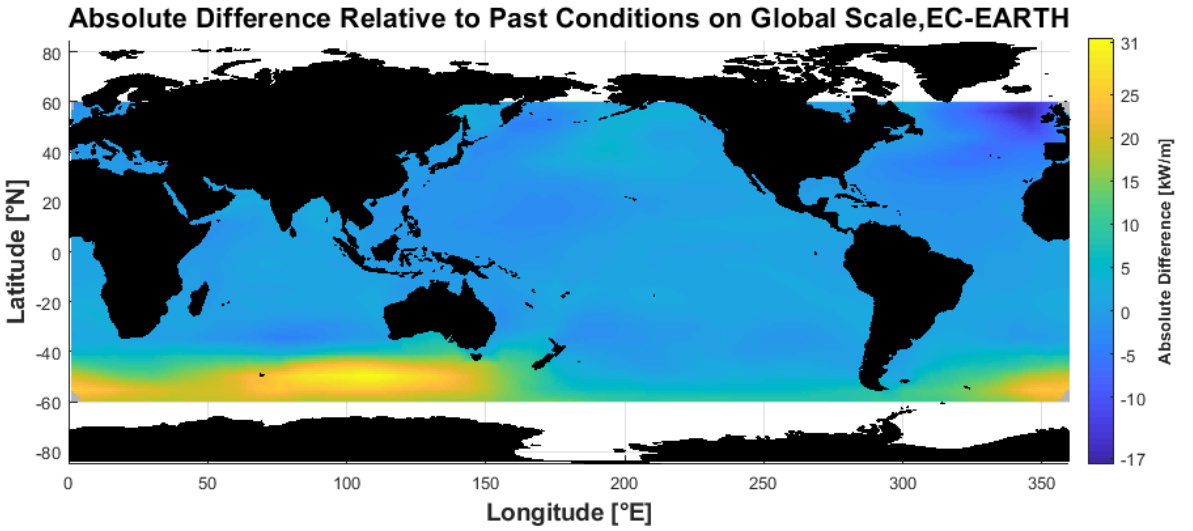

Figure 5.7: Wave power's bias of EC-EARTH model relative to past conditions.

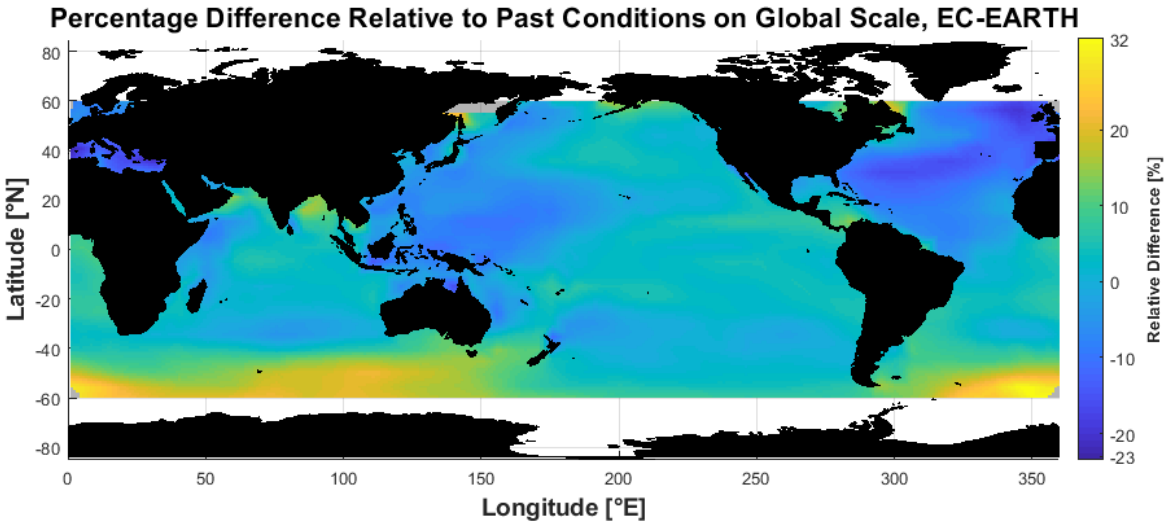

Figure 5.8: Wave power's relative differences of EC-EARTH model relative to past conditions.

5.1.3 Results of GFDL-ESM2M model

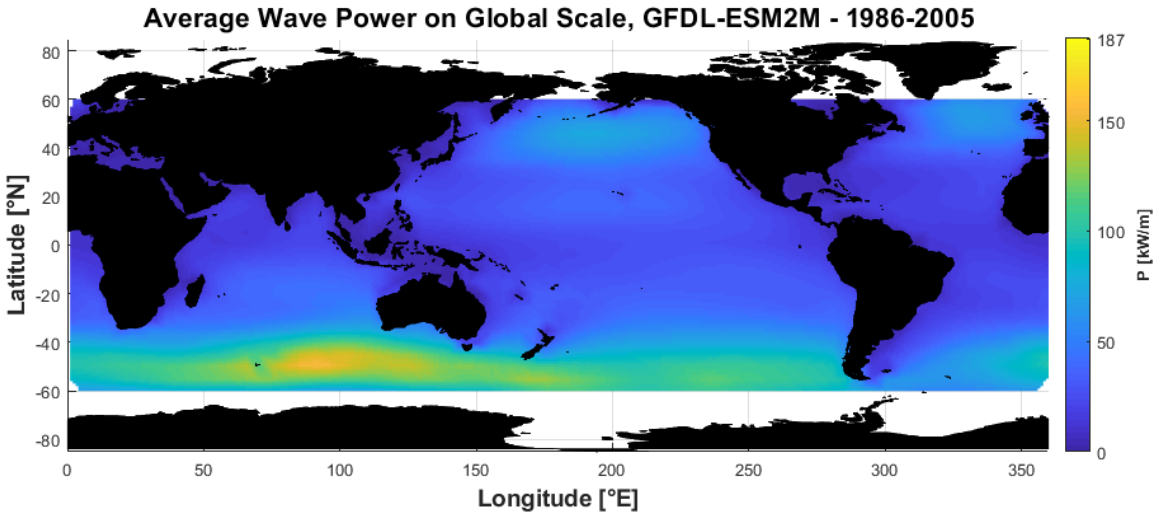

Figure 5.9: Wave Power results of GFDL model in past conditions

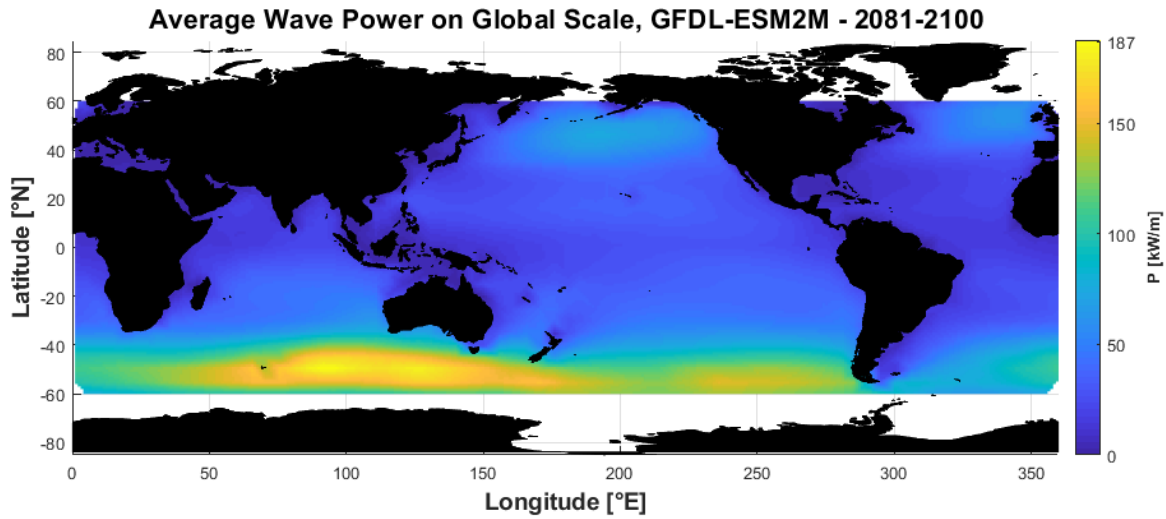

Figure 5.10: Wave Power results of GFDL model in future conditions

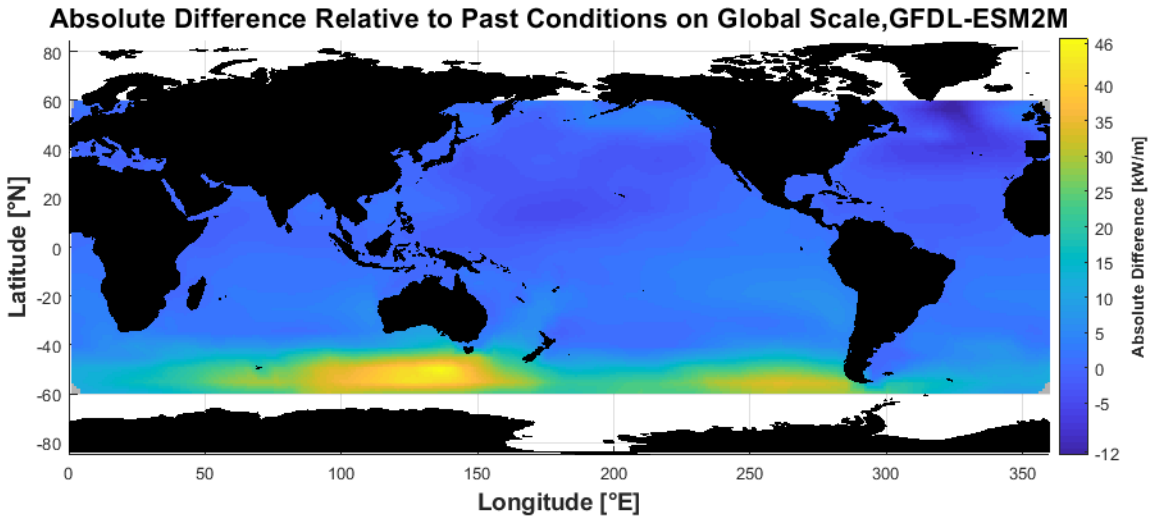

Figure 5.11: Wave power's bias of GFDL model relative to past conditions.

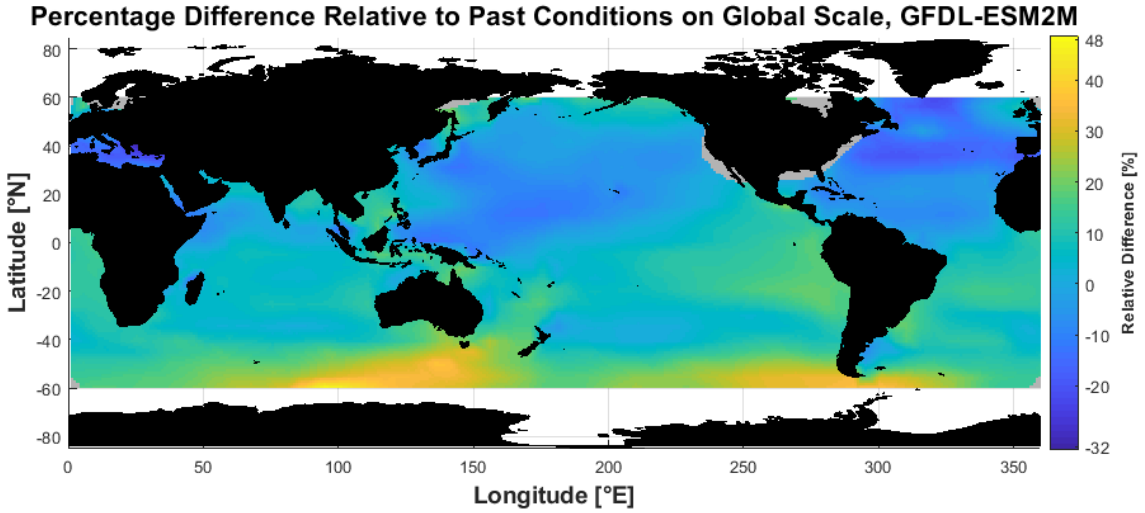

Figure 5.12: Wave power's relative difference of GFDL model relative to past conditions.

5.1.4 Results of INMCM4 model

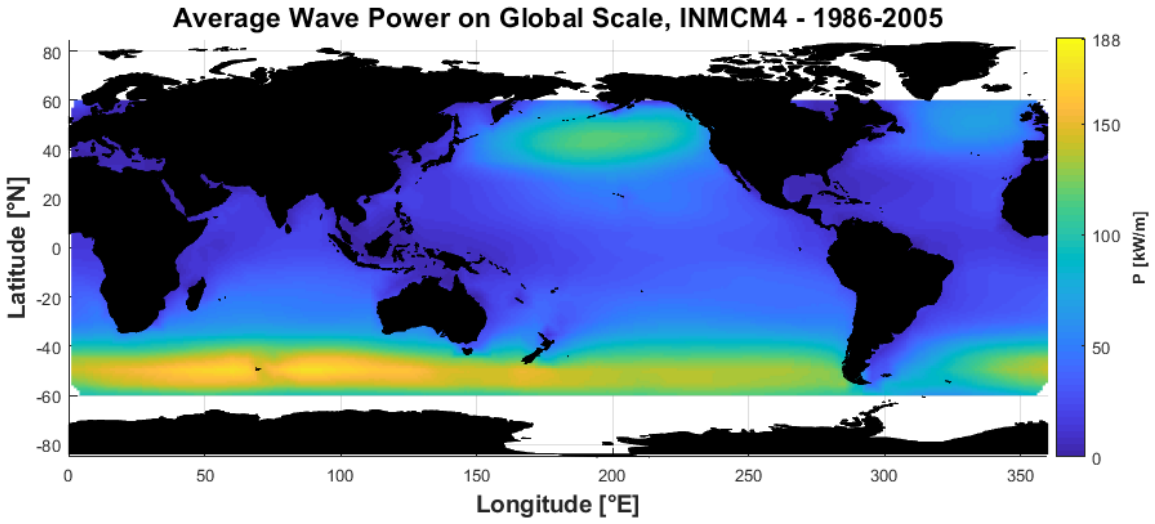

Figure 5.13: Wave Power's results of INMCM4 model in past conditions

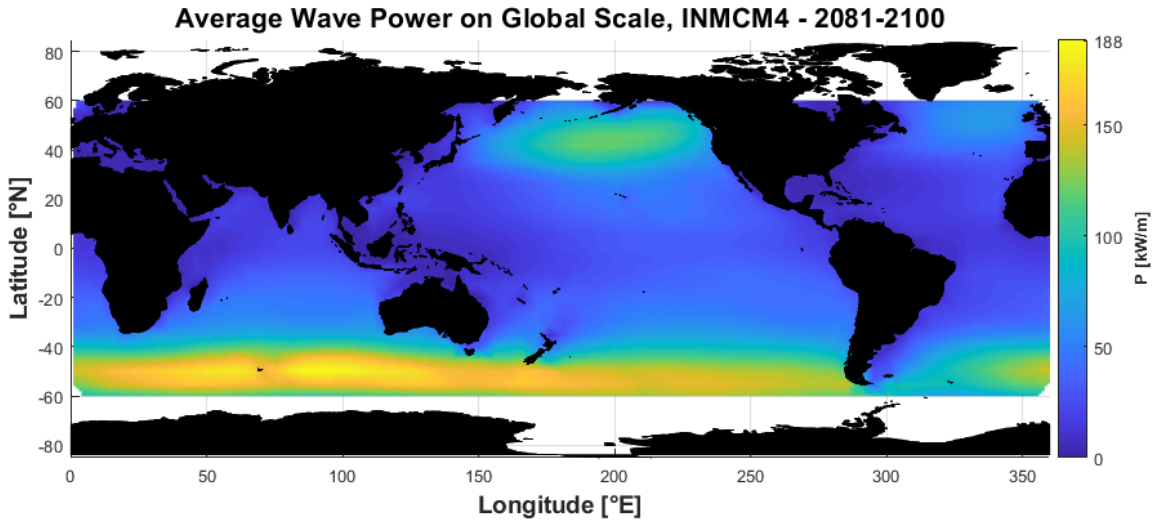

Figure 5.14: Wave Power's results of INMCM4 model in future conditions.

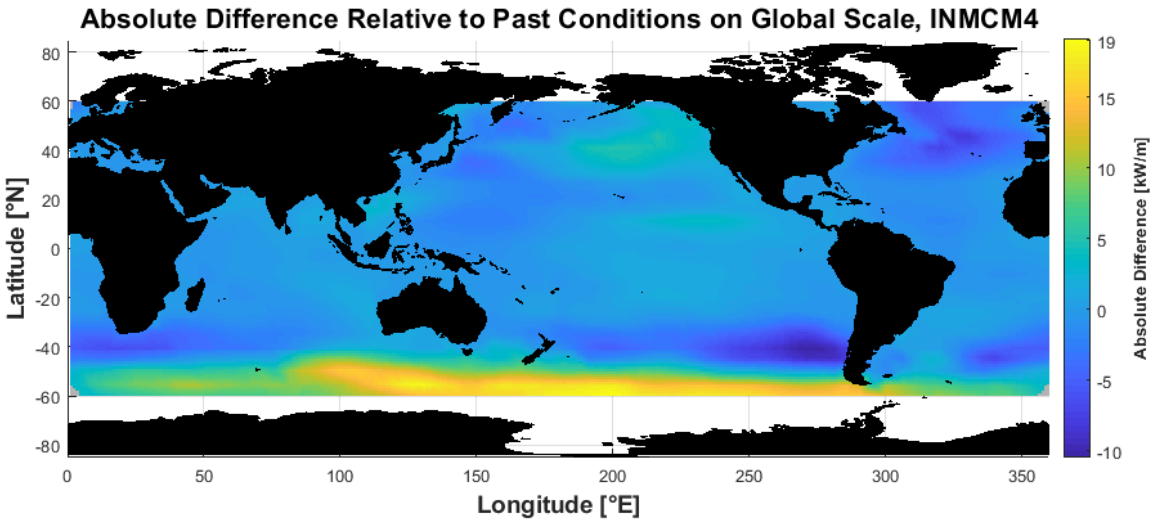

Figure 5.15: Wave power's bias of INMCM4 model relative to past conditions.

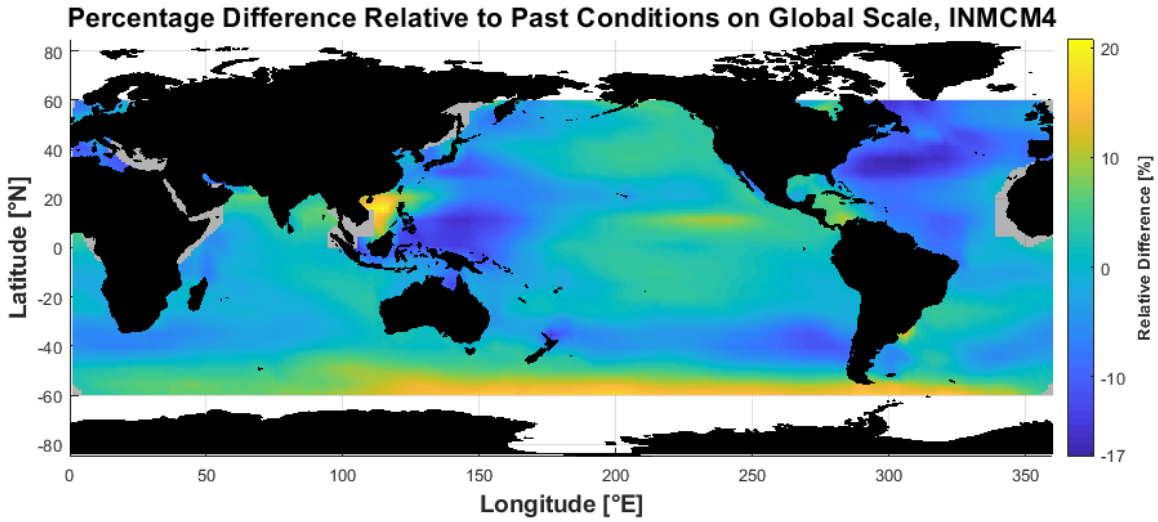

Figure 5.16: Wave power's relative difference of INMCM4 model relative to past conditions.

5.1.5 Results of MIROC5 model

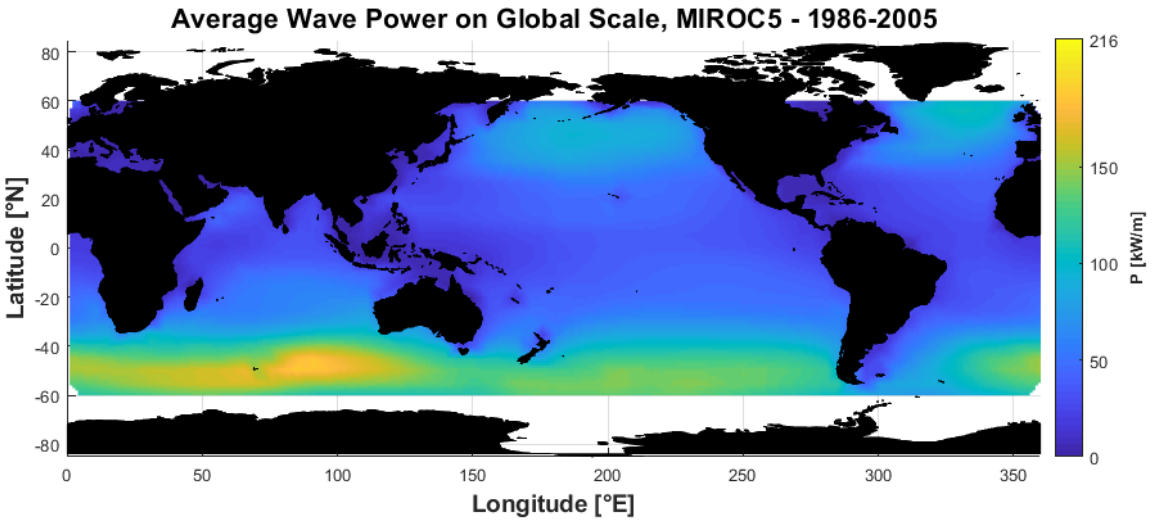

Figure 5.17: Wave Power's results of MIROC model in past conditions.

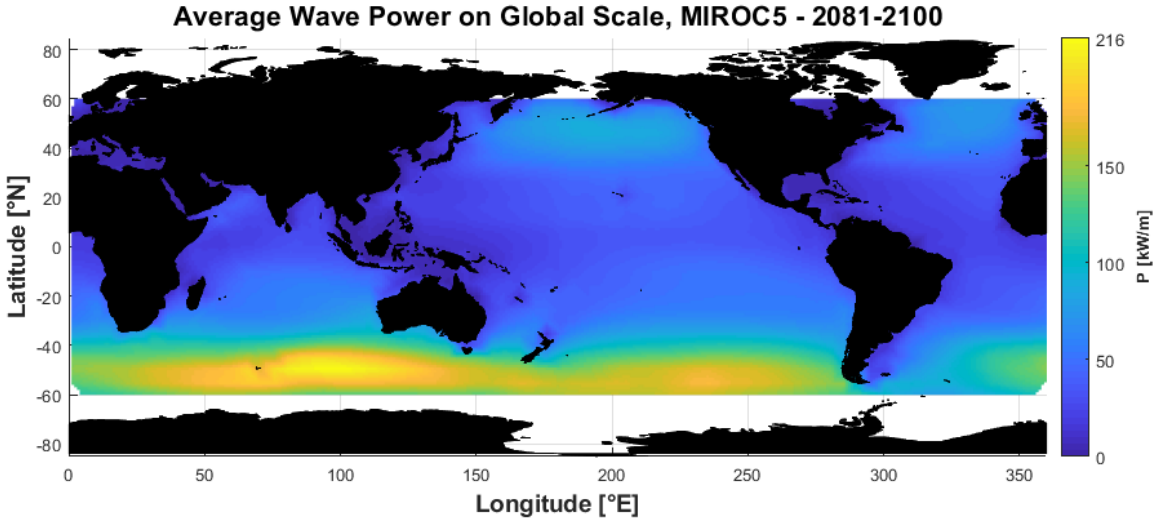

Figure 5.18: Wave Power's results of MIROC model in future conditions.

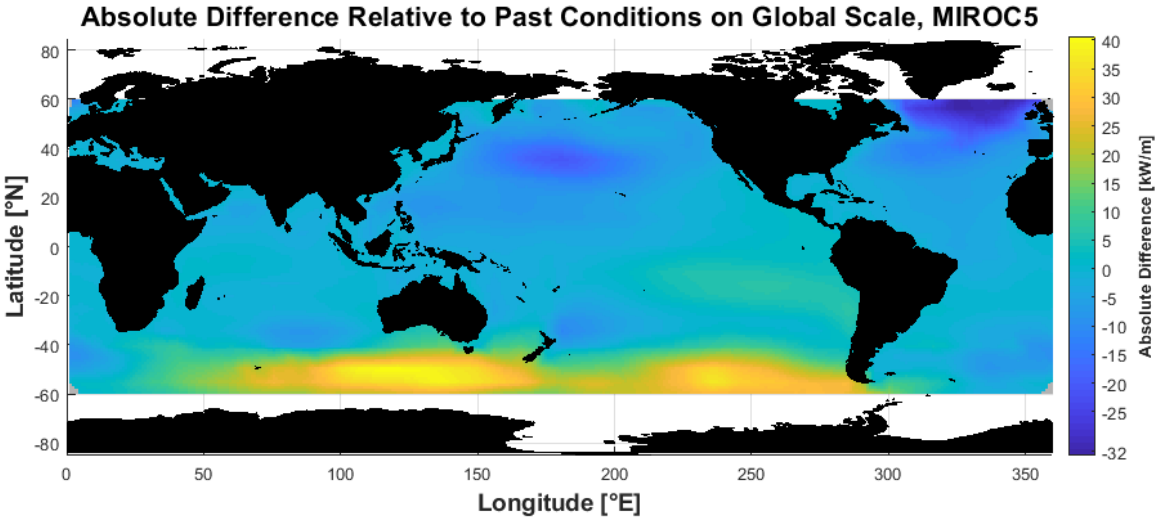

Figure 5.19: Wave power' bias of MIROC5 model relative to past conditions.

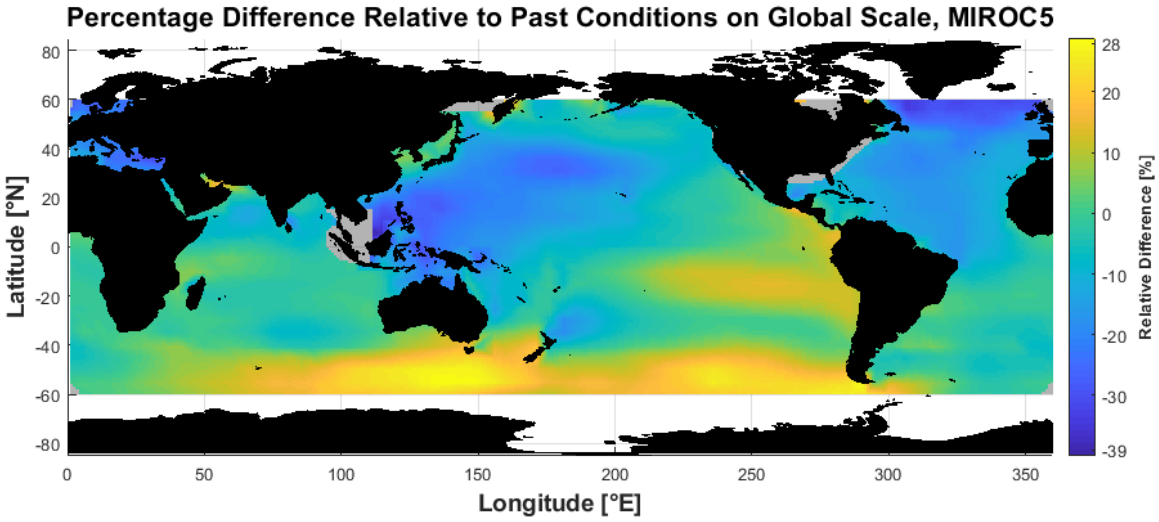

Figure 5.20: Wave power's relative difference of MIROC5 model relative to past conditions.

5.1.6 Results of model ensemble

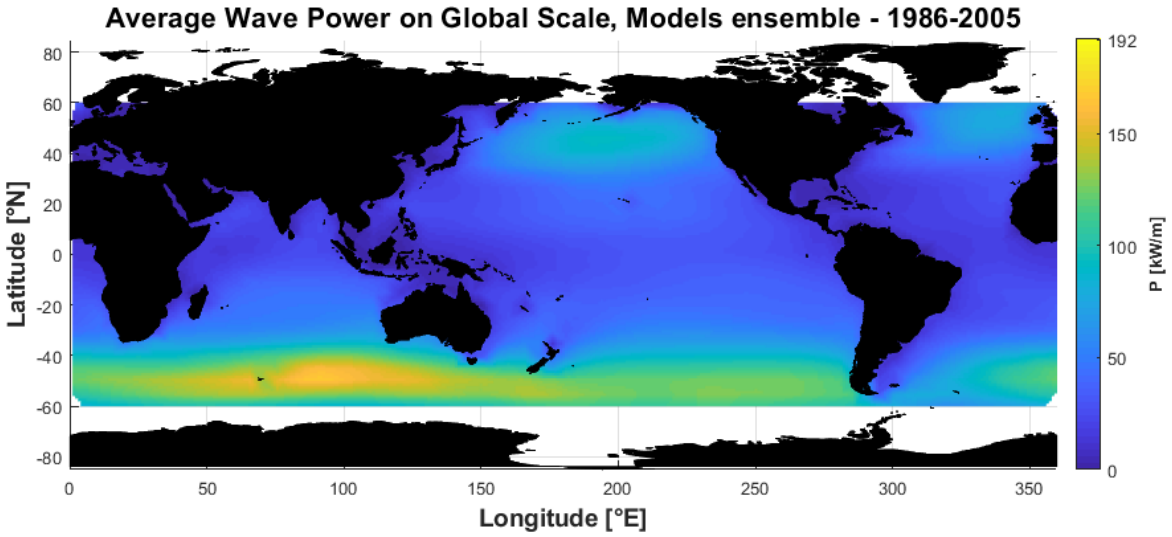

Figure 5.21: Wave Power's results of model ensemble in past conditions.

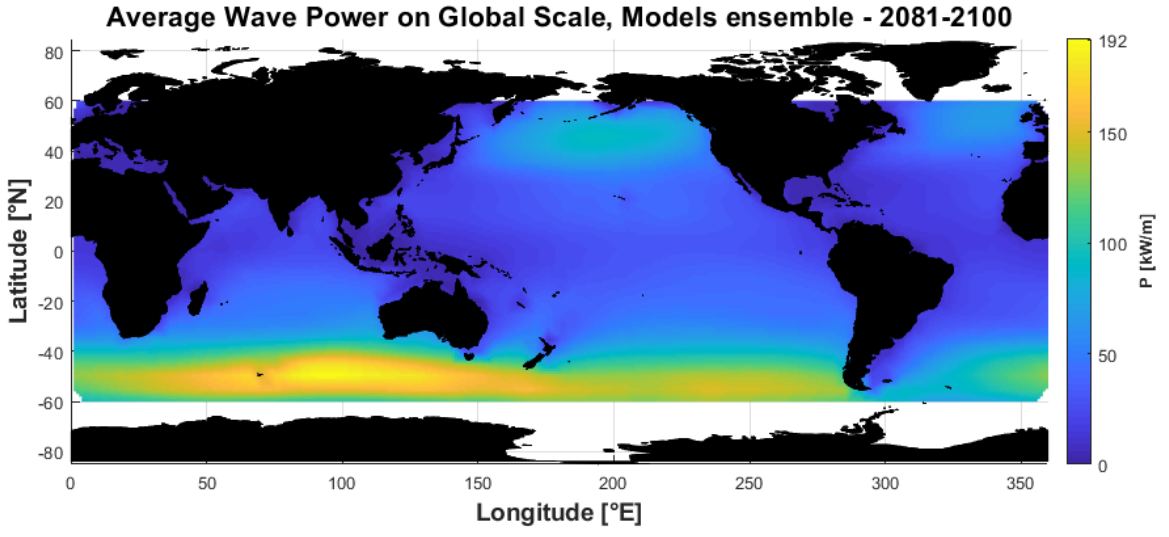

Figure 5.22: Wave Power's results of model ensemble in future conditions.

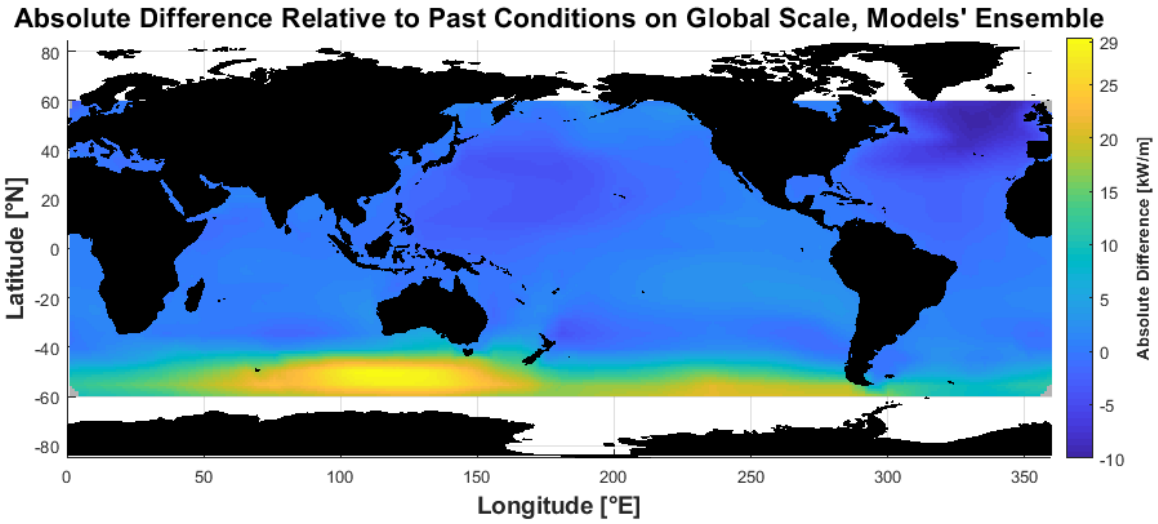

Figure 5.23: Wave power's bias of model ensemble relative to past conditions

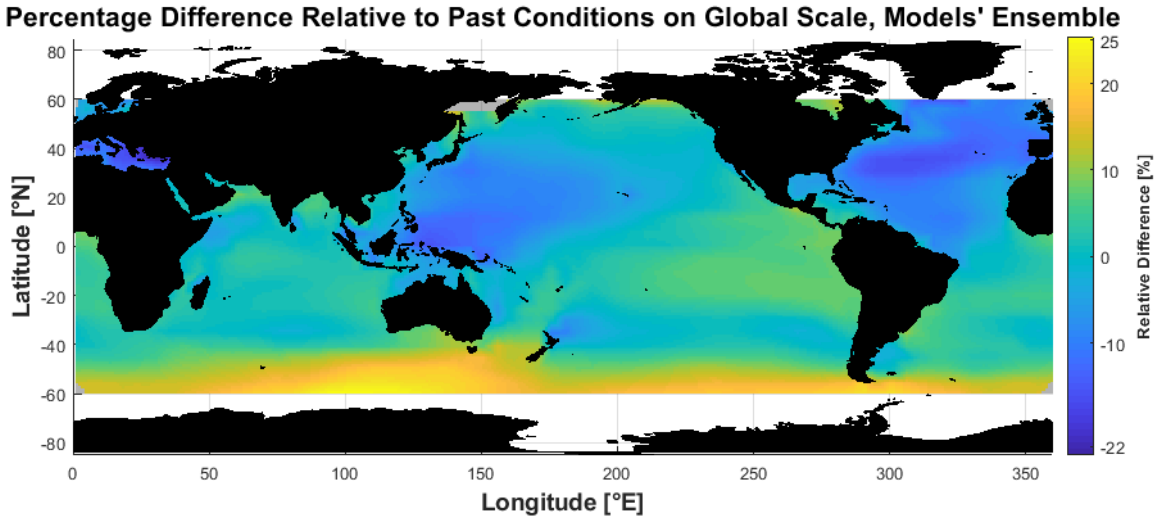

Figure 5.24: Wave power's relative difference of model ensemble relative to past conditions.

5.1.7 Wave Power divided for areas

The wave power was also computed dividing the oceans in eleven areas (described in *section 4.2.3* and illustrated in *figure 4.6*) in order to understand the energy potential of single oceans and how their wave power will change along with climate change. Twelve graphs, one per each area and a global one, are represented in the past and future conditions (*figure 5.25*). The points which compose the five coloured lines are the esteemed average monthly wave powers of every model. In *figure 5.26* the results of the absolute difference between the two time series are plotted.

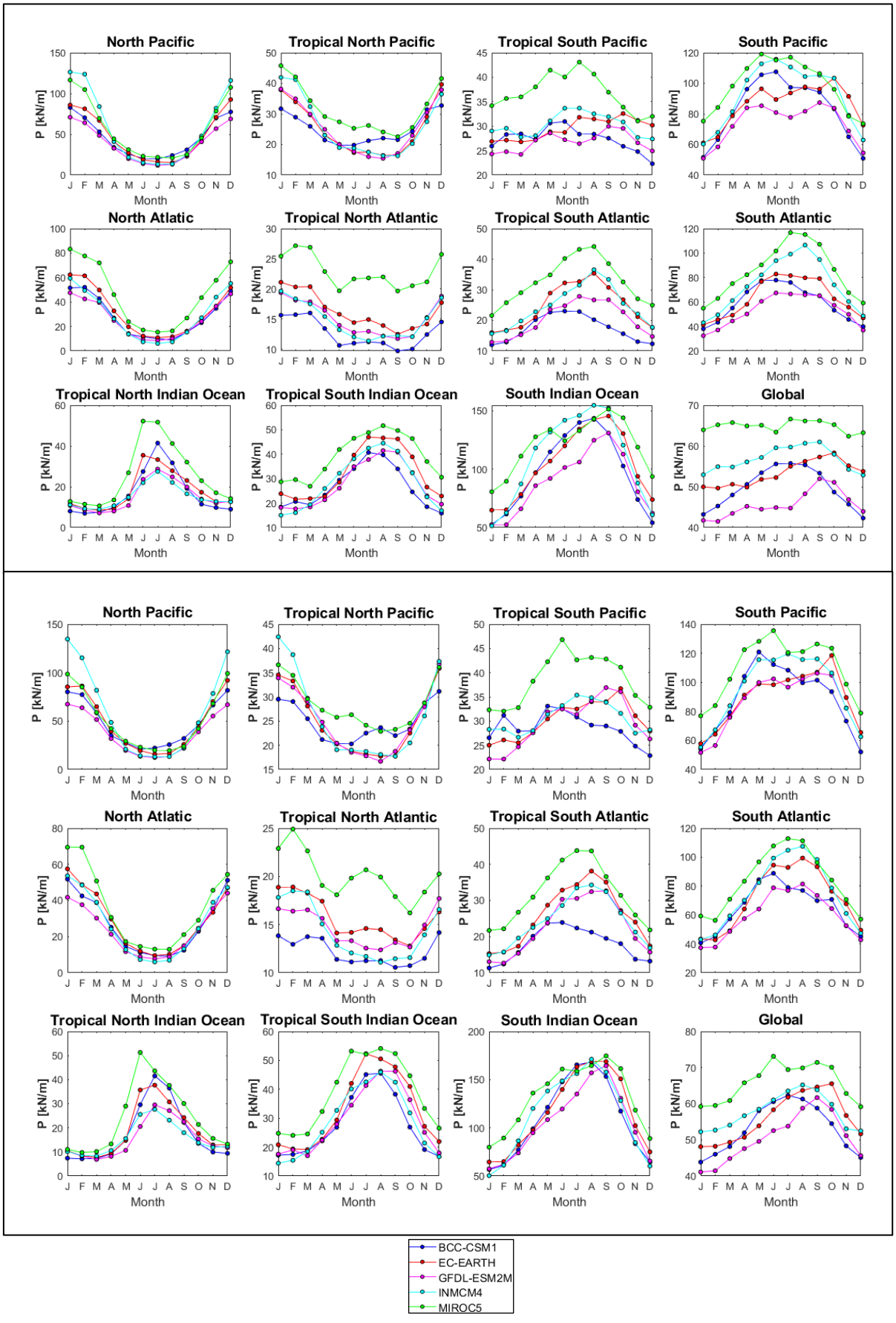

Figure 5.25: Monthly average of the wave power divided by ocean areas in 1986-2005 (upper panels) and 2081-2100 (lower panels).

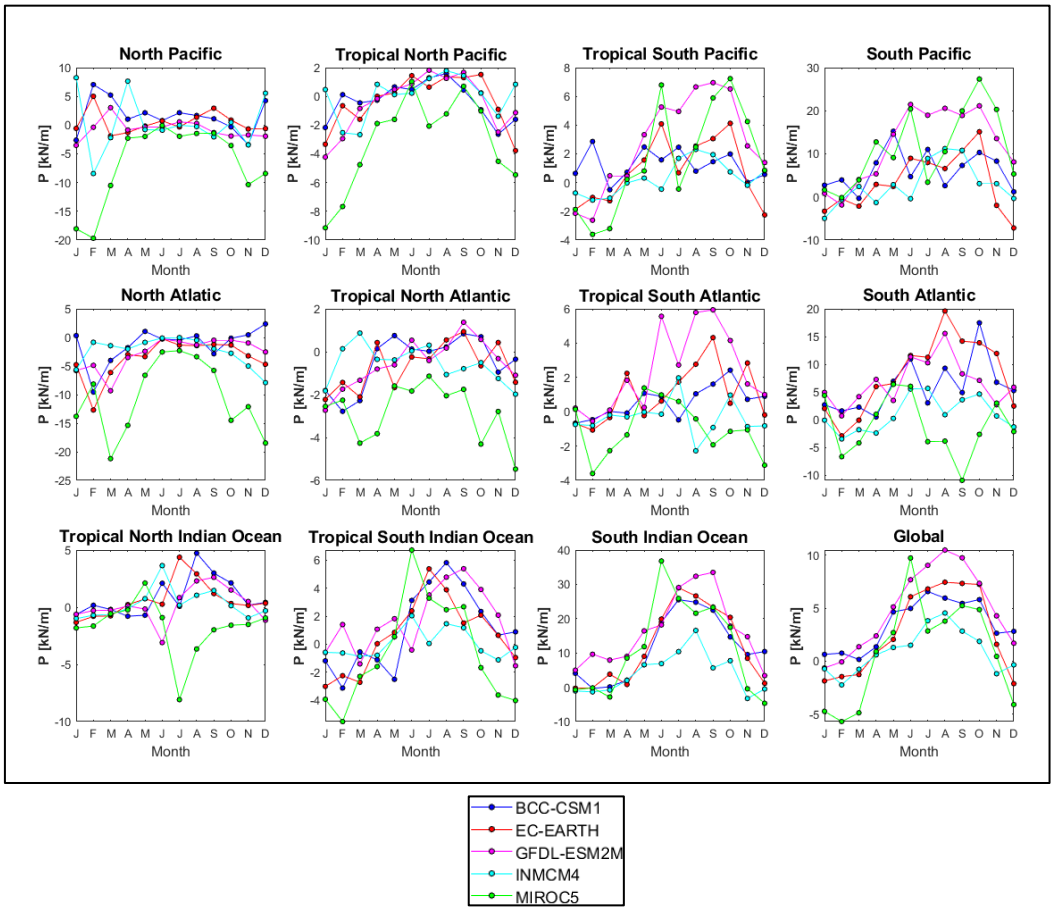

Figure 5.26: Bias of monthly average's wave power between the future and the past conditions.

5.2 Results of the Monthly Variability index

The results of MV index have been computed using formula [5] of *section 4.3.3* and will be shown, as wave power, with global colormaps. The computation has produced:

- Six past conditions' plot of MV index, one for every model and one of model ensemble
- Six future conditions' plot of MV index, one for every model and one of model ensemble.
- One absolute difference of MV between the model ensemble's results of future relative to past conditions.

- One relative difference of MV between the model ensemble's results of future relative to past conditions.

Due to some outliers' values in recurrent area of the models it was established a maximum value of monthly variability index:

$$MV_{max}=3$$

This decision was also made in order to distinguish better the variations of the index on the maps which would have been thin with a larger colour's scale.

In the results that will be shown in the following sections grey areas similar to those presented in *section 5.5.1* can be noticed. These grey areas differentiate themselves from wave power's ones and state the excluded points which in this case have a triple nature:

- Points without an enough number of data inside the twenty years' time interval.
- Points with outlier values.

The limit of data for considering valid a point was set at 14600 data out of 58400, which means 5 years out of 20.

The other excluded points were those whose calculation generated excessively high results. This problem occurred in points that were usually near the coast and therefore belonging to the model's data points of the small grid descripted at the start of *section 4.1.3*. In fact, the small sides of the grid caused in these points not accurate results in the computation of used models, so that very small values of wave power (of the order of 10^{-2} kW/m) invalidate the MV's calculus.

It is important to mention that the excluded points are not the same for each model. Since the model's nature is different these computational lacks can change between the models.

The MV's plotted results, presented below consist of the output of models and models' ensemble for the two studied periods (*figures 5.25 to 5.36*) and the absolute and relative differences between the MV of the mean's ensemble (*figures 5.37 and 5.38*).

5.2.1 Results of the BCC-CSM1-1 model

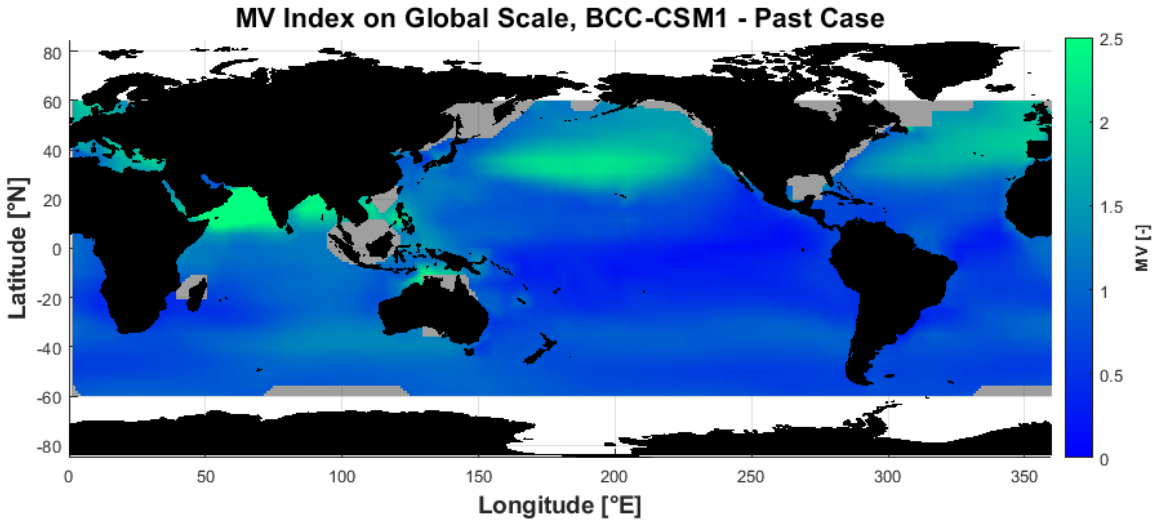

Figure 5.27: MV's results of BCC model in past conditions.

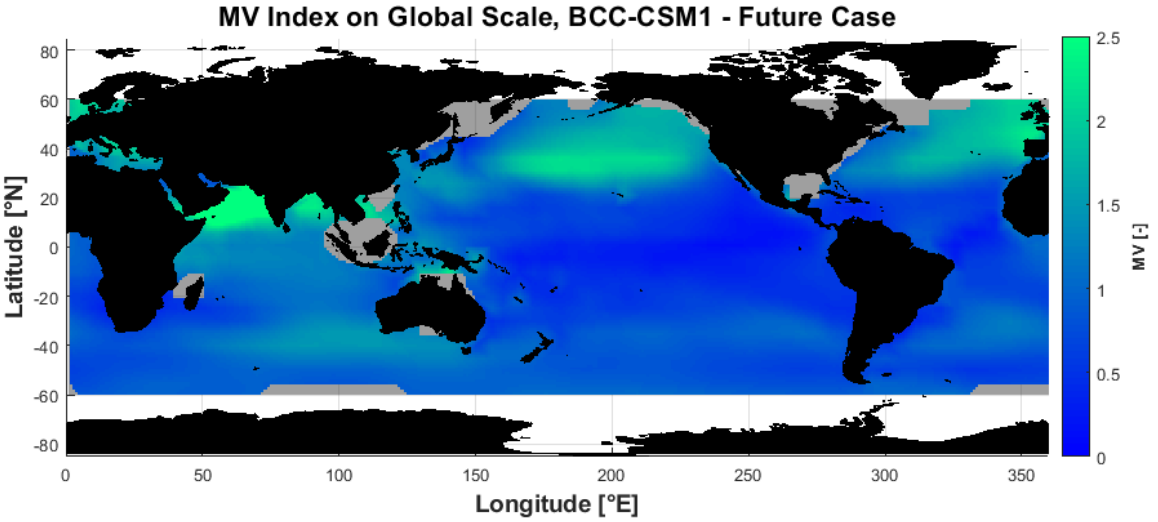

Figure 5.28: MV's results of BCC model in future conditions.

5.2.2 Results of the EC-EARTH model

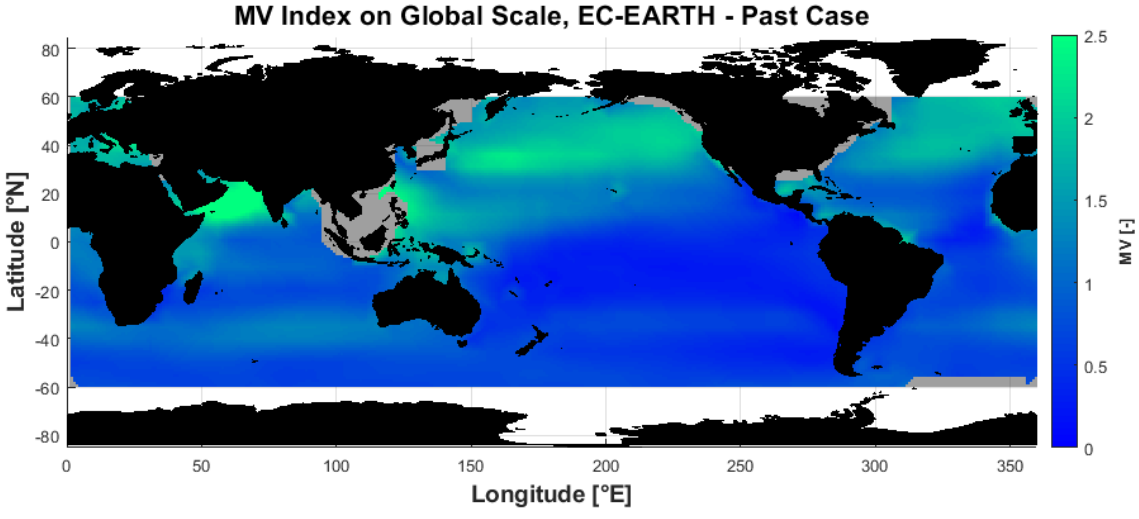

Figure 5.29: MV's results of EC-EARTH model in past conditions.

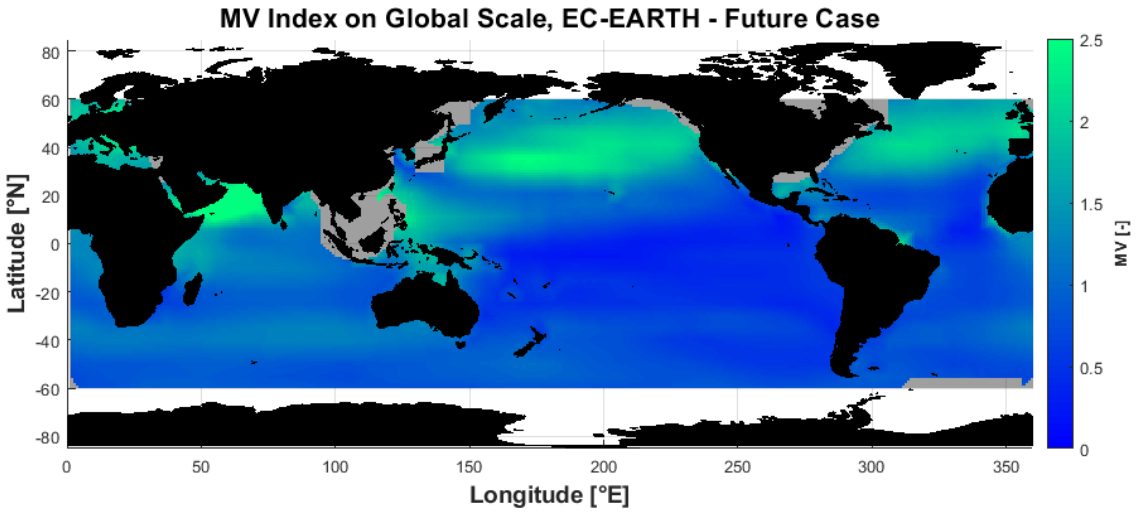

Figure 5.30: MV's results of EC-EARTH model in future conditions.

5.2.3 Results of the GFDL-ESM2M model

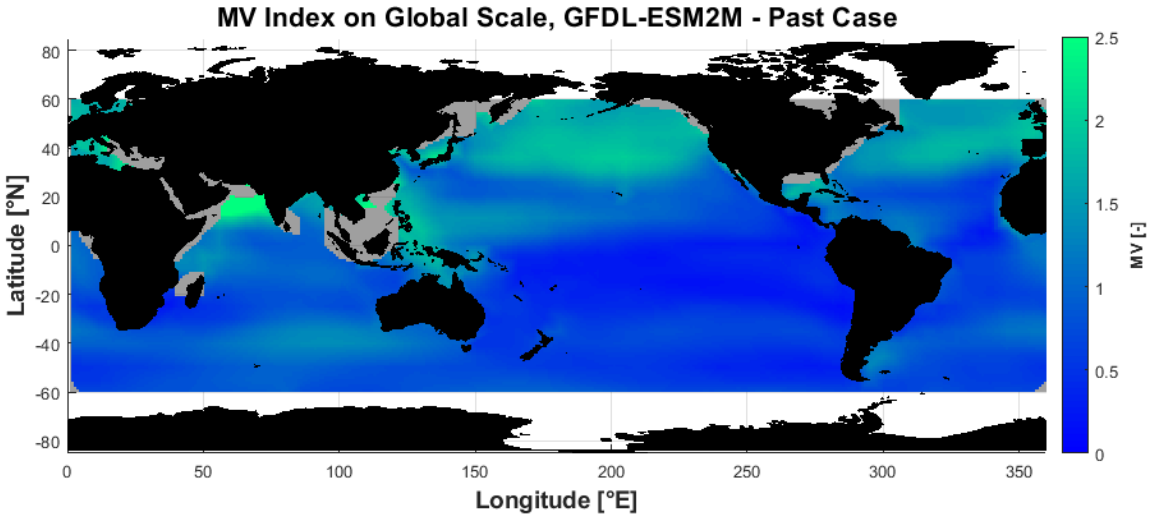

Figure 5.31: MV's results of GFDL-ESM2M model in past conditions.

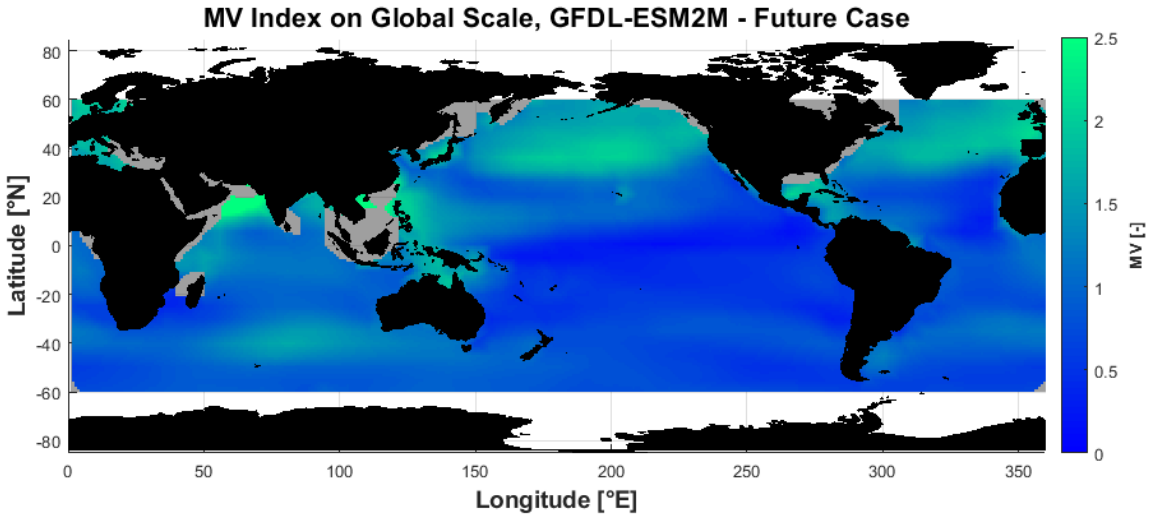

Figure 5.32: MV's results of GFDL-ESM2M model in future conditions.

5.2.4 Results of the INMCM4 model

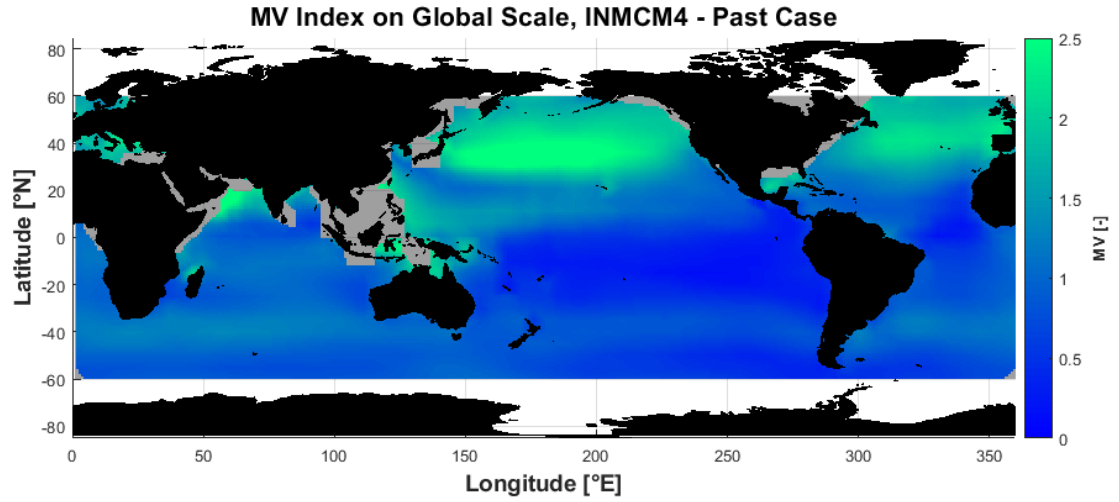

Figure 5.33: MV's results of INMCM4 model in past conditions.

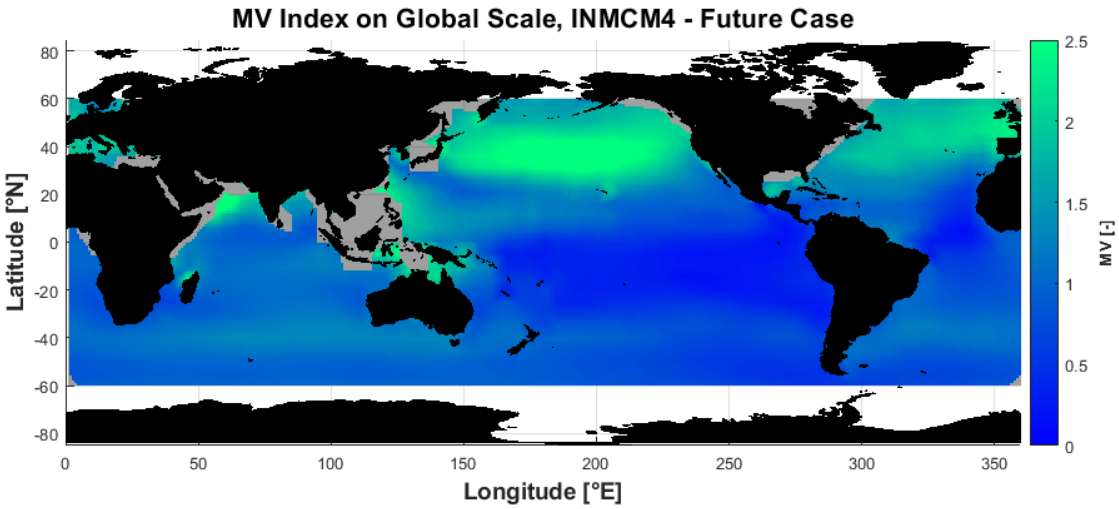

Figure 5.34: MV's results of INMCM4 model in future conditions.

5.2.5 Results of the MIROC5 model

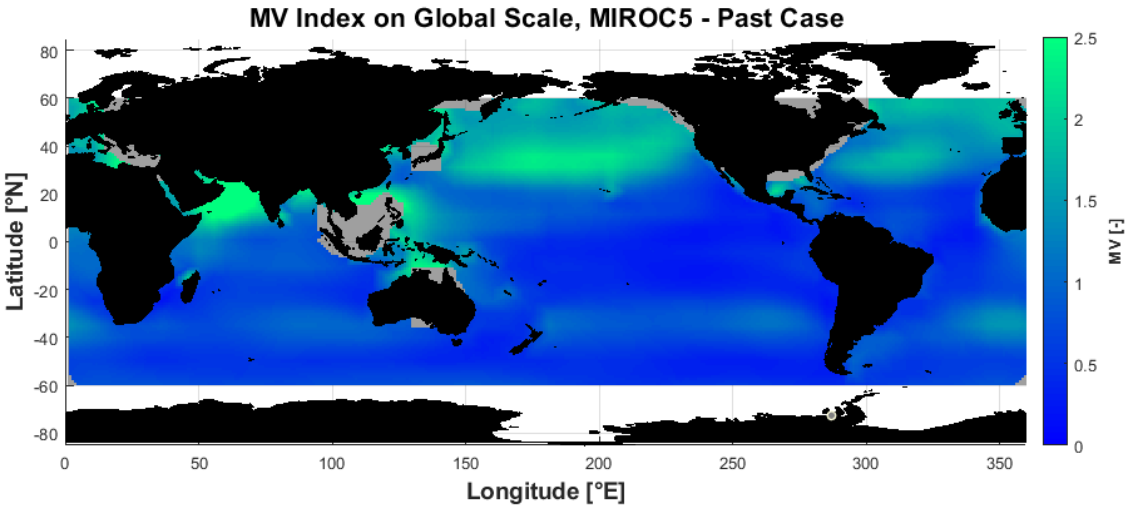

Figure 5.35: MV's results of MIROC5 model in past conditions.

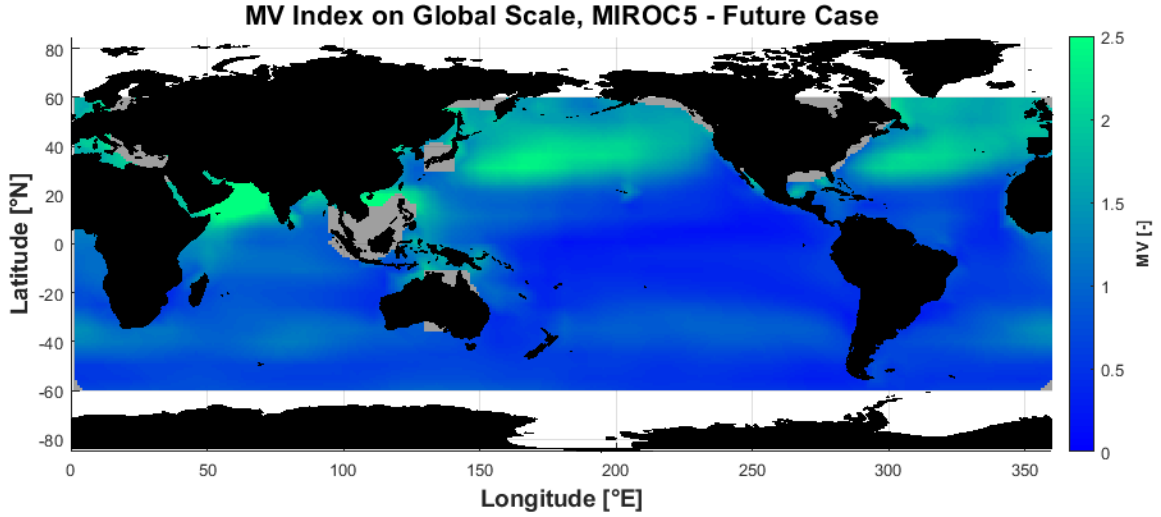

Figure 5.36: MV's results of MIROC5 model in future conditions.

5.2.6 Results of the models' ensemble

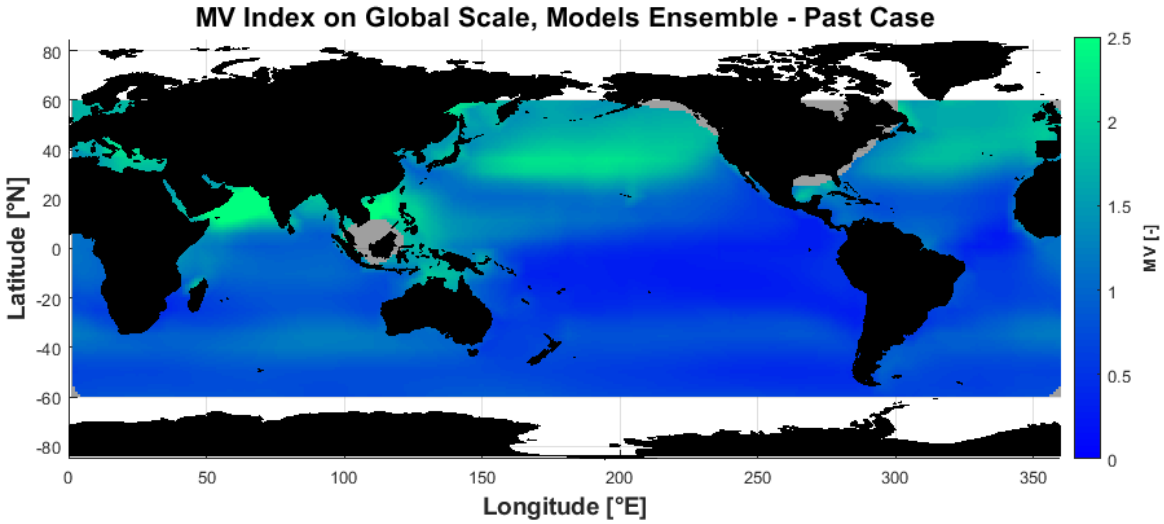

Figure 5.37: MV's results of model ensemble in past condition.

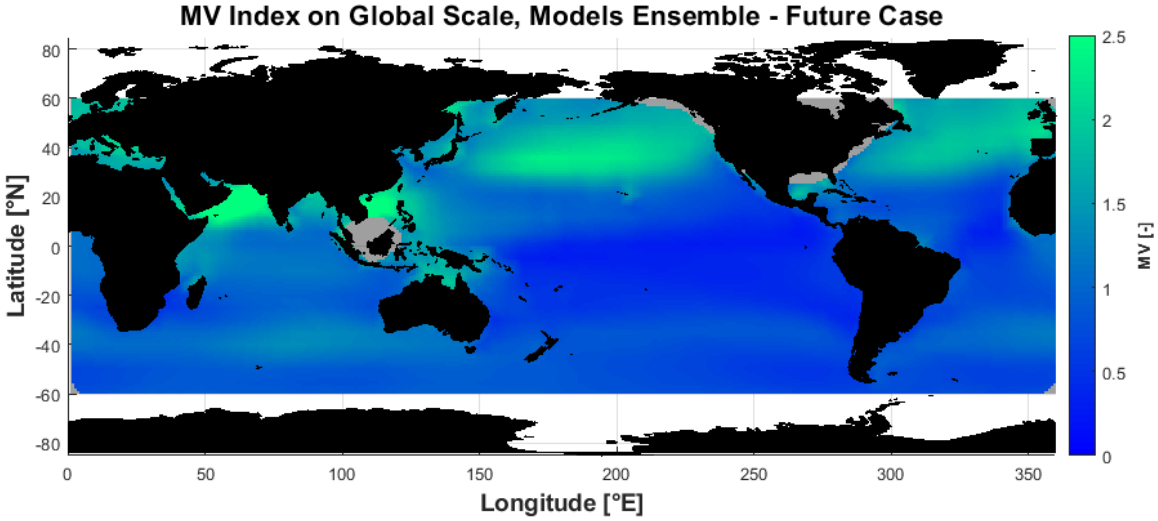

Figure 5.38: MV's results of model ensemble in future condition.

5.2.7 Bias and relative difference of MV between past and future

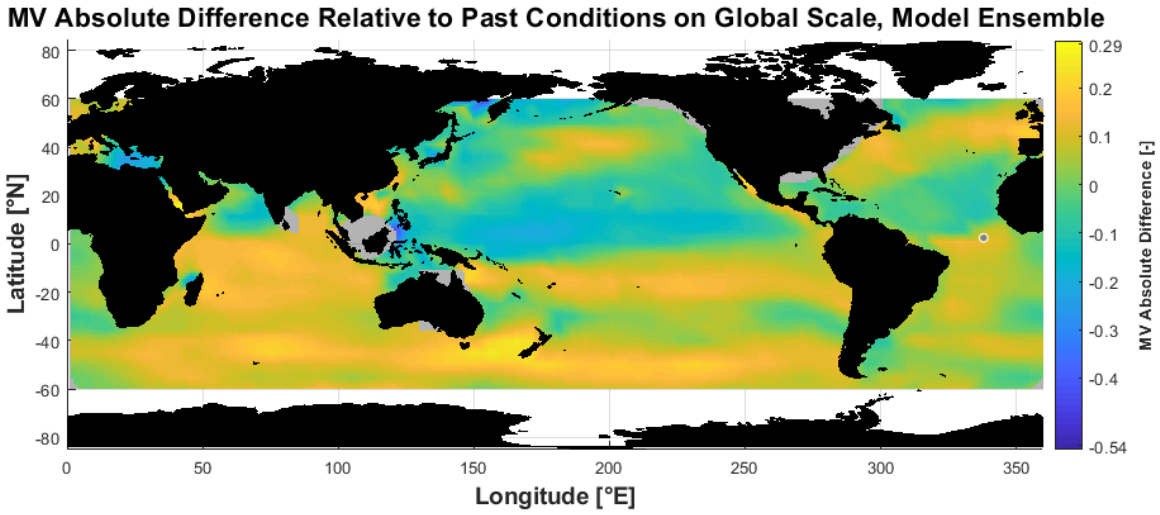

Figure 5.39: MV's bias of models' ensemble relative to past conditions

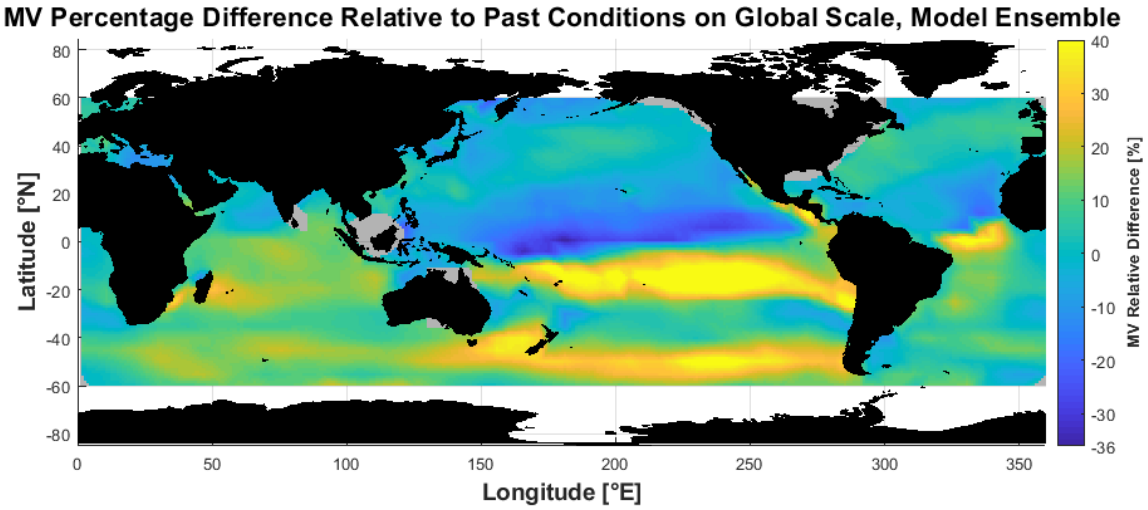

Figure 5.40: MV's relative difference of models' ensemble relative to past conditions

5.3 Results of Seasonal Variability index

The SV index is similar to MV except for the considered period that, in these case, embraces not the months but the four seasons of the year. Therefore, smaller values will be expected but with similar distribution of peaks. The computation of the SV index followed the formula [6] of *section 4.3.4* and has brought to these results' images:

- Six past conditions' plot of SV index, one for every model and one of model ensemble
- Six future conditions' plot of SV index, one for every model and one of model ensemble.

- One plot of absolute differences of SV between the model ensemble's results in past and future conditions.
- One plot of relative differences of SV between the model ensemble's results in past and future conditions.

For the plot of the results it was inserted a similar condition to MV_{max} for the maximum value of seasonal variability:

$$SV_{max}=2$$

Moreover, the grey areas where the indexes' computation was excluded are similar between the monthly and seasonal variability of same models. The points excluded due to the first of the two reasons listed in *section 5.3* are the same but those excluded for the second reason (very low wave power's values of the order of 10^{-2} kW/m) can differ between MV and SV.

The output's plots below illustrated represent the SV for every model and models' ensemble in 1986-2005 and 2081-2100 (*figures 5.39 to 5.50*) and the difference between models' ensemble of SV index (*figures 5.51 and 5.52*).

5.3.1 Results of the BCC-CSM1-1 model

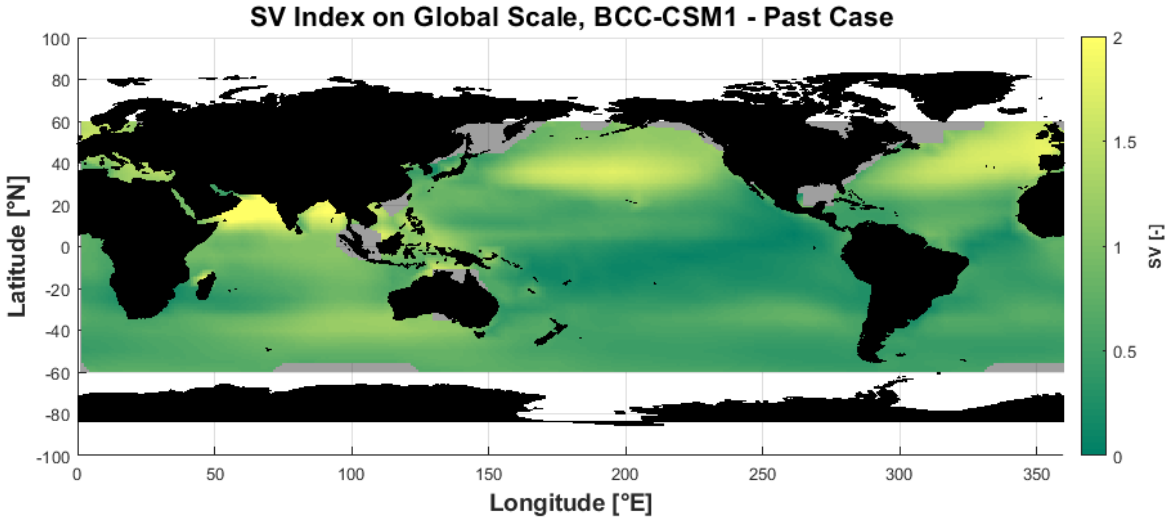

Figure 5.41: SV's result of BCC model in past conditions.

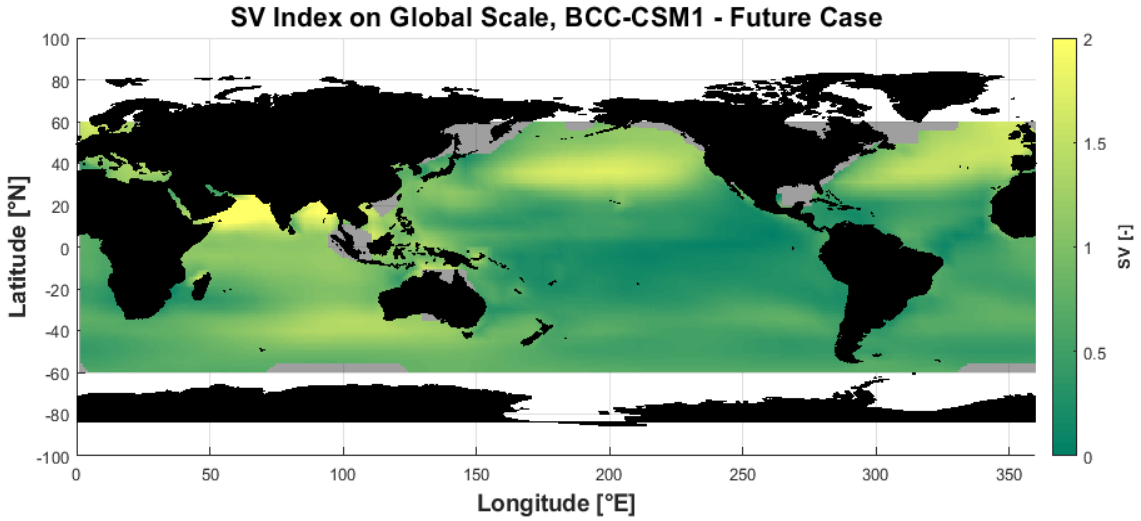

Figure 5.42: SV's result of BCC model in future conditions.

5.3.2 Results of the EC-EARTH model

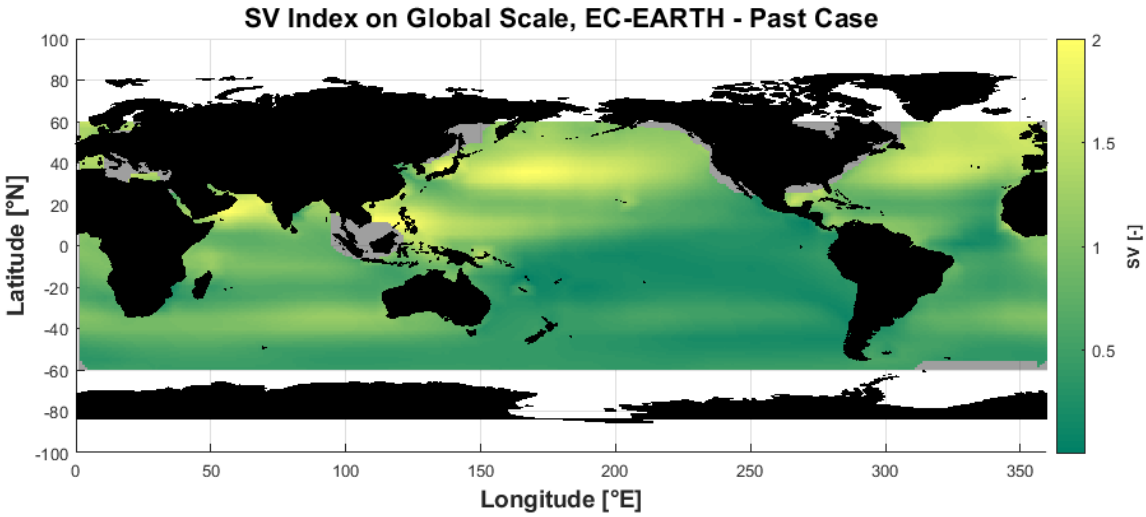

Figure 5.43: SV's result of EC-EARTH model in past conditions.

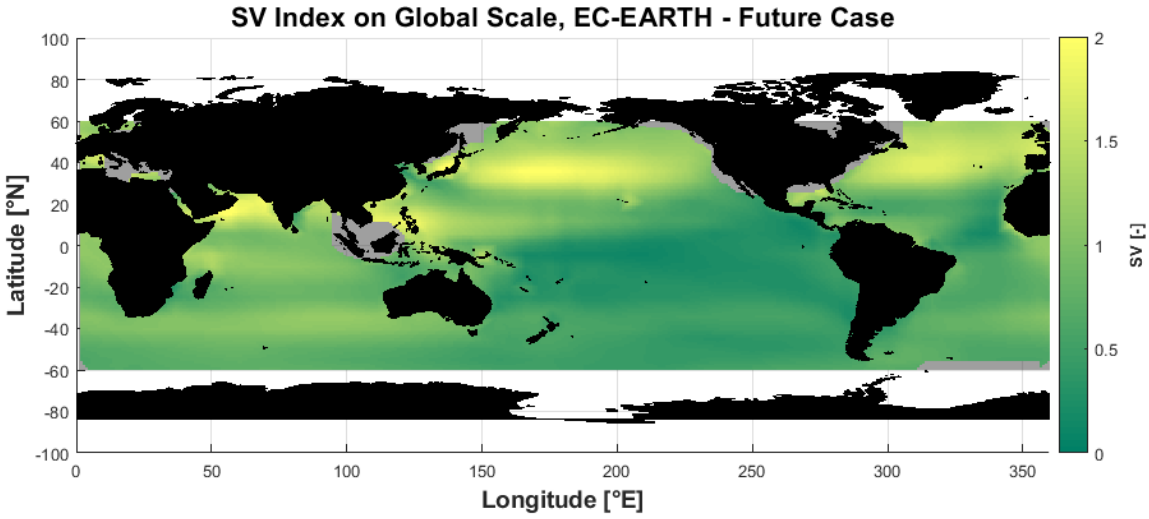

Figure 5.44: SV's result of EC-EARTH model in future conditions.

5.3.3 Results of the GFDL-ESM2M model

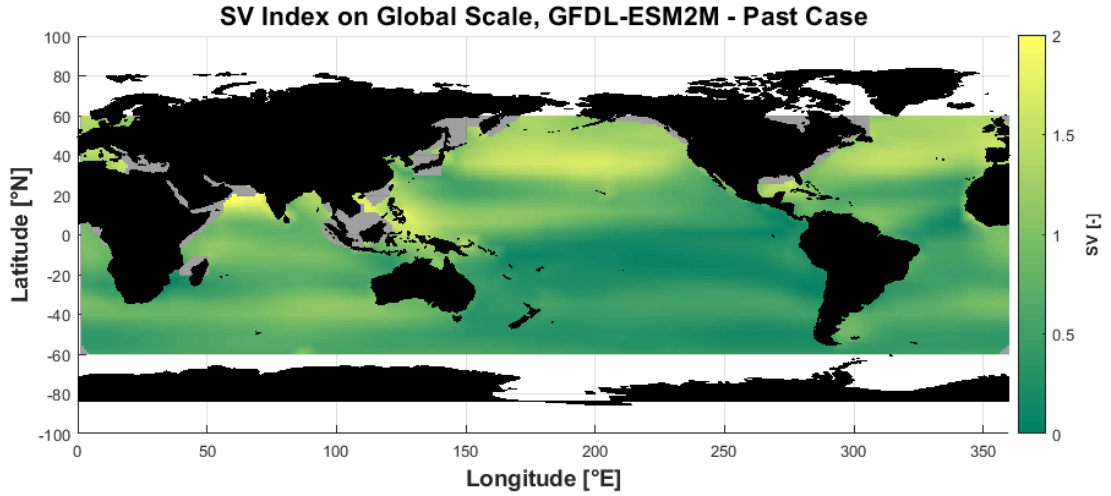

Figure 5.45: SV's result of GFDL-ESM2M model in past conditions.

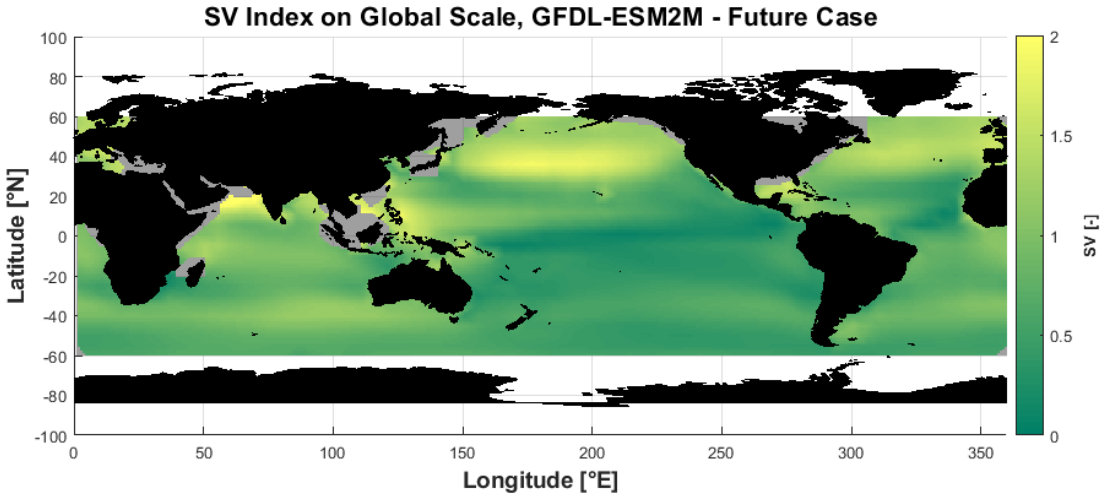

Figure 5.46: SV's result of GFDL-ESM2M model in future conditions.

5.3.4 Results of the INMCM4 model

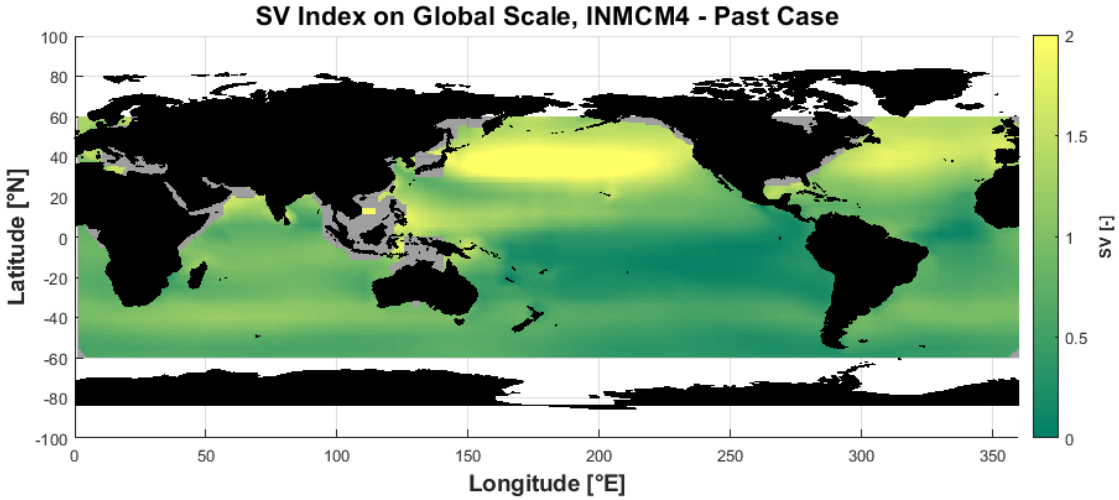

Figure 5.47: SV's result of INMCM4 model in past conditions.

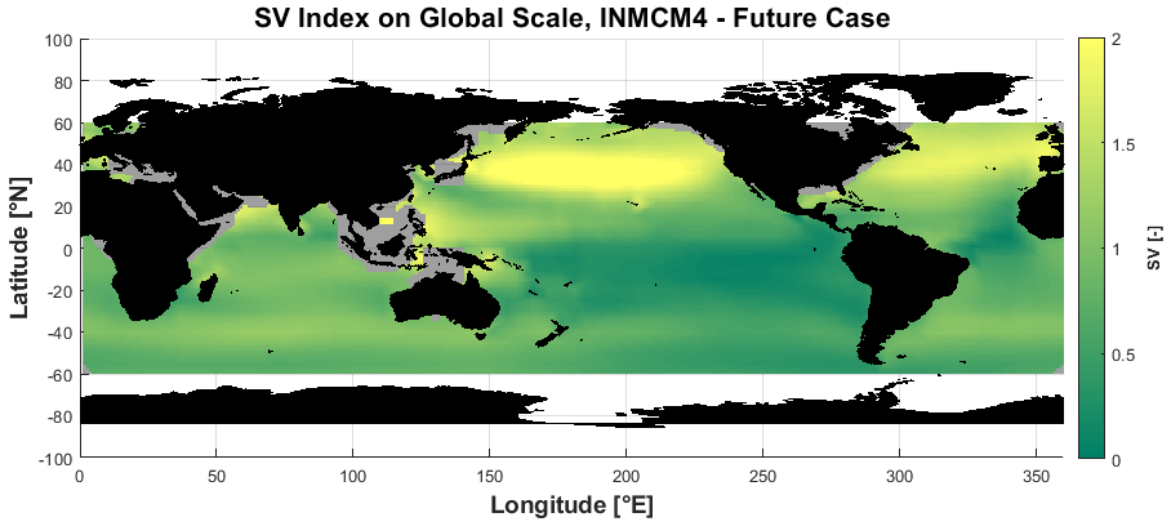

Figure 5.48: SV's result of INMCM4 model in future conditions.

5.3.5 Results of the MIROC5 model

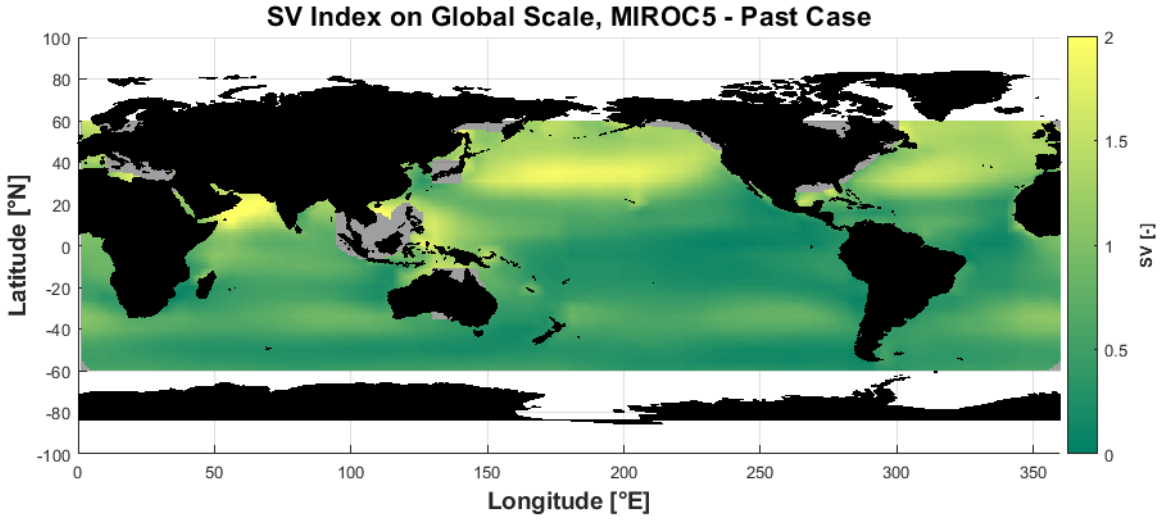

Figure 5.49: SV's result of MIROC5 model in past conditions.

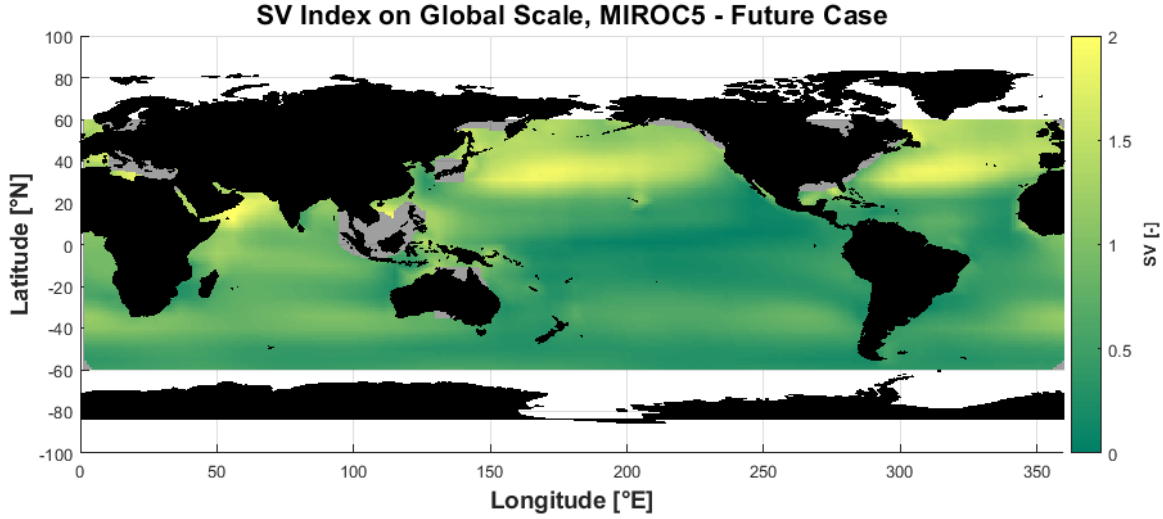

Figure 5.50: SV's result of MIROC5 model in future conditions.

5.3.6 Results of the models' ensemble

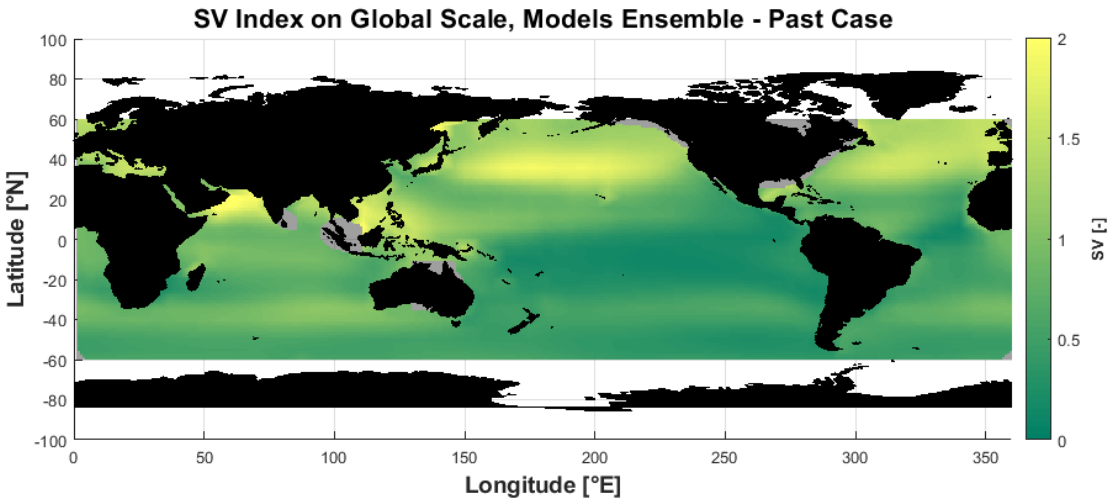

Figure 5.51: SV's result of model ensemble in past condition.

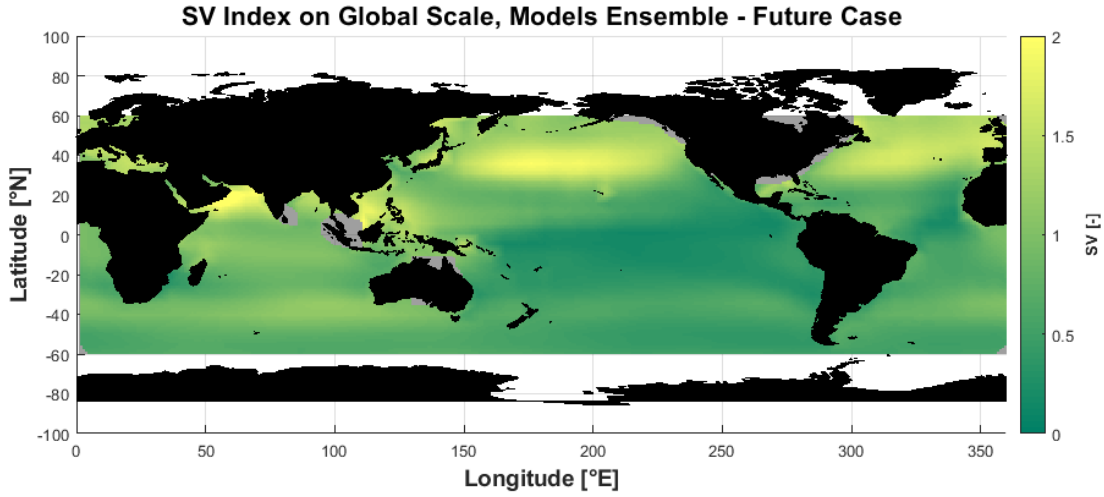

Figure 5.52: SV's result of model ensemble in future condition.

5.3.7 Bias and relative difference of SV between past and future

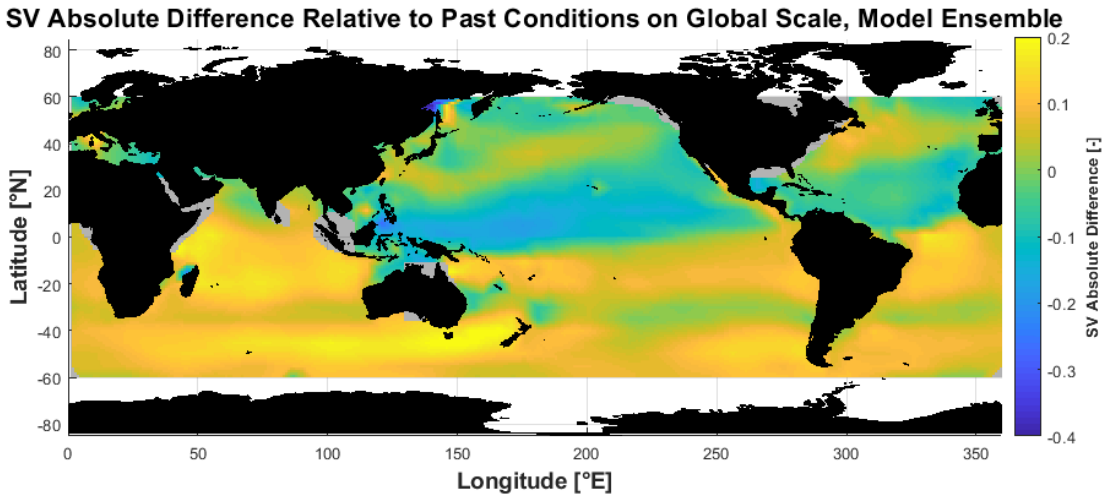

Figure 5.53: SV's bias of models' ensemble relative to past conditions

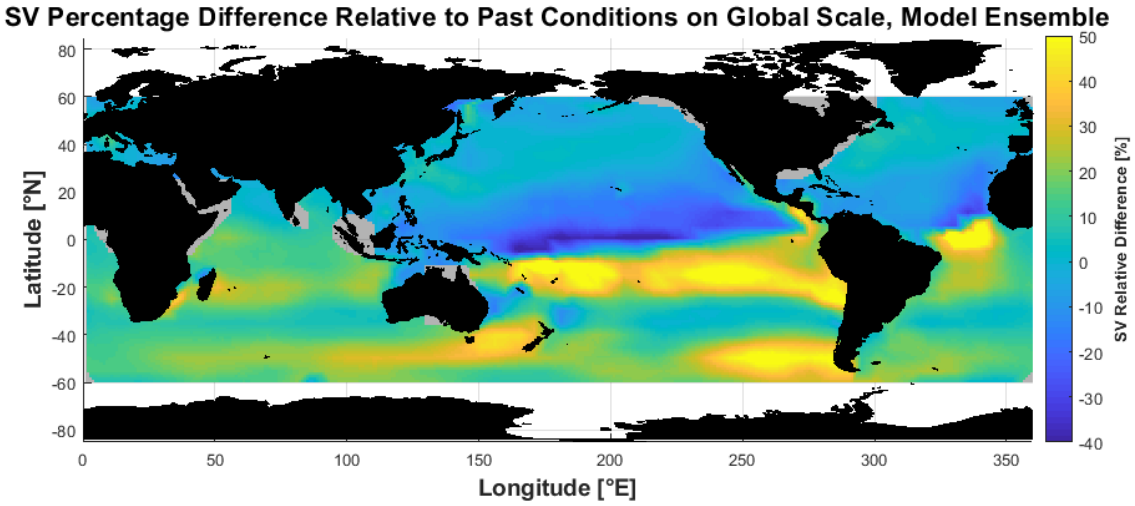

Figure 5.54: SV's relative difference of models' ensemble relative to past conditions

6. DISCUSSION

6.1 Wave Power

6.1.1 Past period

The five results of wave power outputted by the models show a similar distribution of wave energy resource but with certain differences in the values between the models. In general MIROC5 and INMCM4 esteem higher values, GFDL-ESM2M projects the smallest result while BCC-CSM1 and EC-EARTH are placed in the middle.

All the models agree in stating that the southern hemisphere is the one in which most of the energy generated by the waves is concentrated. The ocean that has the largest energy in this hemisphere is the Indian Ocean, where the maximum energy peaks agree on all five models. This specific area is located south-west of Australia.

Subsequently, the ocean with the greatest energy resource is the Pacific followed by the Atlantic Ocean, always in the southern hemisphere. In fact, high values of wave power are concentrated there, not too different from those of the Indian Ocean. Considering the disposition of the continents, it can be seen that these areas are those where the seas are more open, forming fetches that are thousands of kilometres long. This allows the waves generated by ocean storms even far away to reach these areas, contributing to this enormous energy resource which, however, mainly benefits from frequent and strong winds that blow from west to east in most of the year (*figure 6.1*).

In the period from 1986 to 2005 the model which stated the lowest value of the peak was the GFDL-ESM2M (*figure 5.9*) that esteemed 154 kW/m while the highest value was computed by MIROC5 with 187 kW/m (*figure 5.17*). By the way, all the models' peaks are located in the same region, south-west from Australia, as can clearly be seen from the plotted maps. As mentioned, the other high energetic area involves the southern part of the Pacific Ocean, with values a bit lower than Indian Ocean's ones. Here the highest wave power's result is given by MIROC5 and INMCM4 which seem to output more constant values, which slowly decrease moving East. MIROC5 esteems values from 140 to 130 kW/m while INMCM4 projects from 135 to 130 kW/m (*figure 5.13*). The wave energy computed by these two models is around 20 kW/m higher than the other models, which however state a more powerful area in eastern than in western Pacific. Between the southern areas of the three oceans, the Atlantic resulted as the

less powerful one. In this sector the energy resource is higher on the East side under Africa decreasing gradually moving to South America. The highest wave power of this area still belongs to MIROC5 that computed 154 kW/m against 102 kW/m stated by GFDL-ESM2M that has the lowest result of this zone.

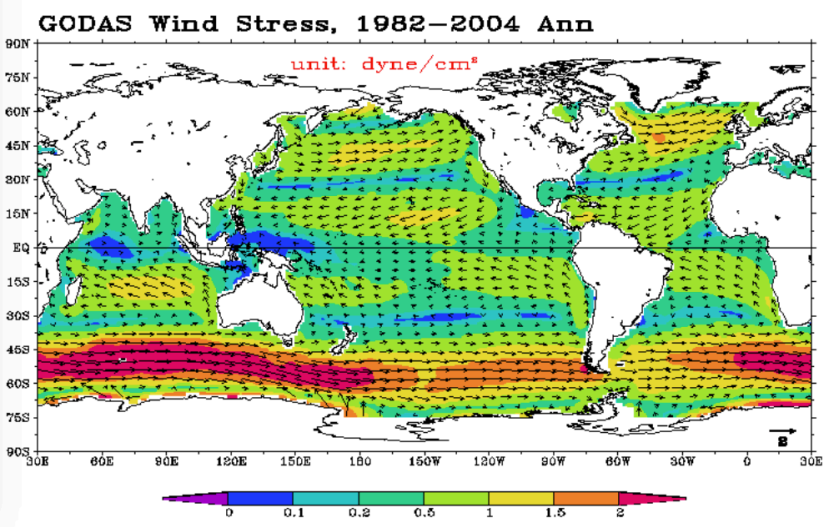

Figure 6.1: Average global wind pattern in the period 1982-2004 (Source: NOAA GODAS).

Among the areas of the northern hemisphere those with greater wave power can only be the Atlantic and Pacific because the northern part of the Indian Ocean has a limited surface due to the existence of the Asian continent. Consequently, this area is less affected by the harsh climate that characterizes the seas at high latitudes and that helps to propagate the waves. This happens in fact in the northern hemisphere of Pacific and Atlantic Oceans.

Apart from MIROC5, the other models esteem the Pacific as more powerful than Atlantic. The peak values that the models show for the North Pacific Ocean range between 115 and 70 kW/m, where the highest value belongs to the INMCM4 model. In the North Atlantic area MIROC5 esteemed a great wave power that reaches 106 kW/m. Its values are around 20 kW/m greater than the second higher model, while the GFDL-ESM2M seems to have the lowest results in both oceans, giving in Pacific and Atlantic 74 and 67 kW/m respectively. All the models, however, shoe a good agreement since the patterns of wave power computed in the oceans seem to be very similar between the models. In the Atlantic ocean the results show that the European side has more energy resource than the American one, while in the Pacific the highest wave power zone is placed in the open ocean from latitude 30°N to north.

The Atlantic area seems to have a high variation of wave power going from North to South. As a matter of fact, the tropical part of this ocean presents the lowest values of wave power between all the oceans' open areas and all the models agree with this pattern. The highest wave power's

values of mid Atlantic zone belong to MIROC5 model as the computation projects values around 25 kW/m while BCC-CSM1's result esteems about 15 kW/m (*figure 5.1*), which makes this model as the less powerful of this zone.

Among the sectors with the lowest wave power computed, there are enclosed areas like Mediterranean Sea, Gulf of Mexico and South China Sea. This result was expected because these seas are less subjected to storms and cannot be influenced by swell coming from afar.

Considering the averaged results of all five models (*figure 5.21*), it is possible to confirm the wave power trend described in the previous paragraphs. The southern hemisphere remains the one with the greatest wave energy resource. The zones with the greatest potential remain the same, being the area located to the south-west of Australia followed by the south of the Pacific and finally the south of the Atlantic Ocean. The sectors located north of the oceans are still considered to be areas of high wave energy density, despite the fact that it does not reach the values calculated in the southern hemisphere. Specifically, the North Pacific has a greater wave power than the North Atlantic.

With regard to the values found, there is a large area between 40° and 60° South and between 50 and 150° East in which on average there is a power of 140 kW/m but with a maximum value of 167 kW/m. The southernmost area of the Pacific Ocean has, according to the model ensemble, a mean wave power of 120 kW/m. This value decreases moving towards tropical waters and reaches values around 30 kW/m along the equator (in the open ocean) and 20 kW/m towards the Asian and American coasts. In the North open ocean there are maximum values between 92 kW/m and 80 kW/m on average, while along the coasts the wave power is reduced to about 50 kW/m.

The Atlantic Ocean, at higher latitudes, has good wave energy, which reaches its maximum off the coast of the British Isles (79 kW/m) and never drops below 30 kW/m at European latitudes. Obviously, the equatorial waters are less energetic, where the lowest limits of 15 kW/m are reached increasing to higher values of wave power going southwards. There, the ocean has a wave energy resource that can reach 120 kW/m south of South Africa.

6.1.2 Future period

With regard to the future conditions projected by the models, the results showed a tendency for all models to estimate an increase in wave power, except for some areas in some models.

Generally, the disposition of areas with both high and low wave energy resource will not shift much between past and future. As was to be expected, the southernmost and northernmost bands of the oceans will remain the most energetic and the equator will have the lowest wave energy values. The power peak values are more likely to change, but as already mentioned they will not move geographically. The area with the highest values will always be the area to the south-west of Australia, followed by the South of the Pacific and the Atlantic Oceans and then by the North of the same oceans. Generally, it was less evident in past results that the North Atlantic will have lower power than the North Pacific in all models.

The model with the highest values of wave power is always MIROC5 (*figure 5.18*). The results of this model will reach a maximum peak of 215 kW/m in the southern area of the Indian Ocean but, in general, the whole area will be subject to values above 170 kW/m. In the South Pacific, MIROC5 still estimates higher values than the other models, and in this area projects a resource of about 170 kW/m that only southwards of New Zealand and near South America drops to 130 kW/m. In these two southern areas of Pacific and Indian Oceans, the other models have very similar values and the peaks differ in the four models by only 4 kW/m, with INMCM4 estimating the maximum among the four with a peak value of 187 kW/m (*figure 5.14*). The arrangement of the energy areas is also distributed with similar values in the western zone of the Southern Indian Ocean, where INMCM4 is the most energetic model with values around 160 kW/m while the other three range between 130 and 140 kW/m. As far as concerned the Pacific Ocean, BCC-CSM1 (*figure 5.2*) and INMCM4 (*figure 5.14*) have a slightly more constant energy resource than EC-EARTH (*figure 5.6*) and GFDL-ESM2M (*figure 5.10*), which show a slight drop in wave power around the meridian 210° East. However, the wave power values of the whole area are around 130-120 kW/m except for INMCM4, which exceeds the other three models by about 10 kW/m on average.

The results in the northern part of the Pacific Ocean show how the INMCM4 model calculates values well above the other models, estimating average powers of about 110 kW/m with a peak of 120 kW/m. MIROC5 and BCC-CSM1 models calculate similar results, with an open ocean mean value of 80 kW/m, slightly lower than the 85 kW/m estimated by EC-EARTH but higher than those given by the GFDL model, which has the lowest wave power. In the Atlantic Ocean the wave power is estimated to be higher in the coasts of the British Isles by all models, and has a tendency to decrease moving towards the United States. The highest values always belong to MIROC5, where they oscillate around 70 kW/m, while the second most energetic model in the area is BCC, which is slightly lower. The model that estimates the lowest values for this

area is GFDL-ESM2M, which goes from 62 kW/m on the British coasts to 17 kW/m on the American coasts.

In the equatorial zones, the values of energy power are obviously among the lowest of the open ocean zones. In the Atlantic the MIROC5 model estimates values around 22 kW/m, BCC-CSM1 shows results around 10-15 kW/m, while the other models have intermediate values.

In the Pacific Ocean, on the equatorial fringe, the values are very similar among all the models, ranging from 15 kW/m around the coasts of Oceania to 20 kW/m on the American ones, with a peak in the open ocean around 30 kW/m for all models except for MIROC5 which estimates 40 kW/m. By shifting the attention to parallels at lower or higher latitudes, the energy resource obviously increases, reaching the values described above.

As regards the average projected by the model ensemble (*figure 5.22*), the extreme south of the area considered, in all the oceans, will increase its energy. Below the Australian coasts a peak of 191 kW/m is expected, with a very large area that will exceed 150 kW/m. In the middle of south Pacific the values are about 140 kW/m but a little further north, still in the southern hemisphere, they tend to fall more rapidly than in the past and by the Tropic of Capricorn reach on average 45 kW/m. In the northernmost part of the Pacific Ocean the peak is located in the open ocean and corresponds to 93 kW/m, but along the Japanese and Californian coasts the values drop to an average of 30 and 50 kW/m respectively.

The northern part of the Atlantic Ocean will not exceed 69 kW/m with a distribution very similar to those previously analysed in the individual models and with the wave power decreasing as it moves towards America. The same westward and downward trend is found in the southern area, where the peak of 130 kW/m is at the border with the Pacific Ocean while towards Argentina the energy resource will decrease. The values in the centre of the Atlantic are similar in the calculation to those for the period 1986-2005.

6.1.3 Differences of wave power between future and past periods

Among the five models used in the calculation of present and future wave energy, there are some particularities. In general, all the models show an average increase in wave power, but this is not homogeneous. In fact, there are many areas that have undergone a significant increase against other areas that have decreased their wave power, but the number of the last ones is lower.

Mainly, all the models agree in stating that the southern hemisphere will suffer a greater increase in energy resources compared to the northern hemisphere, which, on the contrary, will suffer for some models a decrease in vast areas of the Atlantic and in part of the Pacific.

MIROC5 and GFDL-ESM2M are certainly the models that calculate the greatest changes, compared to INMCM4 which foresees only small changes. BCC-CSM1 and EC-EARTH models are in the middle, with the last one presenting higher results between both.

The area with the greatest changes will be in the south, between latitudes 40° and 60°. Here MIROC5 and GFDL-ESM2M models predict a change in wave power with positive peaks of 40 and 45 kW/m respectively (*figure 5.19 and 5.11*), corresponding to 25% and 36% (*figure 5.20 and 5.12*) more than in the past. Apart from the peaks, these two models predict an increase of more than 30 kW/m in a large area further south of Australia. In the same area the INMCM4 model estimates the lowest power values of the five, but still corresponds to an increase of about 12 kW/m.

At the same latitudes but further west, in the Pacific Ocean's part near South America, only the results of MIROC5 and GFDL-ESM2M show a forecast of wave power increase that will be relevant, about 30 kW/m. The result, however, is discordant with the other three projections, which do not estimate a change in the resource. As a matter of fact BCC-CSM1 and INMCM4 state a wave power's increase along the limit of the studied area at 60° S (*figure 4.5)* and a decrease around latitude 40° S. Here, mostly INMCM4 esteem that this area could suffer a decrease of the resource with peaks of values equal to -10 kW/m (*figure 5.15*). Moreover, another different result of this zone is computed by EC-EARTH model which does not compute any relevant change in the wave energy's resource.

In the north of the Pacific Ocean, the MIROC5 model estimates a much greater decrease in the resource compared to the other models, with peaks of up to -20 kW/m corresponding to a decrease of 25%. The same MIROC5 estimates that a large part of the Pacific will reduce its wave energy resource, except in the western area contained between the equator and the Tropic of Capricorn, where there will be an increase of about 12%. The other models in the Pacific Ocean do not project major changes. In fact, the differences between future and present values fluctuate around 0, except for INMCM4 that estimates a slight increase of a few kW/m in the Californian area.

Moving the attention to the Atlantic Ocean, all the models agree in calculating a lowering of wave power, more marked in the northern hemisphere than in the southern one. Apart from MIROC5, which at high latitudes calculates a decrease of up to 30 kW/m and, going down

towards the Tropic, estimates average values of -5 kW/m, all the other models seem to agree on a slight decrease in the wave energy resource of a few kW/m. In the northern hemisphere MIROC5 and INMCM4 estimate a condition very similar to the past or with a slight decrease in energy, while GFDL-ESM2M assumes a slight increase of well-distributed values close to 1-2 kW/m. In the midrange there are models BCC-CSM1 and EC-EARTH that do not detect variations in wave power in the upper area but between latitudes 40° and 60° S estimate an average increase of 10% (*figure 5.4 and 5.8*) corresponding to about 10 kW/m (*figure 5.3 and 5.7*).

The differences between model ensemble averages in past and future conditions show that there will be areas where changes will be significant, both negative and positive, and areas where wave power will remain almost unchanged (*figure 5.23 and 5.24*).

The area that will undergo the greatest change will be, as usual, the southern band of the oceans, where there are the greatest variations, both absolute and relative. In fact, in a point of this area there will be a gap between the future and the present of 29 kW/m of wave power, corresponding at that point to an increase of 20%. The whole area south of Australia, however, shows an increase of at least 20 kW/m.

In the northern part of the Pacific Ocean, in the western half, the model ensemble foresees a vast area where the energy resource will decrease its values between 5 and 13%, lowering the wave power about 5 kW/m in the points most affected by the changes.

However, the maximum decrease is expected in the northern Atlantic Ocean. The northern area will suffer, according to the models' ensemble, a decrease of up to 9 kW/m, with a large area that will lose at least 5 kW/m. These values correspond to losses of 10-15% depending on the points considered.

Finally, the tropical belt between the equator and 23° S will experience an increase in wave energy resources of 5%, 6% and 3% in average in the Atlantic, Pacific and Indian oceans respectively.

6.2 Monthly Variability Index

6.2.1 **Past period**

With regards to the MV coefficient, from the maps shown in *section 5.3* it can be seen its distribution along the globe. Generally, what emerges at first sight is that if in the calculation of wave power the southern hemisphere was more relevant, in the calculation of MV is the opposite. In fact, it is noticeable that in most areas of the northern hemisphere this coefficient has decidedly higher values. This fact can be appreciated also in the plot of wave power's monthly average divided by regions (*figure 5.25*), where the trends of the North Atlantic, the North Pacific and the Tropical North Indian Ocean are certainly more marked than the other ocean regions. As a matter of fact, the curves that describe the mean monthly energy resource create a more severe difference between high resource months and low resource months.

In the northern hemisphere there are many areas with high MV values, but the arrangement of the areas with maximum values is not entirely uniform between the various models. In the Pacific Ocean there are two different model trends that represent MV. The first trend consists of a more marked central area between parallel 40°N and the Tropic of Cancer while the second trend shows a more scattered pattern from the Tropic to the northernmost areas. The estimation of the INMCM4, BCC-CSM1 and MIROC5 models (*figures 5.33, 5.27 and 5.35*) led to some results that follow more the first trend and between them INMCM4 has the most variable wave power's results. In fact it reaches values of MV up to 2.75 while MIROC5 and BCC-CSM1 esteem values that are not higher than 2.2. Moreover INMCM4 and MIROC5 extend their high values from open ocean to the coasts. On the contrary, BCC-CSM1 shows results more relevant in open ocean but along the coast drops to lower values around 1. The other trend, followed by EC-EARTH and GFDL-ESM2M, does not mark a band with high values but shows also that in the northernmost areas both models esteem constant values in the range 1.5-1.8, although EC-EARTH in general exhibits higher results.

In the Indian Ocean the maximum values of monthly variability are found in the Arabic Sea. Here some models have found points to exclude, but in the remaining points the results of MV reach the value of 4 in BCC-CSM1 and around 3 in the other models. So all models agree in evaluating this area as one with great variability, but the fact of having points that have been excluded creates some doubts on the Arabic Sea's values. However, considering the wind patterns and that this sea is influenced by monsoons and typhoons during some months of the year, the values are considered acceptable but with a certain degree of uncertainty.

A similar situation happens in the Mediterranean Sea, where the easternmost side of the sea also presents excluded points. However the results esteem values in the range 1.5-2 with some exceptional higher value in MIROC5, but the presence in the literature of other studies (Besio, Mentaschi and Mazzino, 2016) which analysed in a deeper way this area confirms the reliability of the results despite the excluded points' problem.

In the North Atlantic Ocean, the five models display very similar patterns. Except from MIROC5 that shows a low decrease of MV between the middle of the ocean and the European coasts, the other models estimate the eastern area as the most variable. In particular, INMCM4 has a large area where MV values of 2.1 are reached. The remaining models (GFDL-ESM2M, EC-EARTH and BCC-CSM1) calculate the ocean sector near Europe as the most energetically variable, with values up to 2 and large areas with MV greater than 1.8.

In the southern Atlantic Ocean, the values seem to agree in almost all the analysed area. In the area between the parallel 40°S and the Tropic of Capricorn all the models esteem higher values than in the rest of the ocean. The east side is more variable than the west side of this Ocean, especially for MIROC5, which estimates the peak value of 1.4 while BCC-CSM1 reaches 1 being the lowest result for this ocean.

Also in the other oceans, the areas of the south that are more sensitive to variations over the months, according to all models, are found in the ocean belt enclosed approximately from parallels 25°S to 45°S, where the maximum MV values reached are between 1.1 and 1.3. MIROC5 seems to compute lowest results in the Indian Ocean as it estimates MV values smaller than 1 all over the ocean, while in the Pacific Ocean the model with the lowest results is EC-EARTH which does not esteem MV values greater than 0.7. The INMCM4 and BCC-CSM1 models agree in calculating very constant values along the whole range described above with mean values over 1.2 in the Indian Ocean and 0.8 in the Pacific Ocean. In general, the Indian Ocean is more variable since the results are not lower than 0.7 in all models, while in the Pacific Ocean, from the equator to the tropic the values are included in the range 0.2-0.4.

With regard to the model ensemble results of the MV coefficient, they assume a slightly more homogeneous distribution of the individual results of each model (*figure 5.37*). The maximum values are always found in the northern hemisphere. In the Pacific and Atlantic, at very similar latitudes, they reach 2.2 and 1.9 respectively, with large areas northernmost the oceans with MV greater than 1.7. Moreover in the Atlantic, the part close to the European coasts outputted higher MV values than American coasts, which in turn are a bit more variable than the Asian ones in the Pacific Ocean. In the Indian Ocean, the zone of the Arabic sea appears to have major

intraannual changes but, as stated above, in this region there is a threshold of uncertainty in the reliability of the results. In the southern hemisphere the results are lower than in the North and the Indian Ocean shows more uniform values that are mot lower than 0.7 and reach a peak of 1.2. On the other hand, the Pacific Ocean's equatorial fringe results as the most energetically constant zone as its MV is close to zero (0.3) in a large portion of ocean. Finally, the values found in the Mediterranean Sea seem to be reliable when compared with those obtained by Besio et al. (2016), since they remain under 1.9 in all the sea.

6.2.2 **Future period**

In the future computations the INMCM4 model is the one that projects a more variable energy resource while the other models agree in most of the areas with similar results and patterns.

In the North Atlantic, in all models high values of MV are expected, reaching up to 2.4, in the area extending from America to Europe. From the parallel located at about 30°N to the north, values not smaller than 1.6 are recorded in vast areas in all models. Among them, that with the lowest values is BCC-CSM1 (*figure 5.28*), especially in the north-west zone. On the contrary, MIROC5 and INMCM4 (*figure 5.36 and 5.34*) are the models with the largest surface with high variability of wave power, occupying a major part of the North Atlantic Ocean with peaks of 2.1 and 2.4 respectively.

In the Pacific Ocean, approximately between parallels 25°N and 45°N, three models agree to consider a maximum monthly variability around 2.25, while the INMCM4 and GFDL-ESM2M (*figure 5.34 and 5.32*) models estimate the highest (2.8) and the lowest peaks (2.0). Moreover GFDL-ESM2M and BCC-CSM1 project that the area with higher results will not extend to the eastern and western extremes of the ocean, as opposed to the other models, which spread their regularity towards the continents.

In the northern Indian Ocean there are areas where the value of MV is very high, reaching 3.7 in the BCC-CSM1 model and more than 3 in all models in the Arabic Sea. For this area, the considerations about the reliability of the results made before are still valid.

As regards the southern hemisphere, its variability is much lower than that of the northern hemisphere. The maximum values in this hemisphere are found in the GFDL-ESM2M model, which estimates MV up to 1.6 between Australia and Africa. The other models project here, however, very similar values, being MIROC5 the model which gives the lowest results, in which a peak of 1.1 and large areas with values smaller than 0.9 are found. After the Indian

Ocean, the Atlantic Ocean is the second most variable of the southern hemisphere. Here the pattern is similar for all models and the values are around 1.2, with MIROC5 having the highest values (1.4) in the usual band near Africa. Finally, the Pacific Ocean does not seem to experience intraannual wave power's variability since the results are around 1 in all models.

However, the zones foreseen to have a more constant wave power are the equatorial ones, because obviously they are less subject to meteorological changes during the year. The central Pacific area has the lowest values in all models. In fact, in this area the minimum peaks of 0.15-0.20 are reached in the models. The Atlantic Ocean in the equatorial zone also undergoes low monthly changes, although its values are slightly higher than in the Pacific Ocean. In fact, INMCM4 results the model with the lowest MV reaching the minimum peaks of 0.3 that increase moving to Africa, where values over 1 are reached by all models.

Considering the results given by the model ensemble, the MV coefficient provides definitive evidence of the great intraannual variability of the wave power in the northern hemisphere compared to the southern one (*figure 5.38)*, as predicted by the results of the individual models.

In the northern hemisphere, the Tropic of Cancer marks two different areas of MV in a rather distinct way. In the upper zone it is possible to find the maximum results (2.1 in the Atlantic Ocean and 2.3 in the Pacific) with values that do not fall below 1.3 at any point. Also the areas near the Asian coasts have a large mean monthly variability around 1.5, but near the Chinese coast there is a point considered as outlier that outputted too much high values and that gives to this area a reliability uncertainty. The same happen in the Arabic Sea but with the difference that these high results are more supported by meteorological events. In Atlantic and Pacific Oceans, from the Tropic of Cancer to the Equator, the values drop to 0.5 in both oceans, except for the west side of the Pacific, where the model ensemble estimates results around 1.

The equatorial zone of the Pacific is the ocean space where wave power conditions vary less than any other. In fact, we can see in *figure 5.38* a large area where MV values remain on average smaller than 0.5 with a lower peak of 0.25 in the Pacific, while wave power's projections in the Indian Ocean are more variable with MV values about 1.1. At the same latitude but in Atlantic waters there is the second most energy stable area, where the lower peak is 0.3 and the values do not exceed 0.9.

Finally, the Mediterranean sea presents values of MV that do not exceed 2 and vary not being smaller than 1.6 on the west side and 1.3 on the east side.

6.2.3 **Differences of MV between future and past periods**

Analysing the calculated differences between the periods 1986-2005 and 2081-2100 it is possible to notice how and in what entity the monthly variability of the wave power will change and especially what places are projected to change. Focusing on *figures 5.39 and 5.40* it can be seen that the expected changes will took place mostly in horizontal bands, where the wind patterns operate (*figure 6.1*).

However, in general it can be stated from the images that the area that will undergo the highest relative increases of MV is the South Pacific, where just southern than equator an average increase of 0.10 is expected in MV values, with a maximum of 0.13 that will correspond in percentage to an average increase of 50% in the monthly variability of the energy resource. Moreover, another great change, in relative terms, in this area is expected at low latitudes, where an increase of about 35% corresponding up to 0.20 of MV is projected. By contrast, the greatest diminution of monthly variability is expected in the northern hemisphere by the models ensemble. Except for the northern part of the ocean which states a very small relative increase, the rest of the Pacific Ocean will sustain more constant wave power values along the months, represented by averaged decreases up to -35% and -20% in tropical waters. This decrease of relative values corresponds to an absolute difference between past and future averaged computed results of -0.15 in the tropical area.

The Atlantic Ocean will suffer similar patterns to those of the Pacific. As a matter of fact, it will be affected by an increase located in the southern hemisphere, a decrease in north tropical waters and an increase in the northernmost part of the northern hemisphere. By the way, the entity of these changes is projected to be less marked than those of the Pacific. The zones of ocean close to both African and American continents project an increase of MV up to 40%, which is high due to the low values of MV in that zone. In fact, this increment corresponds to an increase of 0.10 in MV. As already said, the tropical waters of northern hemisphere are projected to decrease their MV and this change is quantifiable in a -10% on average. In the southern hemisphere, the monthly variability differences between the two periods are projected to increase on the west side while the east side, near Africa, will produce a more constant wave power.

On average, the Indian Ocean will experience a MV increase in almost completely its surface, calculated from the model ensemble, equal to 0.14 in equatorial waters and up to 0.2 in the band between the tropic of Cancer and the latitude 45°S. The percentage of increase of this ocean is

computed giving a relatively uniform pattern, with a general increment of 15%. The only sector that will suffer a slight decrease will be the Arabic sea (-5% on average).

Finally, the Mediterranean Sea is projected to change its MV values in negative on the east area and in positive between Spain and Italy, but these changes correspond to results lower than 10% in both positive and negative variations.

6.3 Seasonal Variability index

6.3.1 Past period

The seasonal variability, covering a longer period than the monthly variability, will obviously have lower values, but the patterns of the values compared to those of MV will be very similar. In fact, it can be seen that also in this case the northern hemisphere is clearly more subject to variations compared to the southern hemisphere.

The two oceans that have a more variable resource are the Pacific and the Atlantic. The last one in the northern part is high influenced by the alternation of weather seasons, which confer relevant values of SV in almost all the portion of the sea above parallel 25°N where in fact, in any model's results, drop below the value of 0.8. Among the models, the one that has a larger surface of high values is INMCM4 (*figure 5.47*), while that with smaller SV is GFDL-ESM2M (*figure 5.45*). The first model shows a peak of 1.85 and high results all over the northern part of the Atlantic, while the other reaches a maximum value of 1.56 and, in general, exhibits less relevant values.

In the Atlantic's southern areas of the northern hemisphere, the arrangement of SV values is very similar in all models. Around the coordinates 5°N 330°E, the minimum values are reached and oscillate between 0.1 and 0.2, while between latitudes 30°S and 40°S the maximum values of the southern Atlantic occur and are obtained by MIROC5 (1.1) although the other models have more constant patterns with higher mean values.

The northern Pacific Ocean presents high values of SV, located mainly in open ocean and more precisely around latitude 35°N, above which all models reach at least SV=1.6 and where INMCM4 computes the peak as 2.4. In particular, GFDL-ESM2M and BCC-CSM1 (*figure 5.45 and 5.41*) estimate the seasonal variability with values below the average. Moreover, the second of both results to be the one showing more constancy in the energy resource along the Asian

coasts where, on the contrary, MIROC5 and INMCM4 (*figure 5.49 and 5.47*) foresee strong variations in wave power. This trend is less marked in the EC-EARTH and GFDL-ESM2M models (*figures 5.43 and 5.45*), but they estimate high results in the middle of the northern Pacific Ocean as like as MIROC5 does.

As far as the equatorial and tropical zone are concerned, SV values drop significantly as expected, and the absolute minimums are included in the range 0.07-0.15 (INMCM4 and EC-EARTH respectively). In this oceanic region, the seasonal variability remains low almost everywhere. In fact, it almost never exceeds 0.4 except near the Oceania's coast. Finally, in the southernmost part of the Pacific Ocean the values do not increase significantly, reaching peaks of 0.5-0.8, depending on the model and located for all of them in the usual southern hemisphere's band.

Moving the attention to the Indian Ocean, it can be seen as MIROC5, which is usually the model that estimates higher values, here computes the lowest results. In fact, in the southern part it reaches the maximum value of 0.9 in the south-west of Australia. In this region, representing according to all models the area with the greatest variability of the Indian Ocean, the other results have values not less than 1 and up to 1.2 (BCC-CSM1 and EC-EARTH). In the tropical zone, near the Indian coasts, high values have been computed as it happened in the MV, but the low reliability of the results is still present in this sea.

For what concern the results obtained by the model ensemble, it can be seen from *figure 5.51* that the values in the southern hemisphere of the Indian Ocean, as well as the values in the southern Atlantic, thanks to a very good correspondence of all models in these areas, are very similar to those described for singular models.

In the North Atlantic Ocean, the results are quite homogeneous from the Tropic to the north, reaching the SV peak of 1.6 (in open ocean and near the British Isles) and never falling below 1, except near the coast of Africa, where values around 0.8 are detected.

A very similar situation occurs in the north of the Pacific Ocean, where values slightly lower than the Atlantic ones have been obtained (1.9), and where even along the coasts there are significant values strongly influenced by the results obtained by MIROC5 and INMCM4 in these seas. The minimum values found in the equatorial zone of the Pacific Ocean are equal to 0.15, but a very large area has SV values not higher than 0.4, especially in the eastern part of the ocean while the west side, near Oceania, reaches higher values up to 1.1.

In the South Pacific the values of seasonal variability remain very constant oscillating around 0.6 near the band between the tropic and 45°S. At these latitudes, in the other oceans, the results are higher than the Pacific ones. As a matter of fact, in the Indian Ocean the peak, located south-west of Australia, reaches 1.1 with other values not being lower than 0.9 while in the Atlantic Ocean the maximum value is estimated to be 0.9.

Finally, for what concerns the Mediterranean sea, the results exhibit a value of 1.5 in most part of the region, except for the area below Spain where the SV coefficient is esteemed around 1.

6.3.2 Future period

In the computation under future conditions the INMCM4 model is still the one with higher values and also can be noticed that the patterns of seasonal variability remain similar to the past ones but with an increase in some zones, mostly in the Atlantic Ocean.

In the north Indian Ocean, BCC-CSM1 (*figure 5.42*) is the only model which esteems extreme values while other models, in spite of evaluating in this area a great SV variability, outputted more balanced values. However, this ocean is considered by all models as the most variable. All models, in fact, project mean SV values near 1 in this area, with only MIROC5 (*figure 5.50*) esteeming 0.9. In the southern part, under the tropic's latitude, the model that computes the highest values is BCC-CSM1, which calculates a maximum of 1.4. The remaining models show lower values in the results, but the same tendency of SV to increase its values in this area, located around the latitudes of Australia and South Africa.

In the Pacific Ocean, at the same latitudes, the wave power is projected to change over the seasons less than in the Indian Ocean and, in fact, the values here are considerably lower. Except EC-EARTH model (*figure 5.44*) which gives the lowest results, the other models esteem a similar peak value around 0.8. These values, although being low, are greater than those obtained near the equatorial zone, where the absolute minimums are between 0.9 and 0.10 with large areas having SV values over 0.3, except for Asian tropical areas, where SV is higher. This symbolizes that the wave power remains constant practically all year, especially in the EC-EARTH model as shown in *figure 5.44*. On the contrary, in the northern Pacific the seasonal variability is much more relevant. The maximum value of SV (equal to 2.3) is reached in INMCM4 (*figure 5.48*), while BCC-CSM1 computes the lowest peak (1.7). This is also the model with the smaller area of high variability values. In fact, unlike the other models, BCC-

CSM1 has high values in the open ocean which then decrease more quickly than other models going towards the coast.

In the North Atlantic Ocean there is another area that has great variability. Here, in particular the models INMCM4 and MIROC5 calculate areas where SV reaches 1.85, but the remaining models also estimate a high tendency of the energy resource to seasonal variability. The patterns in which SV decreases are similar to those already seen for MV and correspond to the Tropic of Cancer in the west and the parallel 30°N in the east side of the ocean. Above this imaginary boundary, the results state that SV never falls below 1. Finally, in the southern hemisphere of the Atlantic Ocean, the model with the highest values is INMCM4 which estimates a maximum of 1.1 around South Africa but, in general, the variability of these waters is much lower than that of the northern hemisphere.

Analysing the average results of the five models (*figure 5.52*), the trend of seasonal variability in the areas of the southern hemisphere is very similar to those of the individual models, given the great coincidence that they present in these areas. The mean values of the northern hemisphere confirm the main property of this hemisphere, definitely subject to seasonal weather changes. Here, from the latitude corresponding to the Tropic of Cancer to upper latitudes large areas with high results of SV are estimated, especially in open ocean.

As mentioned above, the Pacific and Atlantic Oceans show high SV values, and their peaks are respectively 2.0 and 1.7 in the northernmost area of the northern hemisphere. Both oceans tend to decrease SV values moving towards the coasts. The Pacific Ocean presents a disparity between the Asian zone, which is more variable with mean SV around 1.3, compared to the American area which is more constant with lower values around 1. The Atlantic Ocean changes its SV more slowly and, in fact, along the coast of Africa and America it reaches 1.0 while the European coasts are still presenting great variability (SV=1.6).

Finally, in the Mediterranean Sea the eastern zone has more constant seasonal wave power values and the model ensemble gives a value of 1.0 while, focusing on the western part, the highest values that can be reached are around 1.5.

6.3.3 Differences of SV between future and past periods

From *figures 5.53 and 5.54* of *section 5.4.7*, the differences between the models' ensemble of SV in past and future conditions can be analysed. These differences represent both absolute and relative values.

There, it can be noticed that the variation of SV follows the same patterns of MV and states that in the southern hemisphere there will be a significant increase of the seasonal variability, while the northern hemisphere will generally sustain a decrease of such coefficient.

Firstly, the Atlantic Ocean is expected to increase on average its variability, but this increase will happen mostly in the southern part where SV will have an increment between 0.1 and 0.15. This result around the equator corresponds to high increases in percentage values, due to the low values of SV coefficient. As a consequence, a slight absolute increase determines increments up to 80% in this area. In the tropical waters of the northern hemisphere a reduction of 20% in SV is projected, while northernmost another increase takes place between Europe and America.

On the contrary, in the Pacific Ocean it is expected that the energy resource will be regularized on a large part of its surface. This phenomenon promises to be strongly marked in the equatorial belt and partly in the tropical bands. More precisely, in the northern tropical waters a decrease of SV between -10% and -35% is expected, which in absolute terms corresponds to a difference of -0.18. Moreover, a high increase of seasonal variability is also projected in the southern tropical waters, around 40% (0.1 in absolute value). The area that will suffer major increments in absolute difference will be located near Australia, where an increment of 0.2 in SV is estimated.

For what concerns the Indian Ocean, the results state that it will increase its variability less regularly than MV, being however from 10% to 25%, with a range of absolute values between 0.18 and 0.05. On the contrary, the Arabic Sea, that increases MV values between past and future, will not change its SV index.

Finally, the Mediterranean Sea does not show significant changes in SV although there is an outlier located near Italy, that outputted a singular high value. As a matter of fact, the pattern of this sea resulted to have percentage values relative to SV changes close to 0%.

7. CONCLUSIONS AND FUTURE DEVELOPMENTS

7.1 Conclusions

The results obtained and discussed in the previous *chapter 6* have mainly confirmed the expectations, a sign of their reliability that can be considered suitable. This consideration has been possible also thanks to the fact that the results of this work are consistent with the studies previously carried out in this field, which, although they do not analyse the impact of climate change on energy resources, they studied the present wave power that is similar to the one estimated in the period 1986-2005 of this work.

On the basis of the model ensemble, it can be observed that the southern hemisphere is the one with the greatest energy potential, especially in the south-east of the Indian Ocean, where in the past mean values of 167 kW/m were reached. Nevertheless, this band also reaches great energy values in the other oceans. In the northern parts of the northern hemisphere there are also areas with high energy potential, in the Pacific more than in the Atlantic, which although they do not reach the average wave power of the south, they have significant values. In future projections, the wave power patterns will remain the same, but according to model results their values will differ from the past. Due to climate change, more changes will occur at higher latitudes where the climate is more severe. In fact, it has been obtained that the southern hemisphere will undergo a generic increase in wave power along its entire southern belt and in particular the Indian Ocean will suffer the greatest increases in wave power, which will be well distributed over its entire surface with vast areas that will increase by more than 20 kW/m. In the northern hemisphere, on the other hand, the entire Atlantic Ocean will decrease its energy resource while the Pacific Ocean will suffer a drop in wave power mainly in the Asian area as is expected to happen in the Mediterranean Sea.

The results of the monthly and seasonal coefficient of variability have shown that the northern hemisphere will be more affected by changes in the resource over the months and the seasons, a reflection of the fact that this hemisphere will be more exposed to climatic differences between the winter and summer periods. In the computation of the variation of these coefficients between the two time periods, the greatest increases caused by climate change are always expected in the southern hemisphere more than in the northern one, where, on the contrary, a decrease in the variability of the resource is foreseen. In particular, also in this case, the Indian Ocean will undergo an increase in MV and SV in a much more distributed way than

the other oceans and the greatest absolute variations are expected near Australia. However, the major variations in percentage will occur along two bands of the southern Pacific Ocean. On the contrary, the northern hemisphere is projected to make more regular its wave power in areas near the equator. In fact, the MV and SV coefficients will decrease in a large area of the Pacific Ocean and in a relative vast region of the Atlantic Ocean. Moreover, in the northern areas of these two oceans the results project an increase in the monthly variability in the open Pacific Ocean and in an entire section of the Atlantic Ocean that will also reach the European and American coasts. Finally, on a seasonal scale, this variation will be slightly different along the European coast but will increase instead on the Asian coasts of the Pacific Ocean. As far as the Mediterranean Sea is concerned, no major changes in the variation of the resource over the course of the months and seasons are expected, although, as already mentioned, a general lowering of the average wave power has been projected.

Consequently, it is possible to affirm that, from the point of view of the available wave power resource, the southern hemisphere will mainly benefit from climate change, in particular the countries surrounding the Indian Ocean, which will have a greater energy resource to take advantage of. The opposite can be said for the European and American countries surrounding the Atlantic Ocean. Here, the climate change is expected to have a negative effect on the production of energy from the waves. Obviously, although the areas with the highest average wave power are in the open ocean, these values are hardly exploitable given the extreme difficulty and economic cost of operating in so remote areas. Despite this, the coasts that surround these high-energy areas will still be those that can be mostly taken into account for the production of energy from the waves, even if they have values of wave power lower than those from open oceans.

In addition, the increase or decrease in the monthly and seasonal variability coefficients due to climate change is also relevant for the energy production. In fact, the MV and SV indexes can determine the dimensioning of the WEC technologies in an important way. Indeed, a structure built to exploit a constant resource can be dimensioned more efficiently than a structure that has to draw on a variable resource and, therefore, will alternate periods with low energy to periods with too much energy, when the wave power is higher than the WEC's power so that it will not be fully exploited. In other words, a more constant resource allows to have structures with a higher capacity factor, designed to operate for longer at more constant powers.

On the basis of this, since the southern hemisphere and, in particular, the entire Indian Ocean will suffer an increase in the coefficients of variability, they will be disadvantaged by climate

change, which will increase the difference in resource from one month to the other and, therefore, will contribute to a more irregular production of energy by wave energy converters (WECs). On the other hand, in the northern hemisphere, since there will be an improvement in the constancy of wave power, climate change could lead to a more efficient WEC operation. However, this will not happen in the whole hemisphere, since the European and American coasts are projected to deal with an increase in MV and SV as well. Consequently, climate change will also bring disadvantages in those areas that, among other things, are now those where most of the research and testing of WECs is being carried out.

7.2 Future developments

Among the possible future developments of this work there is the implementation of the same process but using a greater number of points, reminding that only 1310 points out of 32516 available from the models have been considered. Consequently, the development of a computation on a larger number of points could lead to even more detailed results since it would require minor energy power's interpolation and, in other words, a shorter distance between subsequent points.

Another future application could be to carry out a similar process but applied more specifically to the coasts. Since the application of wave energy technologies takes place on-shore or near-shore for reasons of economic, operational and maintenance feasibility, it becomes a logical consequence to carry out a more in-depth study of the wave power's variations caused by climate change on coastal areas. Consequently, a future development could be to study these areas using only the models' points of the coastal zones or, alternatively, by carrying out the same process as for this thesis but with a new specific model's computation, targeted to these areas, that foresees the realization of an even denser points' grid.

Finally, a specific study on some closed seas could be carried out in order to ensure greater reliability of results in seas such as the Mediterranean, the Chinese Sea and the areas belonging to the Oceania's archipelagos. It may be useful to develop a computation only on these areas so that the results obtained could include a greater number of points and, therefore, have greater reliability.

8. **REFERENCES**

Ardhuin, F., Rogers, E., Babanin, A.V., Filipot, J.F., Magne, R., Roland, A., van der Westhuysen, A., Queffeulou, P., Lefevre, J.M., Aouf, L., Collard, F. (2010). Semiempirical dissipation source functions for ocean waves. Part I: definition, calibration, and validation. Journal of Physical Oceanography, 40, 1917–1941.

Arinaga, R.A., Cheung, K.F. (2012). Atlas of global wave energy from 10 years of reanalysis and hindcast data. Renewable Energy, 39, 49-64.

Besio, G., Mentaschi, L., Mazzino, A. (2016). Wave energy resource assessment in the Mediterranean Sea on the basis of a 35-year hindcast. Energy, 94, 50-63.

Casas-Prat, M., Sierra, J.P. (2013). Projected future wave climate in the NW Mediterranean Sea. Journal of Geophysical Research, 118, 3548–3568.

Casas-Prat, M., Wang, X.L., Sierra, J.P. (2014). A physical-based statistical method for modeling ocean wave heights. Ocean Modelling, 73, 59–75.

Casas-Prat, M., Wang, X.L., Swart, N. (2018). CMIP5-based global wave climate projections including the entire Artic Ocean. Ocean Modelling, 123, 66-85.

Charles, E., Idier, D., Delecluse, P., Déqué, M., Cozannet, G. (2012). Climate change impact on waves in the Bay of Biscay, France. Ocean Dynamics, 62, 831–848.

Cornett, A,M. (2008). A global wave energy resource assessment. In: International offshore and polar engineering conference, Vancouver, Canada, pp. 318-326.

Dean, R.D., Dalrymple, R.A. (2004). Coastal processes with engineering applications. Cambridge University Press, Cambridge, UK.

Déqué, M., Rowell, D.P., Lüthi, D., Giorgi, F., Christensen, J.H., Rockel, B., Jacob, D., Kjellström, E., de Castro, M., van den Hurk, B. (2007), An intercomparison of regional climate simulations for Europe: Assessing uncertainties in model projections. Climatic Change, 81, 53–70.

EMEC, Pelamis Wave Power. (http://www.emec.org.uk/about-us/wave-clients/pelamis-wave-power/).

Grabemann, I., Weisse, R. (2008). Climate change impact on extreme wave conditions in the North Sea: an ensemble study. Ocean Dynamics, 58, 199–212.

Gonçalves, M., Martinho, P., Guedes Soares, C. (2014) Assessment of wave energy in the Canary Islands. Renewable Energy, 68, 774-784.

Guillou, N., Chapalain, G. (2015). Numerical modelling of nearshore wave energy resource in the Sea of Iroise. Renewable Energy 83, 942-953.

Gunn, K., Stock-Williams, C. (2012). Quantifying the global wave power resource. Renewable Energy, 44, 296-304.

Harrison, G.P., Wallace, A.R. (2005). Sensitivity of wave energy to climate change. IEEE Transactions on Energy Conversion, 20, 870-877.

Hemer, M.A., Fan, Y., Mori, N., Semedo, A., Wang, X.L. (2013). Projected change in wave climate from a multi-model ensemble. Nature Climate Change, 3, 471–476.

Hemer, M.A., McInnes, K.L., Ranasinghe, R. (2012). Climate and variability bias adjustment of climate model-derived winds for a southeast Australian dynamical wave model. Ocean Dynamics, 62, 87.

Hemer, M.A., Trenham, C. (2016). Evaluation of a CMIP5 derived dynamical global wind wave climate model ensemble. Ocean Modelling, 103, 190–223.

Iglesias, G., Carballo, R. (2010). Offshore and inshore wave energy assessment: Asturias (N Spain). Energy, 35, 1964-1972.

Iglesias, G., Carballo, R. (2011). Wave resource in El Hierro e an island towards energy self-sufficiency. Renewable Energy, 36, 689-698.

IPCC (2007). Climate change 2007, The physical science basis, in: Contribution of working group I to the fourth assessment report of the Intergovernmental Panel on Climate Change, edited by: Solomon, S., Qin, D., Manning, M. Cambridge University Press, Cambridge, UK, 2007.

IPCC (2013). Climate change 2013, The physical science basis, in: Contribution of working group I to the fifth assessment report of the Intergovernmental Panel on Climate Change, edited by: Stocker, T.F., Qin, D., Plattner, G.-K., Tignor, M., Allen, S.K., Boschung, J., Nauels, A., Xia, Y., Bex, V., Midgley, P.M. Cambridge University Press, Cambridge, UK, 2013.

Knapp, W., Böhm, C., Keller, J., Rohne, W., Schilling, R., Holmén, E. (2003). Turbine development for the Wave Dragon energy converter. Proceedings of the Hydro 2003 Conference, Croatia.

Liberti, L., Carillo, A., Sannino, G. (2013). Wave energy resource assessment in the Mediterranean, the Italian perspective. Renewable Energy, 50, 938-949.

Lionello, P., Cogo, S., Galati, M.B., Sanna, A. (2008). The Mediterranean surface wave climate inferred from future scenario simulation. Global Planetary Change, 63, 152–162.

Mackay, E.B.L., Bahaj, A.S., Chellenor, P.G. (2010a). Uncertainty in wave energy resource assessment. Part 1: historic data. Renewable Energy, 35, 1792-1808.

Mackay, E.B.L., Bahaj, A.S., Chellenor, P.G. (2010b). Uncertainty in wave energy resource assessment. Part 2: variability and predictability. Renewable Energy, 35, 1809-1819.

Makai Ocean Engineering, (2013). Makai to add 100-Kilowatt turbine generator to the Hawaii OTEC Facility in Kona. (https://www.makai.com/2013_04_29_makai_100kw_otec_facility/).

Mori, N., Shimura, T., Yasudaa, T., Masea, H. (2013). Multi-model climate projections of ocean surface variables under different climate scenarios–future changes of waves, sea level and wind. Ocean Engineering, 71, 122–129.

Mori, N., Yasuda, T., Mase, H., Tom, T., Oku, Y. (2010). Projection of extreme wave climate change under global warming. Hydrological Research Letters, 4, 15–19.

NS Energy (2019). 2019. Simec Atlantis decommissions 1.2 MW SeaGen tidal project in Northern Ireland. (https://www.nsenergybusiness.com/news/simec-atlantis-seagen-tidal/)

Nikulin, G., Kjellstrom, E., Hansson, U., Strandberg, G., Ullerstig, A. (2011). Evaluation and future projections of temperature, precipitation and wind extremes over Europe in an ensemble of regional climate simulations. Tellus A, 63, 41–55.

Rolandez, G., Abgottspon, A., Staubli, T. (2014). Discharge measurements at La Rance tidal power plant using current meters method. 10th International Conference on Innovation in Hydraulic Efficiency Measurements, Itajubá, Brazil.

Rusu, L., Guedes Soares, C. (2012a). Wave energy pattern around the Madeira Islands. Energy, 45, 771-785.

Rusu, L., Guedes Soares, C. (2012b). Wave energy assessments in the Azores Islands. Renewable Energy, 45, 183-196.

Sierra, J.P., Casas-Prat, M., Campins, E. (2017b). Impact of climate change on wave energy resource: The case of Menorca, Spain. Renewable Energy, 101, 275-285.

Sierra, J.P., González-Marco, D., Sospedra, J., Gironella, X., Mösso, C., Sánchez-Arcilla, A. (2013). Wave energy resource assessment in Lanzarote (Spain). Renewable Energy, 55, 480-489.

Sierra, J.P., Martín, C., Mösso, C., Mestres, M., Jebbad, R. (2016). Wave energy potential along the Atlantic coast of Morocco. Renewable Energy, 96, 20-32.

Sierra, J.P., Mösso, C., González-Marco, D. (2014). Wave energy resource assessment in Menorca (Spain). Renewable Energy, 71, 51-60.

Sierra, J.P., White, A., Mösso, C., Mestres, M. (2017a). Assessment of the intra-annual and inter-annual variability of the wave energy resource in the Bay of Biscay (France). Energy, 141, 853-868.

Stopa, J.E., Filipot, J.-F., Li, N., Cheung, K.F., Chen, Y.-L., Vega, L. (2013). Wave energy resources along the Hawaiian Island chain. Renewable Energy, 55, 305-321.

Taylor, K.E., Stouffer, R.J., Meehl, G.A. (2012). An overview of CMIP5 and the experiment design. Bulletin of the American Meteorological Society, 93, 485-498.

Tolman, H.L. et al. (2014). User manual and system documentation of WAVEWATCH III version 4.18. U.S. Department of Commerce, National Oceanic and Atmospheric Administration, National Weather Service, National Centers for Environmental Prediction, Technical Report.

Torre-Enciso, Y., Ortubia, I., Lopez de Aguileta, L.I., Marques, J. (2009). Mutriku wave power plant: from the thinking out to the reality. Proceedings 8th European Wave Tidal Energy Conference, Uppsala, Sweden, pp. 319-329.

Vicinanza, D., Contestabile, P., Ferrante, V. (2013). Wave energy potential in the northwest of Sardinia (Italy). Renewable Energy, 50, 506-521.

Wang, X.L., Feng, Y., Swail, V.R.(2014). Changes in global ocean wave heights as projected using multimodel CMIP5 simulations. Geophysical Research Letters, 41, 1026–1034.

Wang, X.L., Swail, V.R., Cox, A. (2010). Dynamical versus statistical downscaling methods for ocean wave heights. International Journal of Climatology, 30, 317–332.